The role of PFK in the oscillatory yeast strain x2180

by

S.M. Muiyser

Thesis presented in partial fulfilment of the requirements for the degree of Master of Science (Biochemistry) in the Faculty of Science at Stellenbosch University

Supervisor: Dr. D.D. van Niekerk
Co-supervisor: Prof. J.L. Snoep

April 2019

Declaration

By submitting this thesis electronically, I declare that the entirety of the work contained therein is my own, original work, that I am the sole author thereof (save to the extent explicitly otherwise stated), that reproduction and publication thereof by Stellenbosch University will not infringe any third party rights and that I have not previously in its entirety or in part submitted it for obtaining any qualification.

Date: April 2019

Abstract

The role of PFK in the oscillatory yeast strain x2180

S.M. Muiyser

Department of Biochemistry,
University of Stellenbosch,
Private Bag X1, Matieland 7602, South Africa.

Thesis: MSc (Biochemistry)

April 2019

The elucidation of mechanisms involved in glycolytic oscillations in yeast can lead to a deeper understanding of the metabolic organisation in living systems. These oscillations, detected in the concentrations of the glycolytic intermediates of yeast, are a well-studied topic in the context of cell populations and extracts. In a recent study sustained oscillations were detected in individually placed single cells of the X2180 yeast strain in a microfluidic flow-chamber. Literature states that the specific regulation of the phosphofructokinase (PFK) enzyme by the metabolites AMP and ATP are a necessary feature in the glycolytic pathway that enables these oscillations. This regulation was also observed in a previous study where a mathematical model for the oscillatory system was created by numerical optimisation of enzyme kinetic parameters in an experimentally validated detailed model of steady state glycolysis. One of the results of the optimisation was an increased inhibition of PFK by its substrate, ATP.

The aim of the current study was to perform an experimental investigation into the enzyme kinetic characteristics of phosphofructokinase in the X2180 oscillatory strain, as well as in the VIN13 strain, which has not been tested for oscillations. To address this, we used wide-field microscopy to detect oscillations in the X2180 strain and to test for oscillations in VIN13, when they were both cultured under conditions that have been shown to elicit oscillations in X2180. We optimised a protocol for inducing oscillations in our local microscope setup, and subsequently detected oscillations in X2180, and not in VIN13. We were able to optically resolve oscillations on the single cell level which will allow for the investigation of synchronization between cells (a feature that is observed in oscillating populations) in future studies. We then performed a kinetic characterisation of the phosphofructokinase enzyme

in both yeast strains to test whether differences in its regulatory characteristics could be the reason for oscillations in one strain and not the other. We found that there are differences in PFK kinetic parameters of these two strains.

Finally, by using our experimentally determined PFK kinetic parameters in a non-oscillating mathematical model, and following the previously published optimisation steps for other enzymes, we were able to simulate oscillations for the X2180 strain but could not do so for VIN13. From this we conclude that VIN13 requires further kinetic characterisation to be able to determine if it exhibits oscillatory behaviour.

Uittreksel

Die rol van PFK in die ossillerende gisstam X2180

S.M. Muiyser

Department of Biochemistry,
University of Stellenbosch,
Private Bag X1, Matieland 7602, South Africa.

Tesis: MSc (Biochemistry)

April 2019

Die toeligting van meganismes betrokke by glikolitiese ossillasies in gis kan aanleiding gee tot 'n dieper insig van die metaboliese organisasie van lewende sisteme. Hierdie ossillasies, wat in die konsentrasies van die tussenprodukte van glikolise waargeneem word, is 'n goed-bestudeerde onderwerp in die konteks van selpopulasies en ekstrakte. In 'n onlangse studie is volgehoue ossillasies waargeneem in individueel-geplaasde enkelselle van die X2180 gisstam, in 'n mikrofluïde vloeikamer. Bestaande literatuur wys dat die regulasie van die fosfofruktokinase (PFK) ensiem deur die metaboliete AMP en ATP 'n noodsaaklike kenmerk is in die glikolitiese padweg wat hierdie ossillasies moontlik maak. Hierdie regulasie is ook opgemerk in 'n vorige studie waar 'n wiskundige model van die ossillerende sisteem deur numeriese optimering van ensiem-kinetiese parameters in 'n eksperimenteel-gevalideerde model van glikolise in 'n bestendige toestand uitgevoer is. Een van die resultate van die optimering was 'n verhoogde inhibisie van PFK deur sy substraat, ATP.

Die doelstelling van die huidige studie was om 'n eksperimentele ondersoek na die ensiem-kinetiese eienskappe van PFK in die ossillerende X2180 stam, asook die VIN13 stam, wat nog nie vir ossillasies getoets is nie, in te stel. Ons het wye-veld mikroskopie gebruik om ossillasies in die X2180 stam te gewaar en te toets vir ossillasies in die VIN13 stam. Beide kulture is gekweek in toestande wat voorheen bewys is om ossillasies in X2180 te ontlok. Ons het 'n protokol om ossillasies te voorskyn te roep in ons mikroskoop opstelling geoptimeer, en ossillasies in X2180 waargeneem, maar nie in VIN13 nie. Dit was moontlik om ossillasies op enkel-selvlak opties te ontleed, wat voorsiening maak vir die verdere ondersoek van die sinkronisasie tussen selle ('n kenmerk wat waargeneem word in ossillerende populasies) in toekomstige studies. 'n Kinetiese karakterisering van PFK in beide gisstamme is uitgevoer om te toets

of verskille in die regulatoriese eienskappe die oorsaak kan wees van ossillasies in die een stam en nie in die ander nie. Ons het gevind dat daar verskille tussen die kinetiese parameters van PFK van die twee stamme is.

Ten slotte, deur gebruik te maak van ons eksperimenteel vasgestelde kinetiese parameters van PFK in 'n nie-ossillerende wiskundige model, en die vooraf gepubliseerde optimeringstappe vir ander ensieme te gebruik, was ons in staat om ossillasies vir die X2180 stam te simuleer, maar nie vir die VIN13 stam nie. Hieruit kan ons aflei dat VIN13 verdere kinetiese karakterisering vereis om te kan bepaal of dit ossillerende gedrag besit.

Acknowledgements

I would like to express my sincere gratitude to the following people and organisations:

- My supervisors Dr Dawie van Niekerk thank you for always letting me come to you with any problem, big or small. Often allowing me to setup in your office and work so you could help me if I got stuck. Thank you!
- Prof Jacky Snoep for the support over the past years. For never giving up on me and believing in me to compete this project.
- Arrie Arends who every step of the way would moved any obstacles so the project could progress and the words of encouragement, thank you to the world's best lab manager.
- Dr Theresa Kouril for always making time to listen to me, the advice you gave me on my work and helping me whenever I would have problems with the enzyme assaying.
- Kathleen Green, my biggest cheerleader, for always pushing me to play BIG! The entire System Biology lab for being pillars of support through good and bad news. I appreciate each and everyone of you!
- The National Research Foundation (NRF) for funding support.
- My family: parents, in-laws and my beloved sister, for never letting me quit. For loving me and always seeing the best in me.
- Maya Muiyser, for allowing mummy to work. You came into my life in the middle of the project and you are the reason for whom I finished this degree.
- Finally my loving husband, Jacques Muiyser, you are my harshest critic, but without your support over the many years I have been studying none of this would be possible. I appreciate you for always listening to me talk about my work and reading, editing my work and the "supervision" you provided. I love you and look up to you so much, you are my role model!

Dedications

This thesis is dedicated to Jacques and Maya.
"The more that you read, the more things you will know. The more that you learn, the more places you'll go." - Dr Seuss

Contents

List of Figures

List of Tables

Abbreviations

2PG 2-Phosphoglycerate
3PG 3-Phosphoglycerate
ADP Adenosine diphosphate
AK Adenylate Kinase
ALD Aldolase
AMP Adenosine monophosphate
ATP Adenosine triphosphate
BPG 1,3-bisphosphoglycerate
DHAP Dihydroxyacetone Phosphate
ENO Enolase
F16bP Fructose 1,6-Bisphosphate
F26bP Fructose 2,6-Bisphosphate
F6P Fructose 6-Phosphate
G6P Glucose 6-Phosphate
GAP Glyceraldehyde-3-Phosphate
GAPDH Glyceraldehyde-3-phosphate dehydrogenase
Glc_i Internal D-Glucose
Glc_o External D-Glucose
GLK Hexokinase (Glucokinase)
GLT Glucose Transporter
NAD^+ Oxidised Nicotinamide adenine dinucleotide
NADH Reduced Nicotinamide adenine dinucleotide
PEP Phosphoenolpyruvate
PFK Phosphofructokinase
PGI Phosphoglucoisomerase
PGK Phosphoglycerate Kinase
PGM Phosphoglycerate Mutase
PYK Pyruvate Kinase
PYR Pyruvate

Chapter 1

Introduction

1.1 Background

All cells need energy to survive. In the case of budding yeast, *Saccharomyces cerevisiae*, this energy requirement is fulfilled by glycolysis. Yeast glycolysis shares similarities in terms of structure and enzymatic composition with glycolysis in many other eukaryotes. Yeast is also an organism that is easy to culture and characterise experimentally. As such, glycolysis is often studied in this yeast model and is well documented in a recent review [1].

One of the characteristics of glycolysis in yeast is the appearance of glycolytic oscillations. These oscillations can be described as fluctuations in metabolite concentrations of the glycolytic intermediates. This phenomenon has been studied since the 1960s and includes experimental [2–7], and theoretical studies modelling this behaviour to understand causes for its appearance and its regulation [8–11].

Experimentally the detection of glycolytic oscillations has been optimized over the years and various methods of detection have been attempted. It was initially thought that the emergence and control of the oscillations was as a result of a single oscillophore, phosphofructokinase (PFK) [12, 13], but in [14, 15] it was shown that the control of frequency and amplitude, key oscillatory characteristics, was distributed over the pathway and did not reside in a single reaction. It has, however, been suggested that the regulation of PFK by ATP and AMP are characteristics that are required for oscillations to occur, i.e. are essential but not necessarily controlling [16, 17] .

1.2 Problem statement

Glycolytic oscillations are widely studied using mathematical modelling. Ideally the model parameters should be experimentally determined at physiological conditions [18]. Since the first detection of oscillations in yeast cells several mathematical models have been created and used to describe the oscillatory

behaviour of yeast cells and features such as phase shifts and synchronization between cells [16, 19–21]. These models were either core models that served as mathematical abstractions of the oscillatory mechanism, or contained parameters that were obtained from literature, or fitted in a top-down fashion on features of the oscillations. In a recent study [10, 11] an oscillating mathematical model of yeast glycolysis was created by numerical optimisation of parameters in a detailed mechanistic model of steady state glycolysis [22]. This steady state model was originally constructed through *in vitro* characterisation of glycolytic enzymes under the same *in vivo*-like conditions and validated against whole cell glycolysis. The subsequent oscillating model was further validated using published experimental data of metabolites in oscillating yeast cells [11]. This model was also extended to describe oscillations in single isolated cells in a microfluidic flow chamber [7]. One of the results of the optimisation was an increased inhibition of the PFK enzymes by its substrate, ATP, and activation by AMP. Experimental verification of this regulatory characteristic in an oscillating yeast strain has, however, not been conducted.

1.3 Aims and objectives

The aim of this research is to investigate the role of PFK in an oscillatory yeast strain. To achieve this a comparative study is performed between two yeast strains: X2180 and VIN13. X2180 is a known oscillatory strain, for which there exists multiple studies investigating the oscillatory behaviour, and an oscillatory model based on this strain was constructed in [10, 11]. VIN13 has not yet been studied with respect to the detection of oscillations. To meet the aim of the study the following objectives need to be met:

1. Test for oscillations and compare the oscillatory strain X2180 to the VIN13 strain using wide-field miscroscopy. The published protocol [7] has to be optimised for the microscope setup available at the Central Analytical Facilities (CAF) at Stellenbosch University. During this optimisation also test for synchronization in the sample of oscillating cells for possible future studies.

2. Characterise the PFK enzyme in both strains by performing enzyme assays and compare the ATP and AMP kinetic regulation of PFK in the two strains to each other and to previously published kinetics of PFK.

3. Analyse the behaviour of a mathematical model of glycolytic oscillations as a whole, by using the experimentally determined PFK kinetic parameters in the model and testing if an oscillatory model can be obtained for both X2180 and VIN13 strains.

1.4 Thesis outline

The thesis documents the work done to complete the aforementioned objectives and is separated into four main chapters.

- Chapter 2 provides a summary of relevant literature. This literature review equips the reader with the required background information to read the thesis. Based on the studies by [7, 17, 23, 24] the detection of glycolytic oscillations, understanding the growth and harvesting of the cells required for oscillations and the different methods used to detect the oscillatory behaviour, are reviewed. Secondly, the role of PFK in this oscillatory behaviour, and the modelling approaches [10, 11] used to investigate this property is summarised.

- Chapter 3 documents the microscope work done to achieve objective 1. The chapter shows the methodology followed to visualise oscillations under a fluorescent microscope. Additionally, the problems that were encountered are also documented for the purpose of improving future research. The chapter also provides the steps for data processing from the raw data to the final signal and explains the tools used in data analysis. These tools include the Fast Fourier transform (used in determining the frequency of a oscillation signal) and the Hilbert function (describes the extent of synchrony between cells).

- Chapter 4 provides details regarding the PFK characterisation in the oscillatory and non-oscillatory strains and describes the work done to achieve objectives 2 and 3. Similarly to Chapter 3, this chapter shows the experimental protocol used to characterise the effects of ATP and AMP on PFK activity as well as the optimisation steps followed when performing PFK enzyme assays. Finally, it is shown how the model with the fitted PFK parameters was optimized to obtain an oscillatory model.

- Chapter 5 is a summary and also includes recommendations for future work based on the identified shortcomings of the current study.

Chapter 2

Background

2.1 Biology of glycolysis and oscillations

Within each cell are regulated systems that allow the cell to live, grow and replicate. Glycolysis is one of the metabolic pathways necessary for cell function that provides energy and intermediary metabolites [25]. It is one of the most conserved processes and occurs in almost all cell types [25]. This anaerobic process occurring in the cytosol of the cell, shown in Figure 2.1, is catalysed by ten core enzymatic reactions for most eukaryotic organisms. The reactions break down the six-carbon glucose (Glc) transported into the cell by glucose transporters (GLT), to release energy, in the form of adenosine triphosphate (ATP), reduced nicotinamide adenine dinucleotide (NADH) and two triose pyruvate (PYR) molecules. Along the way it forms a number of intermediary metabolites and the pathway can be split into two major phases, reactions that require energy (top part of the pathway) and those that produce energy (bottom part of the pathway). In the top part the glucose is converted to fructose1,6-bisphosphate (F16bP) by attaching two phosphate groups, which are donated from ATP molecules, in the energy requiring reactions catalysed by hexokinase (GLK) and phosphofructokinase (PFK). In the subsequent energy producing reactions catalysed by phosphoglycerate kinase (PGK) and pyruvate kinase (PYK), through substrate level phosphorylation of adenosine diphosphate (ADP) leading to the formation of 2 ATP per GAP, i.e. 2 net ATP are formed per glucose. The dehydrogenase reaction catalysed by glyceraldehyde phosphate dehydrogenase (GAPDH) also leads to the net formation of 2 NADH from 2 nicotinamide adenine dinucleotide (NAD^+). The final products of glycolysis, NADH and PYR are then used in aerobic respiration to produce more energy for the cell [25]. Take note of PFK, which is the enzyme that catalyses the reaction producing F16bP, it is an important point of regulation in glycolysis as it is allosterically controlled by various effectors such as ATP, ADP, adenosine monophosphate (AMP), PEP, fructose 2,6-bisphosphate (F26bP) and citrate [25]. PFK is further discussed in Section 2.3.

Saccharomyces cerevisiae is often used in studies of the glycolytic pathway as it is a model organism which shares multiple similarities with simple eukaryotic cells [26] and it is easy to grow and characterise in the laboratory environment. In this study two strains of *S. cerevisiae* are investigated, namely X2180 and VIN13. Based on an online yeast genome database (https://www.yeastgenome.org) [27], the X2180 strain is commonly used in laboratories for biochemical experimentation and is a strain in which glycolytic oscillations, see Section 2.2, have been detected and widely studied [7, 17, 28, 29]. The second yeast strain, VIN13, was created at Stellenbosch University's Wine Biotechnology Department with properties such as cold-tolerance and it is a strong fermenter making it a popular strain used in the production of aromatic white wines. VIN13, to our knowledge, has not been investigated for glycolytic oscillations. Section 2.2 will describe the biology underlying glycolytic oscillations and provides a summary of what is known on this dynamic behaviour.

2.2 Glycolytic oscillations

Under certain conditions, the concentrations of the intermediate metabolites in glycolysis repetitively fluctuate. This is referred to as glycolytic oscillations [31]. These oscillations are usually visualised by monitoring either the NADH auto-fluorescence or absorbance measurements over time [31]. It is hypothesised that the oscillatory behaviour could be a way for the cell to regulate and coordinate the system's functionality in terms of energy efficiency and cellular communication [32]. Glycolytic oscillations are not the only examples of biological oscillators, with oscillations found in protein synthesis in bacteria at the molecular level, and periodicity in muscular and nervous systems within multicellular organisms, being other well known examples [32].

Oscillations have been visualised in both cell-free extracts and intact cells of *S. cerevisiae*. Research has focused on: 1) investigating the conditions allowing for the observation of oscillations and the study of the subsequent synchronous behaviour that accompanies this phenomenon [7, 33, 34], and 2) investigating the factors that bring about these oscillations by specifically looking at enzymatic control and energy balance [8, 35–37]. The [7, 33, 34] studies have been used to guide the experimental protocol in this study and [8, 35–37] provides the context in which the experimental and modelling results are interpreted and is described in the next Section 2.3.

Oscillations in cell-free extracts occur when the lysate is exposed to a constant and suitably strong flow of substrate, such as glucose or fructose. This is usually achieved by adding trehalose to the lysate where the trehalose is gradually broken down by the enzyme trehalase into glucose, resulting in the continuous flow of the substrate within the lysate [38, 39]. The cell-free oscillations are sinusoidal in shape at higher glucose influx rates or have a saw

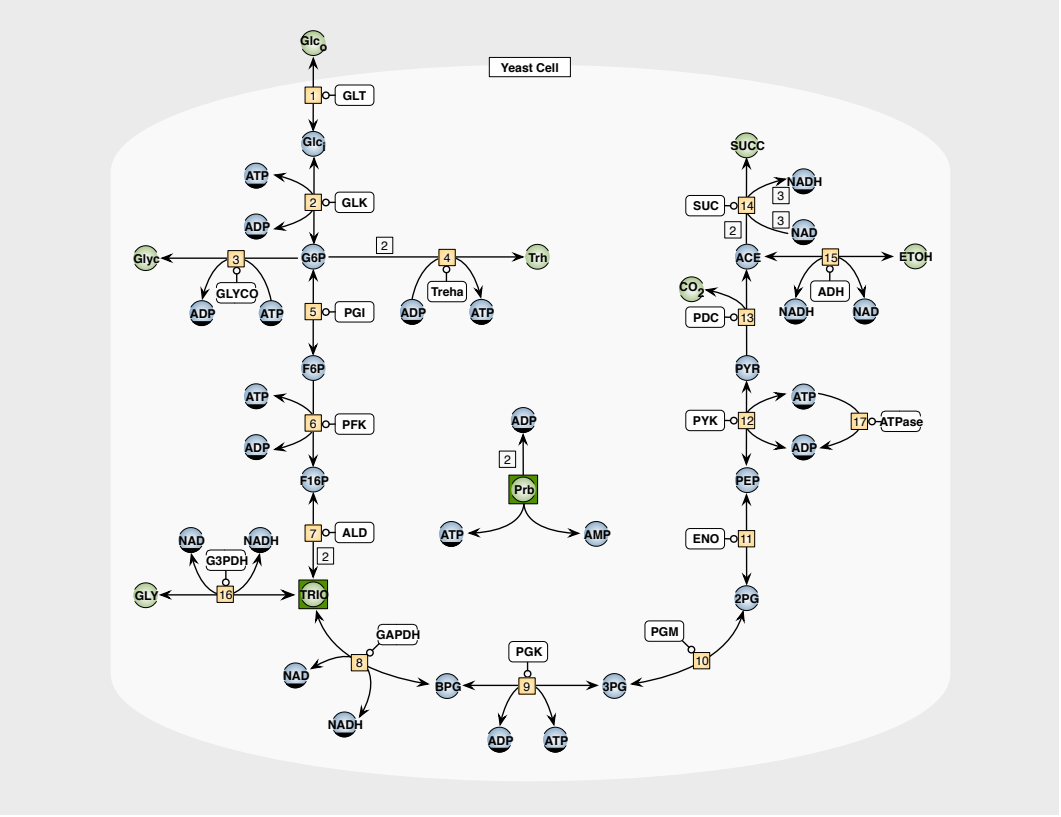

Figure 2.1: Schema of the classical EMP (Embden-Meyerhof-Parnas) pathway of glycolysis in yeast as taken from JWS Online (http://jjj.biochem.sun.ac.za/) [30]. It illustrates the entry of glucose via the GLUT transporters (GLT) into the cytosol of the cell. The enzymes in the pathway are shown by the numbered blocks, the metabolites are the blue balls and the co-factors are represented by the dual coloured balls.First is a kinase reaction **(2)** adds a phosphate group onto the glucose to form glucose-6-phosphate (G6P), an isomerase reaction **(5)** converts the G6P into fructose-6-phosphate (F6P) by rearranging covalent bonds, next is the second kinase reaction **(6)** where a phosphate is added to create fructose 1,6-bisphosphate (F16bP), a lyase reaction **(7)** splits the six-carbon, F16bP, into two triose sugars namely glyceraldehyde 3-phosphate (GAP) and dihydroxyacetone phosphate (DHAP). The (TRIO) box represents DHAP and GAP with the triosephopsphate isomerase reaction between them in equilibrium. GAP is then oxidised by a dehydrogenase reaction to form 1,3 -bisphosphoglycerate (BPG). The BPG produces an adenosine triphosphate (ATP) via a kinase reaction **(9)** to form 3 -phosphoglycerate (3PG), a mutase reaction **(10)** moves the phosphate from the third position of the 3PG to the second position to form 2 -phosphoglycerate (2PG), next a lyase reaction **(11)** removes water from 2PG to create phosphoenolpyruvate (PEP) and finally a kinase reaction **(12)** produces an ATP when converting PEP to pyruvate (PYR).

tooth appearance at lower glucose influx rates [40]. There is an abundance of literature on the oscillations in cell-free extract where these papers point out that most of the glycolytic metabolites oscillate, and that the PFK plays a vital role in the oscillatory behaviour [12, 37, 41, 42].

Oscillations observed in populations of cells were first reported in [35, 43]. These studies used baker's yeast cells that were starved, after which a sucrose pulse was introduced and the cells switched to anaerobiosis, by limiting the oxygen supply to the cells, which initiated a few damped oscillations. Subsequently, oscillations were detected in the glycolytic intermediates, such as G6P, F6P and F16bP, when using enzyme assay methods to quantify intermediate concentrations from aliquots [44]. In [2] it was shown that sustained oscillations can be achieved by the addition of cyanide, which is an aldehyde trap, instead of switching to anaerobiosis. The cyanide binds to acetaldehyde thereby maintaining the acetaldehyde at the right concentration for single cells to oscillate and for the cells to synchronize their oscillations. Thus, in order to detect oscillations in intact yeast cells, the cells are grown until glucose depletion, where the growth rate plateaus and the cells are about to switch metabolism to an alternate substrate (diauxic shift). The cells are then starved for a period of time, and harvested. The addition of a glucose pulse and the subsequent addition of cyanide will then promote the appearance of sustained glycolytic oscillations. Unlike cell-free extracts, where the rate of substrate feed plays a vital role in the appearance of the oscillations detected, the intact cells oscillations are always sinusoidal in shape [45]. Typically, oscillation studies follow the protocol where the cells are harvested at the diauxic shift and then starved to obtain oscillatory conditions. [29] investigated the significance of exactly when the cells are harvested and how it can impact the type of oscillations detected. Cells that are harvested at the log phase, where the cells are growing exponentially and consuming glucose, or the stationary phase, where the cell growth has come to a halt and cells are consuming ethanol, resulted in damped oscillations with only a few cycles observed. However, cells that were harvest at the diauxic shift, where the glucose is depleted and the cells are about to switch to ethanol metabolism, exhibited limit-cycle oscillations. Futhermore [4] also established that the effective concentration of cyanide to yield sustained oscillations in a population is between 3 mM to 8 mM. At this concentration cyanide binds sufficient acetaldehyde to maintain it in a region of concentrations that enable synchronization between the cells.

Most of the intact cell studies are performed in populations of cells as opposed to single cells because of the experimental ease of detecting oscillations in them. This is due to the fact that oscillating cells can synchronise under certain conditions leading to a net oscillating NADH signal from such a population. In [33] it was shown that when two out of phase oscillatory populations were mixed, the amplitude of the detected signal briefly died out after which a gradual recovery occurred due to the formation of one synchronised population. The synchronization is hypothesised to occur as a result of cell-to-cell commu-

nication via the extracellular acetaldehyde (one of the products of glycolysis in yeast) [34]. Acetaldehyde easily diffuses across the cell membrane and stimulates the alcohol dehydrogenase reaction, exerting an effect on NADH which is translated to the upper part of glycolysis. Until fairly recently, however, it was unclear whether the oscillations were a result of the population reaching a certain density or whether cells in isolation could oscillate [7]. This question could not be answered by investigating only populations since the lack of oscillations in a population could be due either to single cells oscillating but not synchronising or cells not oscillating at all. In [46], it was shown that there is heterogeneity at single cell level in a population and that it is possible for cells to oscillate without the population as a whole displaying oscillation. [46] also shows the dependence of the oscillations on the cell density. Properties such as amplitude and the damping of the glycolytic oscillation are directly dependent on the cell density, whereas the period of the oscillations remains independent thereof. Thus there is a certain level of cellular interaction occurring at high cell densities that does affect the appearance of the oscillations. In [47] the dynamics of glycolytic oscillation in single cells, removed from an oscillating population, was investigated. The cells were isolated and fixed onto a coverslip, resulting in a single layer of cells, across which there is a constant flow of glucose and cyanide. The results in [47] showed dynamic behaviour of the population of cells due to the addition of acetaldehyde, however in isolated cells no oscillations were detected.

To date, most of the studies measuring glycolytic oscillation in intact yeast cells were done in a closed batch system or in a system with a slow continuous inflow of substrate. In these studies, the cells are usually visualised using a fluorimeter to detect the fluorescent NAD(P)H. In [19] they investigated the glycolytic oscillations in cell-free extracts using an open system, such as a continuous flow stirred tank reactor (CSTR). The study was able to detect sustained oscillations in this system and by varying the inflow conditions they were able to influence the appearance (shape or period) of the observed relaxation oscillations that is usually found in cell extracts. This setup was then used by [5, 6] to investigate intact cells. This study was also able to show sustained oscillations of the cell suspension when the system is kept at a well defined state by pumping starved cells, glucose and cyanide into the reactor and having excess liquid as an outflow. Some key finding in [5, 6] were the transition from stationary cells to oscillatory behaviour which was mathematically described by a Hopf bifurcation [48]. The bifurcation point is the point at which the cells start to oscillate, at a specific frequency and small amplitude, as a function of a system's parameters, such as glucose concentration or cyanide concentration.

In a more recent study [7] the experimental setup of [47] was optimized and was able to show sustained oscillations at isolated single yeast cell level. The optimized experimental setup consisted of a modified microfluidic system with four inlet channels, where the flow rates of the solutions injected

into the chamber could be controlled. The cells injected into the system, via one channel, were positioned in an array configuration onto the adhesive bottom using optical tweezers. Glucose or a glucose and cyanide solution was then introduced via the other channels. The oscillations were detected by visualizing the NADH fluorescent intensities using an inverted epi-fluorescence microscope. Not only does the study show oscillation at varying flow rates of glucose but the isolated cells exhibit a heterogeneous behaviour, which is a notable phenotypic difference in the cell-to-cell behaviour [23]. In [24] periodic perturbations were employed to investigate the entrainment of the glycolytic oscillations. Oscillating heterogeneous cells were entrained by perturbing the external environment to bring about phase shifts,which is similar to what occurs when single cells synchronise with others. The mechanism was shown to be universal, meaning that regardless of the types of external perturbations (addition of acetaldehyde or removal of cyanide), the cells still synchronised to the signal in a similar fashion.

2.3 The oscillophore

At the molecular level, metabolic regulation is often brought about by feedback or feedforward control processes. Cellular processes have tendency to naturally oscillate and [49] states that this oscillatory behaviour contributes to the operation of regulatory mechanisms within a cell. Therefore, understanding the mechanism of glycolytic oscillation can elucidate the regulatory control of this metabolic pathway [49]. Studies note two possible mechanisms that can cause glycolytic oscillations: [9] attributes it to the inherent instability of the autocatalytic stoichiometry of glycolysis, whereas [8, 35–37] describes the allosteric regulation of PFK, specifically with respect to ATP inhibition, as a key characteristic that is essential for the glycolytic oscillations. The crossover theorem, which is an analysis method used to plot a crossover diagram that shows the phase angle shift between the glycolytic intermediates, indicates control points within the metabolic pathway. In [50] this method was used in yeast extracts to identify PFK and other reactions coupled to the ATP utilization (such as PK) as main steps contributing towards the oscillatory behaviour. Once again, in [3], yeast extracts were used to show PFK as the main contributor to the emergence of oscillations because addition of the metabolites above the reaction (e.g. F6P) elicit oscillation whereas the metabolites below the reaction (F16P) lead to none. Experimental phase angle studies in [51] of intact yeast cells have also shown PFK as a key enzyme in the observed oscillations, and the oscillations in intact cells probably have similar origins and properties to that of cell extracts. Although regulation of PFK might be necessary for oscillations (and is often seen as the oscillophore), it does not have full control of the appearance of the oscillations [14]. In [52] the membrane transporter is described as a rate limiting step that regulates the entry of metabolites into

the cell and can influence the oscillatory behaviour. This is further supported in the study by [53] where the hexose transporter was inhibited and resulted in a lower glucose flux into the cell, which led to a reduced observed frequency of the glycolytic oscillations. Even though the study showed that most of the control lay with the glucose transporter they also conclude that there is possibly one or more steps contributing to the control in glycolytic oscillations. Recent studies make use of a sensitivity analysis called metabolic control analysis (MCA), to determine which reactions exert the most control on the system [54]. When MCA was performed on the current models of glycolytic oscillations in [14], it was found that the control on frequency and amplitude, the characteristics of oscillations, was shared by all enzymes involved in glycolysis and that a single enzyme cannot solely generate or influence the characteristics of oscillation. In [15], based on an analysis method developed in the study, they concur with the findings in [14] and redefine the oscillophore as a culmination of favourable cellular conditions. As such, processes within the cell can be oscillophoric and give rise to the observed oscillatory behaviour. A study [17], employing both experimental characterisation of oscillations as well as mathematical modelling, showed that the regulatory properties of PFK is, in fact, required for oscillations to occur, which will then happen if the rest of the cellular environment is favourable.

In [55], the diploid *S. cerevisiae* strain BY4743, which has a library of sequenced isogenic deletion mutants, and is able to show glycolytic oscillations was used to investigate the effects of deletion of genes that encode glycolytic enzymes. The strain used in the study showed similar glycolytic oscillations to those found in X2180 when the cells are grown and harvested following the same protocol as described in this thesis. The oscillatory behaviour of the mutant strains with deleted genes were visualised and a sensitivity analysis of the oscillatory characteristics was performed on the experimental data obtained. Their findings agreed with the current hypothesis of a shared enzymatic control on the features of glycolytic oscillations. The isogenic deletion mutants specifically with the deletion of hexokinase could still lead to sustained oscillations with smaller amplitudes. On the other hand, the deletion mutants of GAPDH no longer show oscillations. The PFK enzyme is made of subunits, PFK1 and PFK2, which are both shown to have distinct roles in the regulation and control of the glycolytic oscillations. The deletion of both genes knocks out the functionality of PFK and cells do not grow in a glucose rich environment. However, to achieve glycolytic oscillations in a single deletion mutant the PFK2 subunit is required.

Phosphofructokinase is the second priming reaction in glycolysis where the substrate F6P is phosphorylated by coupling it to an ATP hydrolysis reaction. This step is an irreversible reaction committing the cell to glucose metabolism and is pivotal in the regulation of glycolysis [25]. PFK is a heterooctameric enzyme made up of two distinct subunits which is allosterically regulated by various effectors: AMP acts as an activator while its substrate ATP can act

as an inhibitor of the enzyme as shown in Figure 2.2. ATP has two distinct binding sites on PFK: one is a high affinity substrate site and the other a low-affinity regulatory site. Therefore, when the energy requirement for the cell is met the enzyme can "switch off" glycolysis [25], when it is not, high AMP and low ATP work in unison to stimulate PFK and accelerate glycolysis. This complex regulatory pattern of PFK and its relation to oscillations has been the topic of various modelling analyses which will be discussed in the following section.

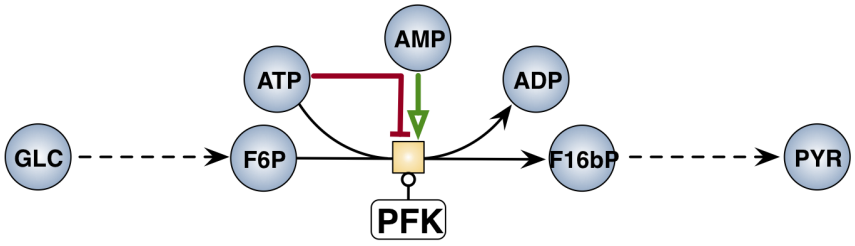

Figure 2.2: Metabolites affecting the PFK-catalysed reaction in glycolysis. The enzyme PFK, as shown by the block, catalyses conversion of its substrates F6P and ATP, to products F16bP and ADP. ATP inhibition is shown by the red line and AMP activation of the enzyme is represented by the green arrow. The description of the abbreviated enzymes, metabolites and co-factors in the schema are in the Nomenclature section of this thesis.

2.4 PFK model

The kinetic modelling of glycolytic oscillations in the complete glycolytic pathway of yeast cells is discussed in Section 2.5, this section details how PFK kinetics is described in the Teusink models [22] and Du Preez model [10, 11] which are under investigation. One frequently used mathematical description of the kinetic mechanism of an enzyme is the Michaelis-Menten equation (equation 2.1 displays its single substrate irreversible form) where the rate at which the product of the enzyme is formed, v, at a specific substrate concentration, $[S]$, is described in terms of maximal rate at saturating substrate concentration, $V_{\max}$ and a Michaelis-Menten constant, K_m, which is the substrate concentration at half maximal rate.

$$v = \frac{V_{\max}[S]}{K_m + [S]} \tag{2.1}$$

Rate constants are typically determined by spectrophotometric assays which detect enzyme activity through changes in NADH absorbance. This requires coupling the enzyme through a common intermediate to an NADH consuming or producing reaction. The Michaelis Menten equation has been generalised

for reversible reactions, multiple substrates and products and various kinetic inhibition phenomena. It can not, however, describe conformational changes in multimeric enzymes induced by species binding to similar sites on subunits leading to reduced or enhanced catalytic activity. For this, the Hill equation and the Monod-Wymann-Changeux equation (MWC) are employed.

In the models of [10, 11, 22] PFK's kinetic mechanism is described using the MWC model (specifically the equation derived in [56]) in terms of F6P, ATP, AMP, F16P and F26bP (fructose 2-6-bisphosphate). ADP (adenosine diphosphate), the product of ATP hydrolysis, is said to have negligible direct effect on the rate of the enzyme and is thus not included. It should, however, be noted that the action of the AK (adenylate kinase) enzyme *in vivo*, converts ADP to ATP and AMP which will affect the activity of the enzyme. The MWC model, also referred to as the concerted-symmetry model, describes a multimeric enzyme composed of identical subunits which are in equilibrium between their T (tense) state (catalytically inactive) and R (relaxed) state (catalytically active). The T state has a low substrate affinity in comparison to the R state conformation of the enzyme. The binding of the allosteric effectors can cause the equilibrium to shift from one state to the other in a concerted manner. The MWC model was originally used to describe the kinetics of a single substrate of an irreversible reaction. [56] modified the model to describe the effect of two substrates, and as previously mentioned, this is the derivation used to describe PFK kinetics in glycolysis. [56] highlights how PFK plays a key role in the glycolytic oscillations observed in biological systems where the autocatalytic property of PFK was recognised to not only be as a result of the feedback activation by the metabolic product (AMP) of the reaction, but also due to the multiple-state function, such as substrate inhibition, of PFK [48]. This led [12, 57] to use the MWC model to describe the kinetics of PFK in their model of yeast oscillations. A similar derivation using the MWC model, describing oxygen binding to hemocyanin, is done in [58]. The MWC model has become a standard in describing allostery of multi substrate enzymes and proteins.

Based on the derivation presented by [56], the rate equation describing PFK in [22] is:

$$v_{PFK} = V_{max} \cdot \frac{g_R \lambda_1 \lambda_2 R}{R^n + LT^n} \tag{2.2}$$

where g_R is the affinity coefficient for the two substrates at the R states, LT^n is the term that accounts for the effectors, $n = 2$ indicates the two subunits (protomers) in PFK as presented in [56], and:

$$\lambda_1 = \frac{[F6P]}{K_{R,F6P}} \tag{2.3}$$

$$\lambda_2 = \frac{[ATP]}{K_{R,ATP}} \tag{2.4}$$

$$R = 1 + \lambda_1 + \lambda_2 + g_R\lambda_1\lambda_2 \tag{2.5}$$

$$T = 1 + C_{ATP}\lambda_2 \tag{2.6}$$

and

$$L = L_0 \left(\frac{1 + C_{i,ATP}[ATP]/K_{i,ATP}}{1 + [ATP]/K_{i,ATP}}\right)^2 \cdot \left(\frac{1 + C_{AMP}[AMP]/K_{AMP}}{1 + [AMP]/K_{AMP}}\right)^2 \cdot \left(\frac{1 + C_{F26bP}[F26bP]/K_{F26bP} + C_{F16bP}[F16bP]/K_{F16bP}}{1 + [F26bP]/K_{F26bP} + [F16bP]/K_{F16bP}}\right)^2 \tag{2.7}$$

Here effectors mediate the displacement of the equilibrium between the T and R states and this is described by the equilibrium dissociation constants K_R for the relaxed state and K_T for the tense state, L_0 is the ratio between the T and R states of the enzyme in the absence of allosteric effectors (T_0/R_0) and C the ratio between the dissociation constants of the two states for an effector (K_R/K_T). Note that the derivation of equation 2.2 is predicated on the assumption that assumed that F6P does not bind to the T state and it is therefore inactive.

2.5 Modelling oscillations in glycolysis

In the field of Systems Biology the mathematical modelling of molecular networks, such as the metabolic pathways, has become the norm. The models usually describe time changes in metabolite concentrations by using ordinary differential equations (ODEs) composed of rates that affect the amount of metabolite concentration by either creating or consuming it. These models provide insights into the functioning and regulation of metabolic pathways [59]. One of the earliest models of glycolysis that included detailed mechanistic descriptions of most of the enzymes involved in the pathway was [60]. The kinetic parameters used in this model were obtained from literature and the model showed dynamic behaviour in the NADH/NAD^+ system which resulted in oscillations where the model predictions closely resembled that found experimentally.

Another well studied model of glycolysis, that has been used in various other studies [10, 11, 61, 62] is the Teusink model [22]. The main aim of [22] was to determine whether *in vitro* kinetic parameters determined for each isolated enzyme, assayed under standardized physiologically relevant conditions, matched the behaviour observed *in vivo*. This lead to the creation of a detailed kinetic model of the steady-state behaviour in the yeast glycolytic pathway, which was constructed from experimentally determined parameters. This was conducted by characterising each enzymatic reaction experimentally

(in cell extract), detailing its mechanism and kinetic parameters, and including branched reactions showing exit destinations of certain metabolites, such as glycogen and glycerol production. The behaviour of an intact whole cell suspension was also determined experimentally to obtain metabolite concentration and fluxes, which was then used as a validation. The reconstituted model was able to successfully predict the systemic behaviour of the glycolytic pathway.

The question addressed in [22] was regarding the *in vivo* predictive power of models constructed from *in vitro* studies , as far as steady state behaviour is concerned. Models of glycolytic oscillations were initially constructed as core models that encapsulated the dynamic behaviour but did not contain mechanistic detail of the reactions in the metabolic pathway [8]. In [21] a model for glycolysis and its corresponding oscillation was constructed using an optimisation approach that was conceptualised in this study by Hynne *et al.* and called the direct method. In the study by [21] an already existing detailed kinetic model was optimised by fitting rate constants and Vmax values from experimental data specifically at the stationary state, where metabolite concentration and rates are independent of time and thus easily described by simple algebraic equations. For the detection of oscillations, the Hopf bifurcation was investigated. This model faired reasonably well in describing some features of the oscillations but not others. In [10] they follow a similar approach as the direct method in [21], but instead of simple algebraic equations, the optimisation is done by integrating the ODEs usually found in mechanistic models. As such the model of [22] is used as a starting point in a series of mathematical optimisation steps. The oscillatory behaviour in a model is usually characterised by an instability in the model. In other words, a system is defined as unstable when there is a perturbation on the steady-state of the variables in a model resulting in the variable moving away from the steady-state. As previously stated, the model is made up of ODEs, and the stability of the system can be investigated by calculating the Jacobian Matrix, M, at steady-state metabolite (S^0) concentrations. This matrix can be interpreted as the sensitivity of the rates to changes in the variables and is illustrated by equation 2.8 described in [10]:

$$M_{S^\circ} = N \cdot \frac{\partial v}{\partial S}\Big|_{S=S^\circ} \tag{2.8}$$

where N is the matrix of stoichiometric coefficients, v the vector of rates and S the vector of metabolites (S^0) denoting the steady state). Equation 2.9 describes the evolution of a perturbation to the steady state in terms of the Jacobian Matrix (M).

$$\frac{d\Delta S}{dt} = M_{S^\circ} \cdot \Delta S \tag{2.9}$$

The stability of the system to perturbations in changes of substrate (ΔS) is encompassed in the eigenvalues and eigenvectors of the Jacobian Matrix where positive eigenvalues denotes the metabolites contributing towards instability in the system. It is however possible that the eigenvalues contain a complex conjugate pair where the real part is positive (indicative of instability). The absolute value of the imaginary component then specifies the tendency to oscillate (describing the frequency characteristic of the oscillator behaviour) and whether the oscillations are sustained limit cycle oscillations. As such, to investigate to what extent certain parameter changes contribute to the oscillatory tendency of the model, control coefficients on the ratio of the imaginary part to the real part is determined for each rate as seen in equation 2.10.

$$C_{vi}^{\frac{\Im\lambda_j}{\Re\lambda_j}} = \frac{\partial \ln \left| \frac{\Im\lambda_j}{\Re\lambda_j} \right|}{\partial \ln v_i} \tag{2.10}$$

In [10] a stepwise iteration was used to adjust parameter values according to this coefficient. This brought the model to the Hopf bifurcation point where a complex conjugate pair of eigenvalues with small positive real part and non-zero imaginary part appeared.

The previsouly mentioned steps to investigate the Hopf bifurcation was the first optimisation performed by [10, 11] to create an oscillatory model, dupreez2, from the non-oscillatory model, dupreez1. The dupreez1 model [10, 11] is very similar to the Teusink model [22] in that it still describes the original steady states even with the few adaptations done:

- The fixed fluxes for trehalose and glycogen synthesis branches were replaced with simple irreversible mass action kinetics.
- The AK reaction was converted from equilibrium to rapid mass action and explicitly represented energy metabolites such as ATP, ADP and AMP rather than assigning energy rich phosphate bonds to describe these metabolites.
- The glycerol branch was expanded by adding an intermediary step.
- The ATPase reaction was changed to simulate saturation kinetics.

The dupreez3 model was further optimized by fitting to some of the characteristics of oscillation such as amplitude and frequency of selected metabolites while dupreez4 additionally accounts for the synchronization of the oscillatory behaviour between cells in a population. For the purpose of this study only the first optimisation step to obtain an oscillatory model (i.e. dupreez1 to dupreez2) is considered.

2.6 Relevance of current study

A thorough literature review has shown that there exists a number of studies towards understanding the underlying mechanism and occurrence of glycolytic oscillations. These studies describe this biological phenomenon from an experimental point of view or via mathematical modelling and have shown that:

- At well defined conditions oscillations can be detected using NADH detection methodologies [4–7, 29, 34].
- The control or emergence of oscillation is not attributed to a single enzyme, as previously hypothesised [12, 13] where PFK was termed the oscillophore, but rather it is as a result of a combined effect of the enzymes in glycolysis [15].
- Allosteric inhibition of the PFK enzyme by ATP and activation by AMP are requirements for oscillations to occur [16, 17].

As such, characterising the effect ATP and AMP have on PFK enzyme in oscillating yeast, and comparing it to already existing models of oscillating glycolysis, is one of the main goals of this thesis.

Chapter 3

Visualising individual oscillations at the population level with microscopy techniques

3.1 Introduction

Glycolysis in *Saccharomyces cerevisiae* is a well described metabolic pathway [63] and studies have shown that under specific conditions the glycolytic metabolites exhibit an oscillatory behaviour. This was first demonstrated through the observation of the fluorescent fluctuations in NADH concentrations within populations of intact yeast cells [31].

In [7] sustained glycolytic oscillations were shown in individual isolated yeast cells. This indicated that even at low biomass concentrations the yeast cells do oscillate. The findings were demonstrated using an experimental technique where the yeast cells were positioned in a microfluidic chamber, and the flow rates across the cells were manipulated to obtain well defined extracellular conditions. In addition to the oscillatory behaviour observed in isolated yeast cells, the experimental results highlighted the heterogeneity of the individual cells [23]. Despite this heterogeneity the authors show how the oscillations of these single cells could synchronise [24].

In this chapter the visualisation of oscillations in both X2180 strain and VIN13 strain of intact cells will be described and discussed, similarly to the work reported by [7, 23, 24]. The isogenetic differences in the two yeast strains are highlighted in [64]: The X2180 strains is commonly used for laboratory experimentation and is said to have poor fermentation properties, whereas VIN13 is a commercially used strain in wine production. For the comparison the cells are grown, harvested and treated in a similar manner to that described in [7, 23, 24]. The visualisation of the cells will however be different to that described in [7] as the fluorescent microscopy facilities at Stellenbosch University were used instead of a microfluidic chamber. This would allow for

future studies to visualise the behaviour of single cells in a population but has the strength of allowing the investigation of synchronization since there is no flow of medium washing away extracellular metabolites as is the case in the microfluidic chamber.

Oscillations in *S. cerevisiae* in the fermentation industries might not a desired phenomenon as it reduces the efficiency of the ethanol production in the bio-reactors [65] and makes control of such fermentations difficult. Studies on macroscopic factors, such as pH, cell biomass density and even carbon dioxide level, have been made to mitigate the oscillatory phenomenon [66]. Since VIN13 is a frequently used strain in wine making, the objective was to investigate if it would exhibit oscillatory behaviour when treated in the same way as the X2180 strain. This was not a criterium by which VIN13 was selected for fermentations and it has not been tested to date.

3.2 Methods

3.2.1 Experimental

Cell preparation and harvest Cells from both strains (X2180 and VIN13) were grown, harvested and treated following the protocol described in [29]:

1. The growth medium used in the agar plates and in which the cells are cultured contains 10 mg/mL glucose, 6.7 mg/mL yeast nitrogen base and 100 mM of potassium hydrogen phthalate (KHP) at a pH of 5.0. The two yeast strains were streaked out from freezer stocks on to media rich agar plates. Starter cultures were made from a single pin colony that is inoculated into a volume of growth media and allowed to grow overnight (overnight starter culture) to an OD above 1.0. The protocol calls for the cells to be grown semi aerobically at 30°C while agitated in a rotary shaker at 160 rpm for 12 to 14 hours until just past the diauxic shift.

2. At the end of the approximate 14 hour growth period, glucose exhaustion was tested by using glucose test strips. Once the culture showed glucose depletion the cells were washed twice with a phosphate buffer (100 mM) by centrifuging the cells at 13 000 RCF for 5 minutes at 4°C, discarding the supernatant and re-suspending the pellet in the buffer.

3. The re-suspended cells (that are now in phosphate buffer) were then placed back in the 30°C rotary shaker to starve for a further 3 hours, after which the cells were harvested by centrifuging the culture. The remaining pellet is then diluted in 5 ml phosphate buffer and kept on ice until used.

Microscope visualisation As previously stated, to visualise cell oscillation, the fluorescent microscopy facilities at Stellenbosch University were used:

1. The Lab-Tek 8 Chambered # 1.0 Borosilicate Coverglass System in which the cells were visualised under the microscope, was coated with a 1 mg/mL concentration of concanavalin A (Con A) solution containing 10 mM Tris/HCl and 100 mM NaCl.

2. The coated chambers were then placed under the ultraviolet (UV) light in the laminar flow cabinet for 30 minutes to allow the surface to become adhesive before the diluted cell suspension was placed in each chamber.

3. Prior to visualization under the microscope, the cell suspension was removed and the chamber was washed with the phosphate buffer to remove any non-adhered cells. This wash step was performed to ensure that only a single layer of cells adhered to the bottom of the chambered cover glass system for unobstructed visualisation.

4. The immobilised cells were covered with a small volume of phosphate buffer to prevent them from drying out or being damaged while being positioned in the microscope.

5. There after a glucose pulse of 20 mM and 5 mM potassium cyanide was then added to the washed, immobilised cells and placed back into the microscope. Note that these concentrations are the final concentrations the cells were exposed to in the chamber and that the stock solutions of glucose and cyanide added compensated for the phosphate buffer initially added to the chambers.

6. The cells were then visualised under the Olympus IX81 inverted fluorescent microscope with CellR imaging software to detect oscillations within the different cells. The objective used was Olympus UPlanApo N 100x with excitation filters of 350 nm for blue light. Emission at 460 nm was detected for the visualization of NADH. For full details regarding the specification of the microscope refer to the specification sheet provided in Appendix A.

7. Images were recorded every three seconds for 15 minutes where the first time point was recorded after the cells were in focus on the microscope. The recording was then paused and the second time point recorded after the solutions was added to the cells. This introduced a delay of between one and two minutes after the addition of the glucose and cyanide.

3.2.2 Analysis

Image analysis During the course of a 15 minute experiment the microscope captures approximately 300 images (one every three seconds). The images are then imported into the ImageJ software package for analysis. The oscillatory behaviour was recorded by detecting the fluctuating fluorescent intensity of NADH. The software stacks the images creating a time lapse of the NADH fluorescence which was captured using the Time Series Analyzer plugin that allows regions of interest (ROI) to be drawn around each individual cell on the image. The pixel intensity measured in each ROI is then plotted as a function of time to visualise the oscillations.

Data analysis The processing of data acquired through microscope imaging is well documented in [67, 68]. As the objective of the study was to specifically investigate oscillatory behaviour, the analysis procedure in [24] was followed:

- The pixel intensity signals are first processed using MATLAB (The MathWorks, Inc.) that has a built-in signal processing toolbox with commands to detrend and smooth the raw data. The data is detrended linearly to compensate for any drift while smoothing is a process by which a running average of the NADH signal is calculated using a window length of 5 data points to compensate for the noise introduced by the imaging equipment.

- This pre-processed data is then imported into Wolfram Mathematica for further analysis. The first analysis performed was a Fast Fourier Transform (FFT) to determine the dominant frequency of oscillation. The Fourier transform is a mathematical operation that is used to transform a function that is presented in its time domain into one that consists of a sequence of sinusoidal signals each with a unique frequency. In this way, the dominant constituent frequencies of a signal can be determined by converting from the time domain to the frequency domain as shown in Figure 3.1 [69]. The fast Fourier transform (FFT) used in Mathematica is an algorithm that determines the discrete Fourier transform (DFT) of a discrete time signal and is often used in such signal processing [70].

- To determine whether or not the population of cells exhibit any synchronous behaviour the instantaneous phase between the oscillating cells is investigated. To this end an analytical signal, $\zeta(t)$ is calculated [71], which comprises the original signal, $s(t)$, and its Hilbert transform, $s_H(t)$, as shown in equation 3.1. In this equation the instantaneous phase, $\phi(t)$, and amplitude, $A(t)$, can be determined from the equation provided by [72]. Using the calculated instantaneous phase of oscillation of the individual cells, ϕ_n, the Kuramoto order parameter, $r(t)$ can be determined using equation 3.2 where N is the number of cells investigated. The

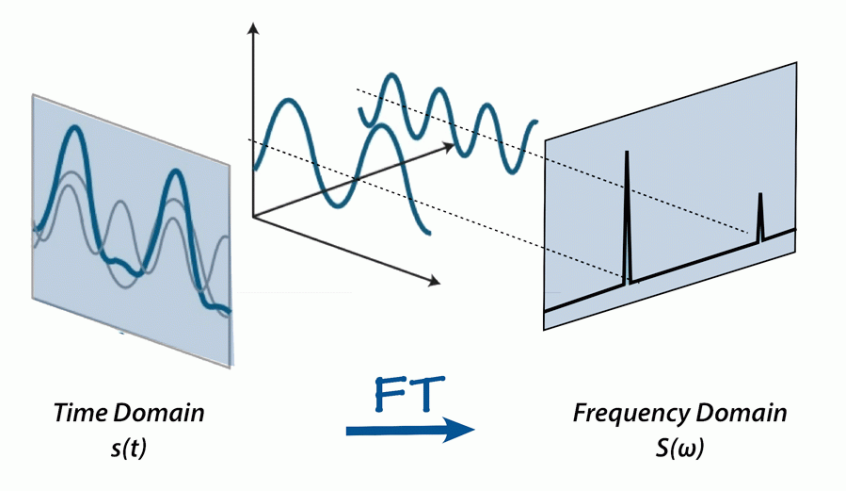

Figure 3.1: Description of FFT illustrating how the original signal - $s(t)$ which is expressed on the time domain can be divided into constituent signals which is describe using a frequency domain - $S(\omega)$ (source: AAVOS Int.[69])

order parameter describes the phase coherence between the individual cell where values between zero and one are calculated (with 1 indicating synchronization) [73].

$$\zeta(t) = s(t) + is_H(t) = A(t)e^{i\phi(t)} \tag{3.1}$$

$$r(t) = \frac{1}{N}\left|\sum_{n=1}^{N} e^{i\phi_n(t)}\right| \tag{3.2}$$

The essence of this method is that it adds the phases as vectors in the complex plane and normalises to the number of cells. If the phases are coherent (synchronized) the result will be 1. If they are not synchronized, this value will be less than one, and in the case of noisy experimental data this value then fluctuates between 0 and 1.

3.3 Results and discussion

3.3.1 Growth curves

The growth curve for the X2180 strain, as seen in Figure 3.2 was recorded to determine exactly when the cultures would reach the diauxic shift when inoculated with the overnight started culture at 1% (v/v) of the total media. The figure shows four different volumes (5 ml, 15 ml, 25 ml and 50 ml) of growth media inoculated with 0.05 ml, 0.15 ml, 0.25ml and 0.5 ml from different starter cultures and hence all start at different optical densities (ODs).

However, eventually once all the glucose is consumed and the growth begins to plateau, an OD of approximately 1.5 is reached in all the cultures. Note that all the cultures took approximately 12 to 14 hours to reach this diauxic shift, which corresponds with a typical growth curve for *S. cerevisiae* [74]. As a result of these findings, for the purpose of the oscillatory experiments, the cultures were grown for at least 12 hours, and subsequently tested to determine if the glucose had depleted, before harvesting the cells for the next step. The growth rate, μ, was calculated using equation 3.3 which is just the gradient of the exponential phase (linear section of the growth curve in Figure 3.2). The growth rate calculated was an average of 0.2883 h^{-1} with a standard deviation of 0.02822 for the X2180 yeast strain where the glucose concentration for the growth is 10 mg/ml = 55.5 mM and thus is indicative of the maximal growth rate, μ_{max}. Whereas in [75] the maximal growth rate reported for VIN13 is 0.5 h^{-1}.

$$\mu = \frac{\ln OD_2 - \ln OD_1}{(t_2 - t_1)} \tag{3.3}$$

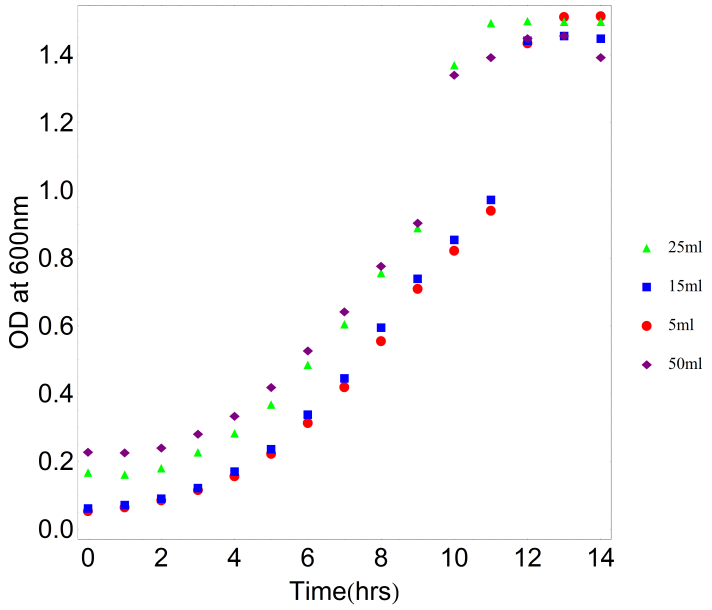

Figure 3.2: Growth curves for the X2180 strain of *Saccharomyces cerevisiae*. Various flask volumes from 5 ml to 50 ml were inoculated with 1% of an overnight starter culture with an OD above 1.0 and the OD reading was taken every hour until just after glucose depletion in the media.

3.3.2 Visualisation of cell oscillation

During the oscillation experiments performed in [7] a 20 mM glucose pulse was introduced at the first time point and some damped oscillations were detected. After approximately 4 minutes a second solution containing both 20 mM glucose and 5 mM cyanide (mixture solution) was added and resulted in the observation of sustained oscillations. Several optimisation steps were taken to be able to visualise the cells using the microscope setup. The well containing a single layer of cells was mounted on the stage above the objective. Note that the microscope has temperature control facilities and is encased in an incubator enclosure (refer to specification sheet for an image of the microscope Appendix A) making it difficult to add any fluids within this confined space. In the current study, in an attempt to mirror the [7] study, during the initial glucose pulse no oscillations were detected, but oscillations were detected after the addition of the glucose/cyanide mixture solution. This is shown in Figure 3.3 where no observable oscillations are present before approximately 6 minutes. A possible reason for not detecting the initial glucose induced oscillations is that the oscillations, if present at all, could have died down during the delay between the glucose pulse and capturing the image. This is not the case when the mixture solution is added where the oscillation are still present and not affected by the time delay introduced. Due to this limitation, it was decided to expose the cells with the mixture solution from the start.

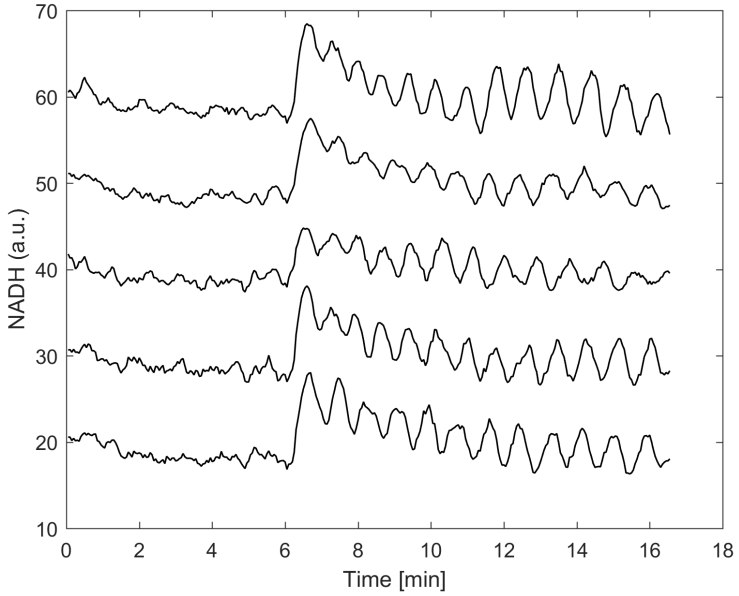

Figure 3.3: Shows the results of an initial experiments where the glucose pulse (t = 2 min) was first introduced, but no oscillation were detected, followed by a second pulse of glucose and cyanide (t = 6 min) causing sustained oscillations.

The wide-field microscope was used to visualise the time-lapsed intrinsic fluorescence of NADH. During one experiment a contrast image of the adhered cells to the well was taken prior to the start of the experiment to show the morphology and placement of the cells. This is shown in Figure 3.4 (a). In comparison, Figure 3.4 (b), shows a typical fluorescent image captured by the microscope during the experiment. The circular numbered shapes seen on the image are the regions of interest (ROI's) placed on each cell for the purpose of measuring the NADH intensities over the time period (using ImageJ).

Figure 3.5 (a) shows the raw data captured for the X2180 strain. Here the pixel intensities are plotted as a function of time for a collection of 10 cells that were selected to demonstrate the data processing procedure. From the raw data it is evident that the signal exhibits an oscillatory pattern. The data was processed as shown in Figure 3.5 (b) to (d) to reduce the noise and drift observed in the raw data as a result of the scatter and focal drift caused by the microscopes light source and imaging camera [67]. Figure 3.5 (c) and (d) show the difference between choosing a window length of 3 data points (9 seconds) or 5 data points (15 seconds) for the smoothing operation, respectively. As the window length is increased, the data becomes increasingly smoothed. A window length of 5 points was selected as it was the optimal number of data points used to get a clear representation of the oscillation.

In Figure 3.6 (a) and (b) the processed signals from 20 selected cells are presented for both the X2180 strain and VIN13 strain, respectively. The complete set of results for all the ROIs, for both X2180 and VIN13, can be found in Appendix A. As shown in Figure 3.6 (a), the X2180 signals exhibit an oscillatory behaviour within the individual cells using this experimental technique. This is similar to the findings of [46] where the cells were treated and visualised using a microscope in the exact same manner as the current study. However, the population of cells were visualised between microscope slides, which is a confined space in comparison to the method used in this study, and still found limit cycle oscillations within the individual cell in a population. Another observation is that the oscillations of the individual cells vary, with regard to frequency, onset and duration and therefore a heterogeneous behaviour is observed. The cyanide that was added, 5 mM, falls with the optimal range between 3 mM and 8 mM that is needed for the observation of oscillation in such batch experiments [4]. Conversely, as shown in Figure 3.6 (b), none of the VIN13 cells demonstrate any oscillatory behaviour.

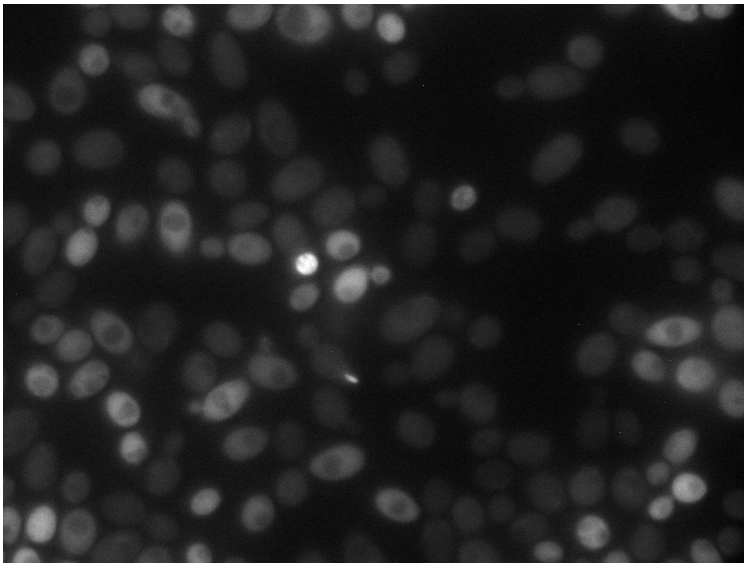

(a)

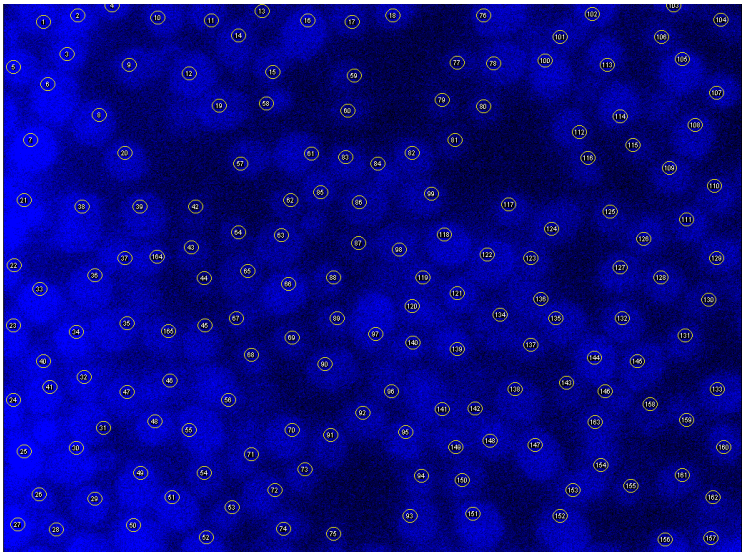

(b)

Figure 3.4: The image (a) shows the high resolution (wide-field transmission) image taken of the X2180 cells with the microscope prior to the start of the experiment. The image in (b) is the image captured during the experiment and using ImageJ all the cells are encapsulated with ROI's measuring the NADH fluctuation in each image.

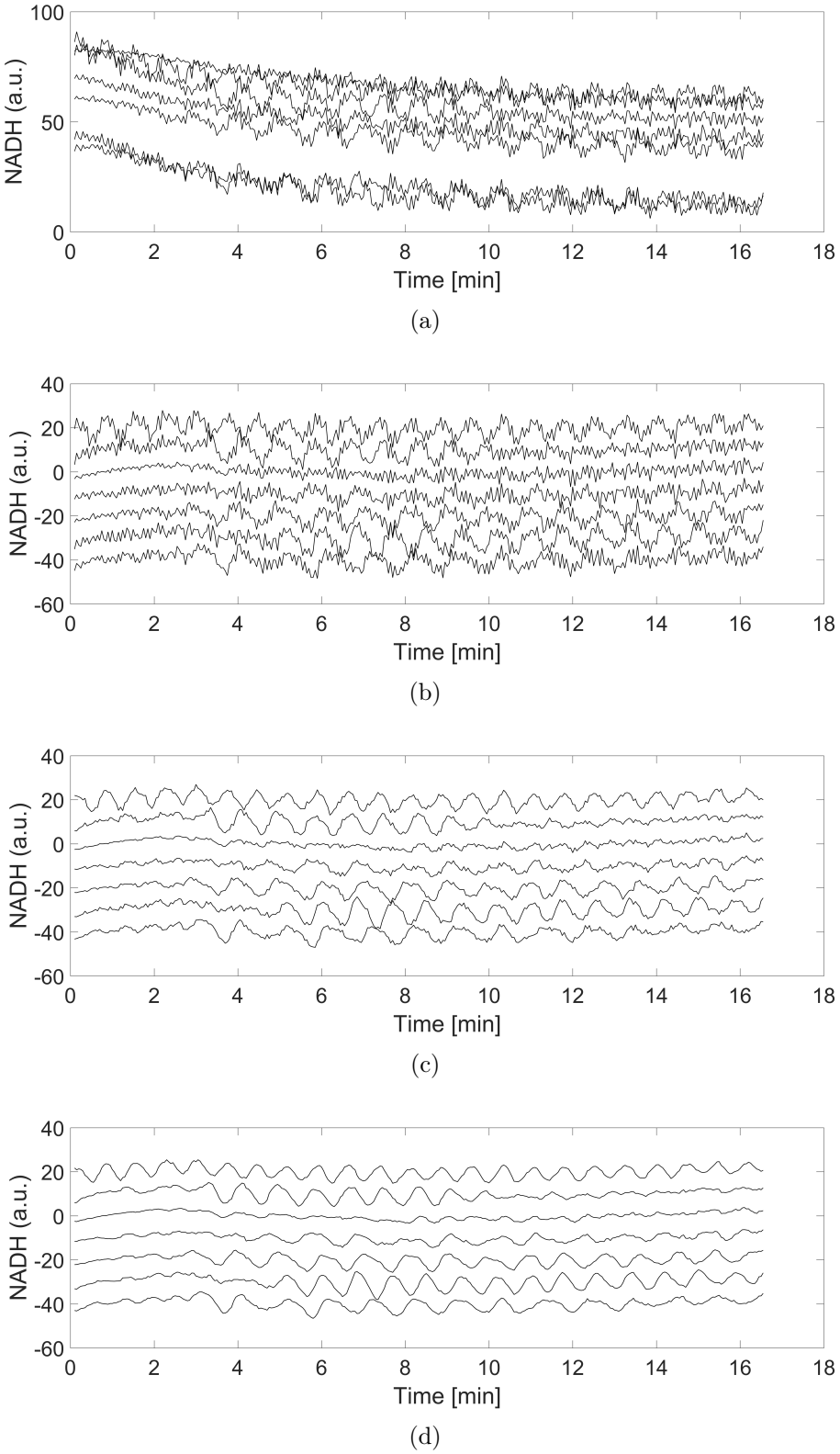

Figure 3.5: Image processing - These graphs show the process taken to optimize the X2180 signal: (a) raw signals, (b) detrended signals and smoothing the data with a window of 3 (c) versus 5 (d) data points.

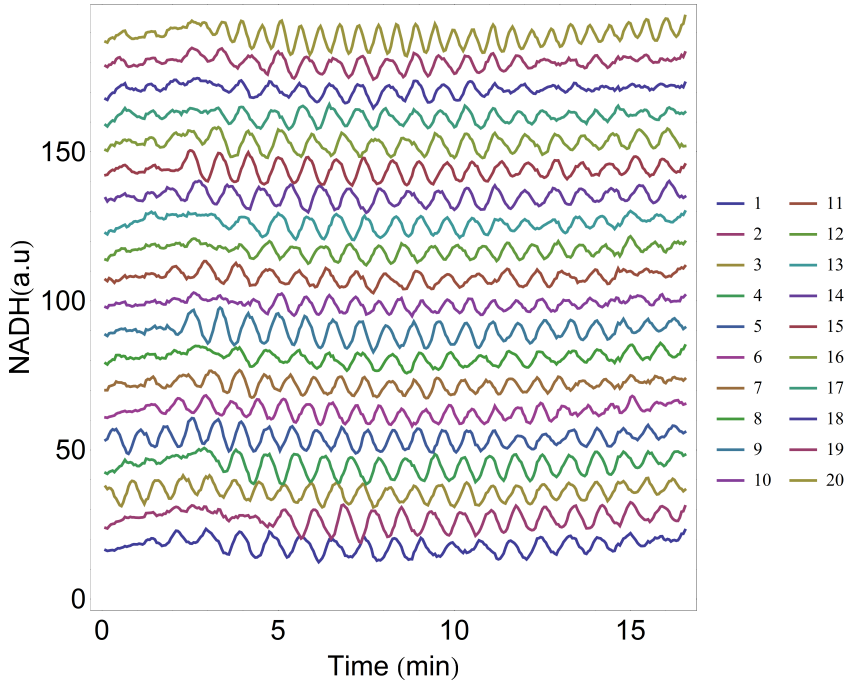

(a)

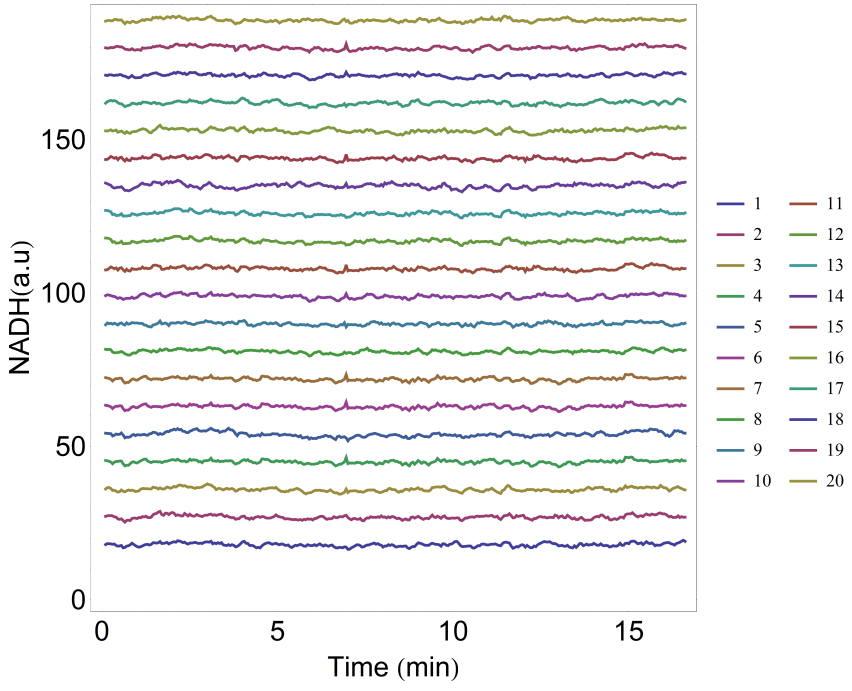

(b)

Figure 3.6: Oscillatory signal in X2180 (a) and VIN13 (b) The graph shows the NADH autofluorescence for 20 individual cells that are offset by 10 units for clarity.

3.3.3 Quantification of cell oscillation

As described in the Methods section, the dominant frequencies of oscillation were determined by means of conversion of the signals form the time domain to the frequency domain. The FFT in Figure 3.7 (a) shows a dominant signal observed at approximately 0.022 Hz (and a period (T) of 45 s) for an individual cell of the X2180 strain. In contrast, the VIN13 strain, which visibly showed no oscillatory behaviour in Figure 3.6 (b) also does not exhibit a similar dominant frequency in the FFT shown in Figure 3.7 (b).

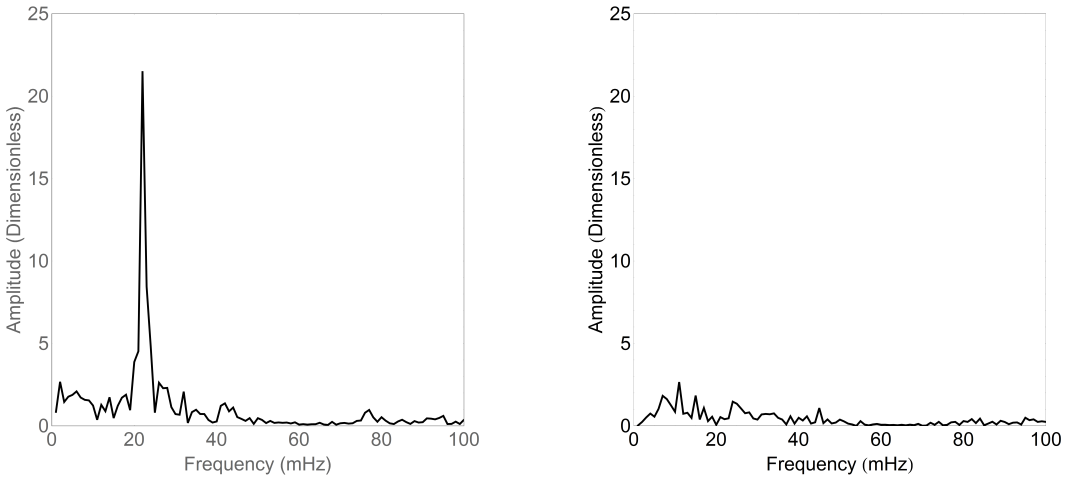

Figure 3.7: FFT for an X2180 oscillatory signal (a) and VIN13 (b) non-oscillatory signal.

A histogram (Figure 3.8) shows the periods of oscillation, quantified through FFT, for each individual cell in the X2180 dataset. From the 160 cells that were imaged, the FFTs showed that approximately 120 cells exhibited oscillations around a period of 40 - 60 s. In [17] it is shown that the period of oscillation is dependent on the glucose concentration and that for the specific conditions used in [7] (which is similar to that used in this thesis i.e. 20 mM), the oscillations have a period of approximately 50 s for the individual cells. According to [47, 76] with very similar conditions ($\approx$ 60 mM glucose and $\approx$ 6 mM cyanide) a period of 36 s in a dense yeast cell population corresponds to the natural frequency observed in NADH oscillations. The mean and standard deviation of the distribution of period of oscillation are 48 s and 15 s, respectively. This means that 66.7% of the cells have a period of oscillation between 33 s and 63 s, which correlates well with the aforementioned literature.

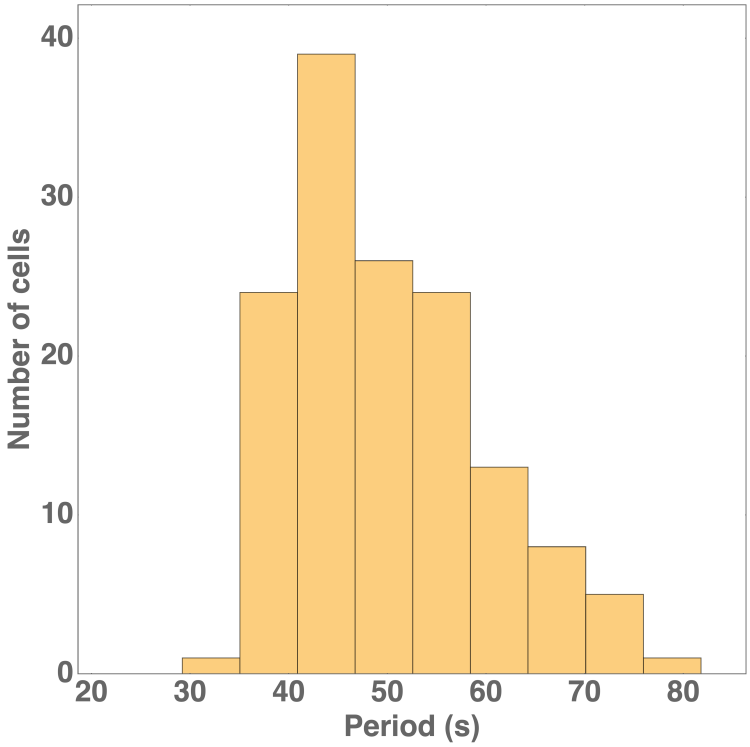

Figure 3.8: Histogram showing the periods of all the signals in the X2180 data set calculated using the FFT.

3.3.4 Testing for synchronization

This section describes an additional investigation done to verify if an analysis methodology used in [24] is applicable to collected oscillatory data using the experimental setup described in this thesis. Therefore it is not a requirement for the final objective of the study but rather the potential for future work. As previously stated, in the results for the oscillatory signal in Figure 3.6 (a), heterogeneity between the individual cells in the population was observed. It was therefore decided to investigate if the oscillations between neighbouring cells in the chamber exhibit synchronous behaviour. In [24] the mechanisms involved in the entrainment of isolated cells to synchronise or desynchronise their oscillations was investigated. In this study [24] they visualise this entrainment by calculating the correlation in instantaneous phases of oscillation between the cells by determining the Hilbert transform of the signals. This analysis method is described in Section 3.2.2. Thus in short the instantaneous phases of oscillation were quantified using Hilbert transforms and an order parameter, $r(t)$, see equation 3.1 [24]. Figure 3.9 (a) and (b) show examples for the NADH signal of neighbouring cells when the oscillations appear to be in synchrony. This is corroborated by the order parameter shown in (c) and

(d) where the order parameter tend to one indicating synchronization of cells. The synchronization seems to be very localised and temporary, usually only between a few cells close to one another. The Appendix A contain more examples of these pockets of synchronization observed in this heterogeneous cell populations.

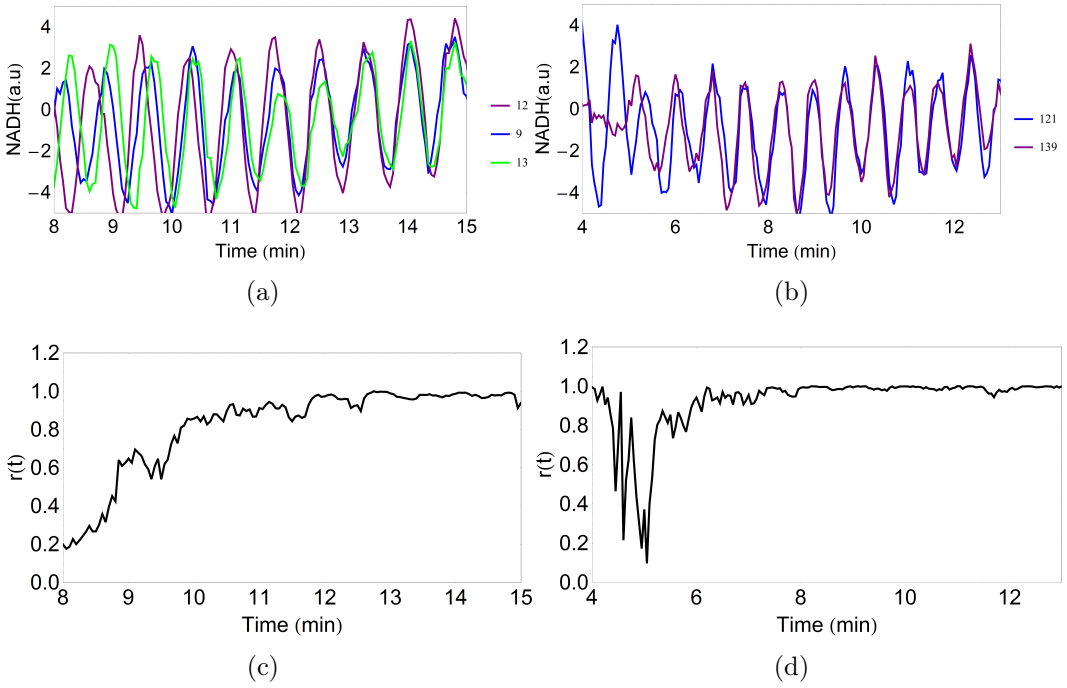

Figure 3.9: Here the NADH signal of the neighbouring cells, as shown in (a) and (b), is used to calculated the instantaneous phase ϕ_n of oscillation using the Hilbert transform. The graph in (c) and (d) show the order parameter, $r(t)$, calculated from the determined ϕ_n. The values close to zero indicates the signal is out of phase with one another and, values close to one denote the cells are synchronised. ROI values are indicated in the figure legends, see also Figure 3.4 (b)

3.4 Conclusion

This chapter addressed the first objective of the study: visually compare oscillatory strain X2180 to VIN13 strain using the published protocol but optimized for the setup available at Central Analytical Facilities (CAF) at Stellenbosch University as well as test for synchronization in the sample of oscillating cells for possible future studies.

To this end, the previously published culturing and visualisation protocols were optimised for our environment. Using wide-field microscopy, flurescent signals of intra-cellular NADH were collected from intact cells of the X2180

and VIN13 strains. After a series of signal processing techniques, oscillations were evident in the X2180 yeast strain (on single cell level), however no oscillations were detected in the VIN13 yeast strain. Although this result does not necessarily mean that VIN13 is unable to oscillate, it does indicate that no oscillations occur when it is treated in the same manner as X2180. This difference could be attributed to inter-strain differences. As such, Chapter 4 documents the investigation of the characteristics of the PFK enzymes of the two strains.

For the oscillating signal further analysis was performed to determine the period of oscillation which was between 40 s - 60 s and corresponds to what is found in literature [7]. Additionally, an analysis method quantifying synchronization was investigated and showed that pockets of synchrony were present between neighbouring cells. Further optimisation will be required to maximise the size of these pockets for further analysis of synchronization. This system does, however, have the advantage that the synchronizing metabolite, acetaldehyde, is not washed away as it is in the microfluidic flow chamber of [7] where no synchronization has been observed.

Chapter 4

Characterisation of Phosphofructokinase

4.1 Introduction

The method for inducing glycolytic oscillations has been detailed in Section 2.3, and consist of: harvesting of the cells at the diauxic shift, starvation for three hours and the introduction of a glucose pulse followed by cyanide. It has been suggested [10, 13, 17] that the regulation of PFK by its allosteric effectors ATP and AMP, is a requirement for oscillations to occur, although it might not be sufficient [17]. Many features of glycolytic oscillations have been studied experimentally: such as the required conditions promoting the observation of oscillations and the study of the synchronous behaviour that usually accompanies the oscillating phenomenon [7, 33, 34]. Others include, investigating the factors such as enzymatic control and energy balance which influences the emergence of oscillation [8, 9, 35–37] and the use of core or mechanistic detailed models of yeast glycolysis [7, 10, 16, 21].

In [10] a detailed mechanistic model of yeast glycolytic oscillations was obtained by performing a series of parameter optimisation steps on a validated model of steady state yeast glycolysis, constructed from enzyme kinetic parameters determined *in vitro* [22]. In [11] this model was validated using a collection of previously published data on oscillations in cell suspensions and cell extracts. During the optimisation in [10] it was seen that the kinetic parameters of PFK, specifically those affecting inhibition by ATP, became increasingly important for oscillations with significant amplitude to occur. Subsequent to the results in Chaper 3 where it was confirmed that the X2180 *S. cerevisiae* strain does oscillate whereas no oscillations were detected in the VIN13 strain, the question was posed whether this difference could be attributed to different PFK kinetics in the two strains. In this chapter the aim of the described work was to characterise and fit the kinetic behaviour of PFK with respect to ATP and AMP for the two strains (X2180 and VIN13) using the rate equation de-

scribing PFK kinetics in the Teusink model [22]. The rate equation used in the Teusink model [22] is based on the MWC model describing a multimeric enzyme regulated by various effectors. The fitted PFK kinetic parameters are then substituted into the non-oscillatory model of the Du Preez model [10, 11], known as the dupreez1 model, and the first optimisation is repeated to test whether an oscillating model can be obtained without changing the parameters of PFK.

4.2 Methods

4.2.1 Experimental

Lysate preparation The cells are grown and harvested following the same protocol described in Chapter 3. However, in order to perform enzyme assays the cell lysate needs to be extracted by breaking open the cell wall using the glass bead extraction method, which is usually used for small volume extractions. The protocol used is an established method used in our laboratory, the procedure is as follows:

1. Glass beads, approximately 0.5 mm in diameter, are cleaned before used for extraction, by soaking overnight in a 1 M HCL solution, after which they are washed and dried in an oven at 150°C.

2. At the very least an equal volume of glass beads is added to the pellet of cells spun down from the starved culture, in order to make sure enough cell material gets exposure to the glass beads. To that an equal volume of extraction buffer is added, to create an environment suitable for the extracted proteins, containing 20 mM KH_2PO_4 with 1 mM PMSF (a protease inhibitor: prevent the breakdown of the extracted proteins) at pH 7.0.

3. The 1:1 mixture of cells, beads and buffer is then vortexed for 30 s, allowing the glass beads to disrupt the cell wall and followed by a 30 s incubation on ice, this is to prevent overheating of the cell suspension.

4. Step 3 is repeated eight times. Once the cycle is complete the mixture is spun down by centrifugation at 13 000 RCF for 10 minutes at 4°C. The supernatant contains the enzymes and cytosolic proteins, referred to as the lysate, while the solid precipitate made up of the glass beads and broken cell wall is discarded. The lysate is stored on ice until required in the subsequent experiment, or stored for short periods (up to 2 hours) in a refrigerator.

Enzyme assay The activity of the glycolytic enzymes were determined using the generalised protocol followed in [22]. In this protocol the enzymes activity was visualised using a spectrophotometer that measured the amount of NADH consumed or formed at an optical density of 340 nm. The PFK characterisation in this study was based on the optimized enzyme assay methodology, inclusion of an Adenylate Kinase inhibitor, used by [77]. These experiments were conducted by linking the enzyme via Aldolase (ALD) and Glycerol 3-phosphate dehydrogenase (G3PDH), which utilises NADH, refer to Figure 4.1. An alternative method to assay PFK activity is by coupling the ADP production of the enzyme to Pyruvate kinase (PK) and Lactate dehydrogenase (LDH). However it was decided to link the enzyme to ALD and G3PDH instead since it allowed for the investigation of ATP with no limitations on the concentration. In contrast, if PFK was coupled to PK and LDH, the concentrations would need to be constrained, because ATP has an inhibitory effect at high concentrations on PK.

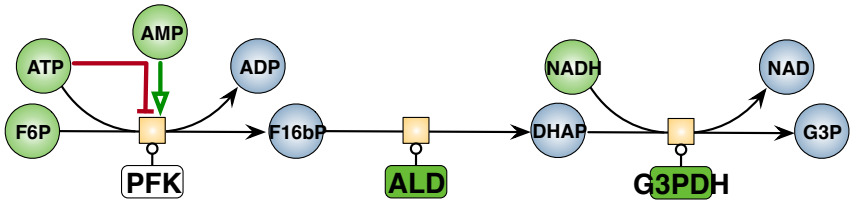

Figure 4.1: The metabolites assayed during the PFK enzyme characterisation. During the enzyme assay experiment the metabolites, co-factors and enzyme presented in green are those added to the lysate. The lysate contains the enzyme being characterised, PFK, and the intermediary metabolites for this enzyme assay. Again the description of the abbreviated enzymes, metabolites and co-factors in the schema are in the nomenclature section of this thesis.

The assays were performed on a *BMG LABTECH SPECTRstar*^{Nano} using 96- well microtitre plate (F-bottom) at 30°C with a total assay volume of 100 μl. The assay volume comprised of 4 μl lysate, obtained through extraction method described in Section 4.2.1, and the following PFK reagents:

- 1 μl ALD (From Sigma-Aldrich: 1 KU Aldolase from rabbit muscle - Product Number: A8811)
- 0.5 μl G3PDH (From Sigma-Aldrich: 1 KU Glyceraldehyde 3-phosphate from rabbit muscle - Product Number: G6751)
- 0.8 mM NADH (From Sigma-Aldrich: β-Nicotinamide adenine dinucleotide, reduced dipotassium salt - Product Number: N4505)
- 0 - 10 mM F6P (From Sigma-Aldrich: D-Fructose 6-phosphate disodium salt hydrate - Product Number: F3627)

- 0 - 10 mM ATP(From Sigma-Aldrich: Adenosine 5'-triphosphate disodium salt hydrate - Product Number: A1852)
- 0.25 mM or 1 mM AMP (From Sigma-Aldrich: Adenosine 5'-monophosphate sodium salt - Product Number: A1752)
- Adenylate Kinase inhibitor at 100 μM (From Sigma-Aldrich: P^1, P^5-Di(adenosine-5') pentaphosphate pentasodium salt - Product Number: D4022)

Depending on the purpose of the experiment F6P or ATP is varied between 0-10 mM. The effect of AMP is investigated at 0.25 mM and 1 mM with an Adenylate Kinase inhibitor at 100 μM (relevance discussed below in Section 4.3). An assay buffer is made up of 500 mM Pipes, 1 M KCl and 100 mM $MgSO_4$ at pH 6.8 and 10 μl is added to the assay, while the remainder of the volume is made up of deionised water to ensure that a total assay volume of 100 ul is attained. Table 4.1 lists the experiments conducted in this study to characterise PFK by investigating the effect that the substrates F6P and ATP and allosteric effector AMP had PFK.

Table 4.1: Description of enzyme assay experiments(in-well concentrations)

Experiment	ATP [mM]	F6P [mM]	AMP [mM]
A	1	0 - 10	0, 0.25 and 1
B	0 - 10	1	0, 0.25 and 1
C	0 - 10	0.75	0, 0.25 and 1
D	0 - 10	0.5	0, 0.25 and 1
E	0 - 10	0.25	0, 0.25 and 1

The spectrophotometer recorded the absorbance of NADH at 340 nm wavelength, taking a reading of the decreasing absorbance every 3 s. The experiments A to E were performed on lysate extracted from one culture where each experiment was conducted in triplicate. The biological repeat for the experiments A to E was also performed in triplicate using lysate extracted from another culture and for every experimental set a control rate defined at 1 mM ATP, 5 mM F6P and 0 mM AMP concentrations was determined which was used to normalise the data to correct for any inter-lysate variation in enzyme expression.

It is expected that at high ATP concentration the PFK activity is inhibited as seen in [10]. This is modulated by allosteric effectors (activators), such as AMP and F26BP, which can attenuate the inhibitory effect [25]. For the F6P saturation curve a 1 mM ATP concentration was selected as an optimal concentration based on [10]. The researchers showed in their oscillatory model that at lower F6P concentration the inhibitory effect of increasing ATP concentration is more prominent. However, for an ATP concentration of 1 mM

at low F6P concentration (0 - 2 mM) it still functioned like an activator promoting PFK activity. In [10, 11] ATP inhibition of PFK was also highlighted by showing that the negative allosteric regulation plays a vital role in causing instability in the system, thereby promoting glycolytic oscillations. This is why it was decided to investigate this effect on PFK by scanning ATP (0 - 10 mM) at low F6P concentrations for both the strains, X2180 (where oscillations were visualized) and VIN13 (no oscillation were detected).

Bradford: Protein determination Using the Bradford method a linear relationship between the concentration of a standardized protein and the measured absorbance readings, taken at 595 nm, can be determined. The protein standards are generated using Bovine Serum Albumin (BSA - Product Number: A2153) for a concentrate range of 0 - 0.5 mg/ml. These concentrations were selected as they are the concentrations where the standard curve is most linear. The lysate is investigated by creating a dilution series consisting of the following: undiluted, 10×, 20×, 50× and 100×. For this investigation only the concentrations that fall in the linear range is calculated and converted to the total protein isolated from the culture. This is achieved by dividing the absorbance reading of the diluted lysate with the gradient of the standard curve and multiplying the dilution factor of the lysate to provide the protein concentration, c_{prot}, of the lysate in mg/ml (≈15 mg/ml for X2180 and VIN13 as determined from the Bradford experiments). A volume of 20 μl of the protein standards and the lysate dilution are pipetted into the 96- well microtitre plate to which a volume of 180 μl of Bradford reagent is added. The Bradford reagent is made up of Brilliant Blue G (0.1 mg/ml) diluted in 95% methanol (0.05 v/v) and 85% phosphoric acid (0.1 v/v), this dark blue solution is then filtered until a reddish/brown colour is attained. The protocol followed in this section is based on work done by [77].

4.2.2 Analysis

Processing of experimental activity data Enzyme activity is often written in terms of U, which describes the enzymes ability to convert substrate and has the units μmol/min. The data obtained from the spectrophotometer during the enzyme assays can be plotted to show how the NADH absorbance changes over time (Δ A/min at 340 nm) where the slope defines the rate of conversion for that substrate concentration. Additionally, the data from the Bradford experiment is used to calculate the protein concentration of the lysate used in the assay.

As such, the activity for PFK is calculated using the following equation:

$$U/\text{mg protein} = (\Delta\text{A/min}) \times \frac{V_{tot}}{\epsilon.l.C_{prot}.V_{lys}} \tag{4.1}$$

where V_{tot} is the total volume of the assay, ϵ is the extinction coefficient of NADH (6.22 mM^{-1} cm^{-1} at 340 nm), l is the path length the light travels through the sample (0.257 cm for the F-bottom 96- well microtititre plates for a 100 μl assay volume - calculated using a standard curve of NADH in assay buffer), C_{prot} is the protein concentration from the Bradford and V_{lys} is the volume of lysate used in the assay (0.004 ml). Equation 4.1 is obtained by writing the spectrophotometer data, $\Delta A/\text{min}$ in terms of the Beer-Lambert law, $A = \epsilon cl$, to obtain:

$$\frac{\Delta\text{A/min}}{\epsilon l} = \frac{n/\text{min}}{V_{Tot}} = \frac{\mu\text{mol/min}}{V_{Tot}} \tag{4.2}$$

The protein concentration, $C_{prot} = \text{mg protein}/V_{lys}$ from the Bradford protein determination can then be incorporated to arrive at:

$$(\Delta\text{A/min}) \times \frac{V_{tot}}{\epsilon.l.C_{prot}.V_{lys}} = \mu\text{mol/min/mg protein} = U/\text{mg protein} \tag{4.3}$$

The final step in processing this data is to normalise the activity calculated for each concentration in an experiment to the activity calculated for the control rate experiment, this is done to be able to qualitatively compare the results between different experiments.

PFK model fitting The Monod, Wymann, Changeux (MWC) equation was used to described PFK kinetics in [22] and is discussed in Chapter 2.4. Equation 4.4 is the rate equation as it appears in the Du Preez model [10]. For the purpose of the discussion here it will be referred to as the PFK model:

$$\frac{a}{b\left(c + \frac{d}{e}\right)} \tag{4.4}$$

where:

$$a = \text{ATP.F6P.gR}(1 + \frac{\text{ATP}}{\text{KmPFKATP}} + \frac{\text{F6P}}{\text{KmPFKF6P}} + \frac{\text{ATP.F6P.gR}}{\text{KmPFKATP.KmPFKF6P}})\frac{V_{\max}}{V_c} \tag{4.5}$$

$$b = \text{KmPFKATP.KmPFKF6P} \tag{4.6}$$

$$c = (1 + \frac{\text{ATP}}{\text{KmPFKATP}} + \frac{\text{F6P}}{\text{KmPFKF6P}} + \frac{\text{ATP.F6P.gR}}{\text{KmPFKATP.KmPFKF6P}})^2 \tag{4.7}$$

$$d = (1 + \frac{\text{ATP.CiPFKATP}}{\text{KiPFKATP}})^2(1 + \frac{\text{ATP.CPFKATP}}{\text{KmPFKATP}})^2(1 + \frac{\text{AMP.CPFKAMP}}{\text{KPFKAMP}})^2 (1 + \frac{\text{CPFKF16BP.F16P}}{\text{KPFF16BP}} + \frac{\text{CPFKF26BP.F26P}}{\text{KPFF26BP}})^2 L0 \tag{4.8}$$

$$e = (1 + \frac{\text{ATP}}{\text{KiPFKATP}})^2(1 + \frac{\text{AMP}}{\text{KPFKAMP}})^2(1 + \frac{\text{F16P}}{\text{KPFF16BP}} + \frac{\text{F26BP}}{\text{KPFF26BP}})^2 \tag{4.9}$$

Here the parameters CiPFKATP, CPFKATP, CPFKAMP, KiPFKATP, KmPFKATP, KmPFKF6P, KPFKAMP and $\frac{V_{\max}}{V_c}$ were determined by fitting the rate equation to the experimental data. These parameters are the maximal rate of the PFK enzyme Vmax, the binding coefficients for the substrates ATP and F6P (KmPFKATP and KmPFKF6P) and constants related to the efffect of the allosteric AMP activation (KPFKAMP and CPFKAMP), ATP substrate activation (KPFKATP and CPFKATP) and allosteric ATP inhibition (KiPFKATP and CiFKATP). No data was collected on the effect of F26bP or the minor effect of F16bP, and parameters related to these species remained the same as in the DuPreez model [10, 11]. Also gR and L0 parameters, characterising the R and T state of PFK where L0 describes the ratio between the states without allosteric effectors and gR is the afficity of the effectors for R state, were not refitted. The fitting was done using the standard *NonlinearModelFit* function in Wolfram Mathematica with the only constraint that the parameters be positive. Once the calculated parameters are included in the PFK model it can be used to simulate and predict the behaviour of PFK under the experimental conditions.

Model analysis The PFK kinetics determined in Section 4.2.2 is incorporated into the non-oscillatory dupreez1 model [10, 11]. The model is then optimized to test for oscillations for both X2180 and VIN13 strains. As explained in [10] and Section 2.5, the stability of the system is investigated by means of a Jacobian Matrix calculation with equation 2.8. The eigenvalues of this matrix is an indication of the oscillatory tendency of the model with all negative eigenvalues indicating a stable steady state and a pair of complex conjugate eigenvalues with positive real parts a stable limit cycle oscillations. In an recursive procedure the control of every (allowed) parameter on the ratio of imaginary to real parts of the complex eigenvalue is determined using equation 2.10 where a positive value implies that an increase in the parameter value (and a negative value that a decrease in the parameter) would increase the oscillatory tendency.

The parameters with positive control are then increased by a certain percentage and those with negative control decreased by the same percentage. The process is repeated, having the effect of decreasing the magnitude of the negative real part of the eigenvalues, until the real part of the eigenvalue passes trough zero, i.e. the Hopf bifurcation point is reached, and the system shows sustained oscillations. As was done in [10], only the rate multipliers, i.e. Vmax values for enzyme catalysed reactions and rate constants for mass action reactions, were changed during the optimisation procedure. In contrast to the

previous study, Vmax of the PFK reactions was kept at its experimentally determined value and not optimised.

4.3 Results and discussion

4.3.1 Enzyme assay

Initial results for ATP saturation-inhibition curves at 2 mM F6P with the activation of AMP for (a) X2180 and (b) VIN13 are shown in Figure 4.2 presented the opposite result to what was expected. At 0 mM AMP (blue symbols) there was the typical ATP inhibitory curve for the higher ATP concentration in the X2180 strain, but for the VIN13 strain no inhibition was visualised at higher ATP concentrations. In both graphs the AMP (yellow = 0.25 mM; green = 0.5 mM and orange = 1 mM) does not act as an allosteric activator but seems to rather inhibit the reaction which was the opposite of what is stated in literature [10]. A possible reason for the result shown in Figure 4.2 was that the AMP introduced in the pathway stimulates the Adenylate kinase catalysed reaction (equation 4.10) which functions close to equilibrium. As a result, introducing AMP to the system promotes the AK to rapidly create ADP from the ATP and AMP thereby effectively reducing the amount of ATP available for the PFK reaction as well as the AMP. Subsequently, an Adenylate Kinase inhibitor P^1, P^5-Di(adenosine-5') pentaphosphate pentasodium salt (A5pp) was used to "block" AK activity. The effect of the inhibitor on the AK was investigated and showed that a concentration of 100 μM was sufficient to suppress the activity of AK.

$$\mathrm{ATP} + \mathrm{AMP} \rightleftharpoons 2\,\mathrm{ADP} \tag{4.10}$$

In Figure 4.3 the effect of ATP on PFK at a F6P concentration of 1 mM (Experiment B) for X2180 is shown. The red dots are at 0 mM AMP, the blue squares at 0.25 mM AMP and the green triangles at 1 mM AMP for the X2180 strain. The AK inhibitor (A5pp) was included with the experiments involving AMP and the results showed the expected ATP inhibitory effect and activation by AMP. Additionally, Figure 4.4 shows the result when comparing the biological repeats. The A and B experiments from Table 4.1, which are the (a) F6P saturation curve and (b - d) ATP scans at 1 mM F6P with varying AMP, were selected to represent the qualitative similarity in the datasets. Since the experimental results between the two lysates, represented as blue and red, were comparable, the data was pooled when performing the PFK model analysis.

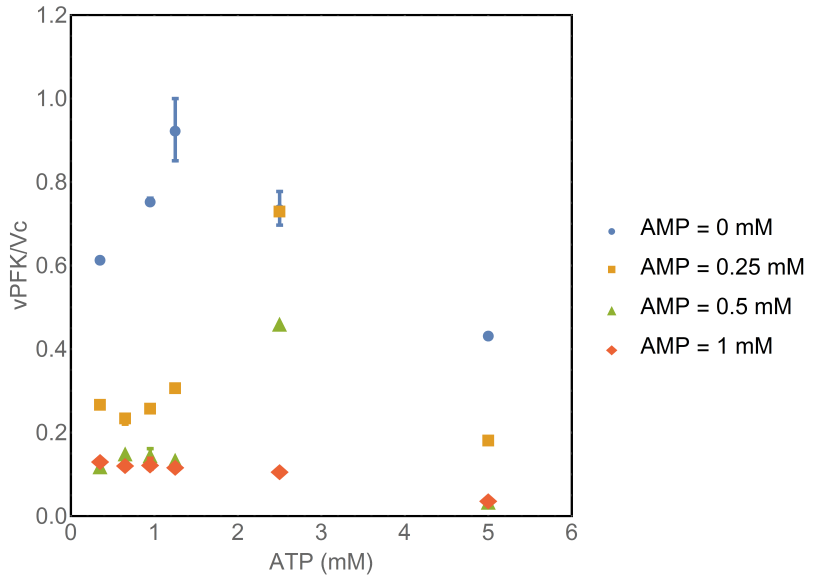

(a)

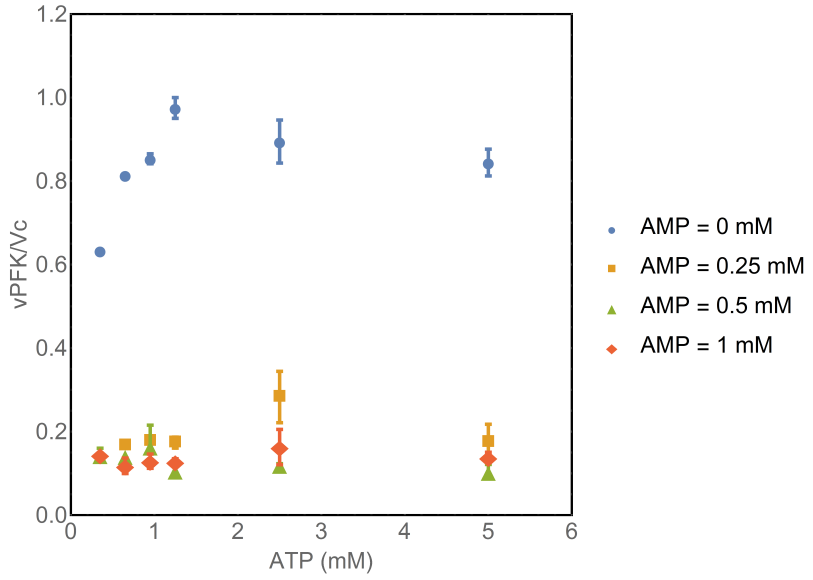

(b)

Figure 4.2: Initial experimental results, showing AMP "inhibition" rather than activation when scanning ATP (0 - 5 mM) and varying the AMP concentration from 0 mM to 1 mM at 2 mM F6P in (a) X2180 and (b) VIN13 eluding to AK reaction utilizing the added AMP (and ATP) resulting in the inhibitory effect observed. The mean of the experimental data is presented symbolically with error bars indicating the standard deviation of the triplicate data (normalised to the control rates).

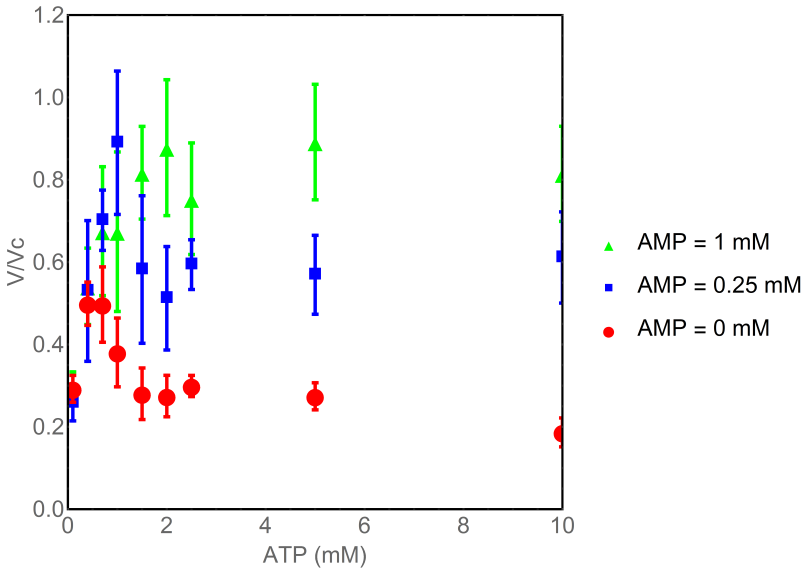

(a)

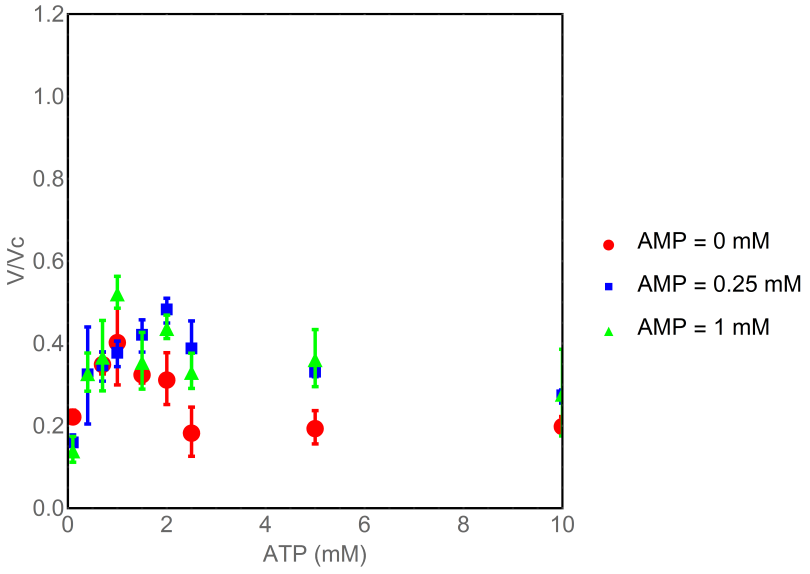

(b)

Figure 4.3: Experiment B: Investigating the effect of ATP on PFK at a F6P concentrations of 1 mM for the (a) X2180 and (b) VIN 13 strain at varying AMP concentrations (red/circular symbol = 0 mM AMP, blue/square symbol = 0.25 mM AMP and, green/triangular symbol = 1 mM AMP). The AMP activation of PFK is visualised in the presence of AK inhibitor (A5pp). The mean of the experimental data is presented symbolically with error bars indicating the standard deviation of the triplicate data (normalised to the control rates).

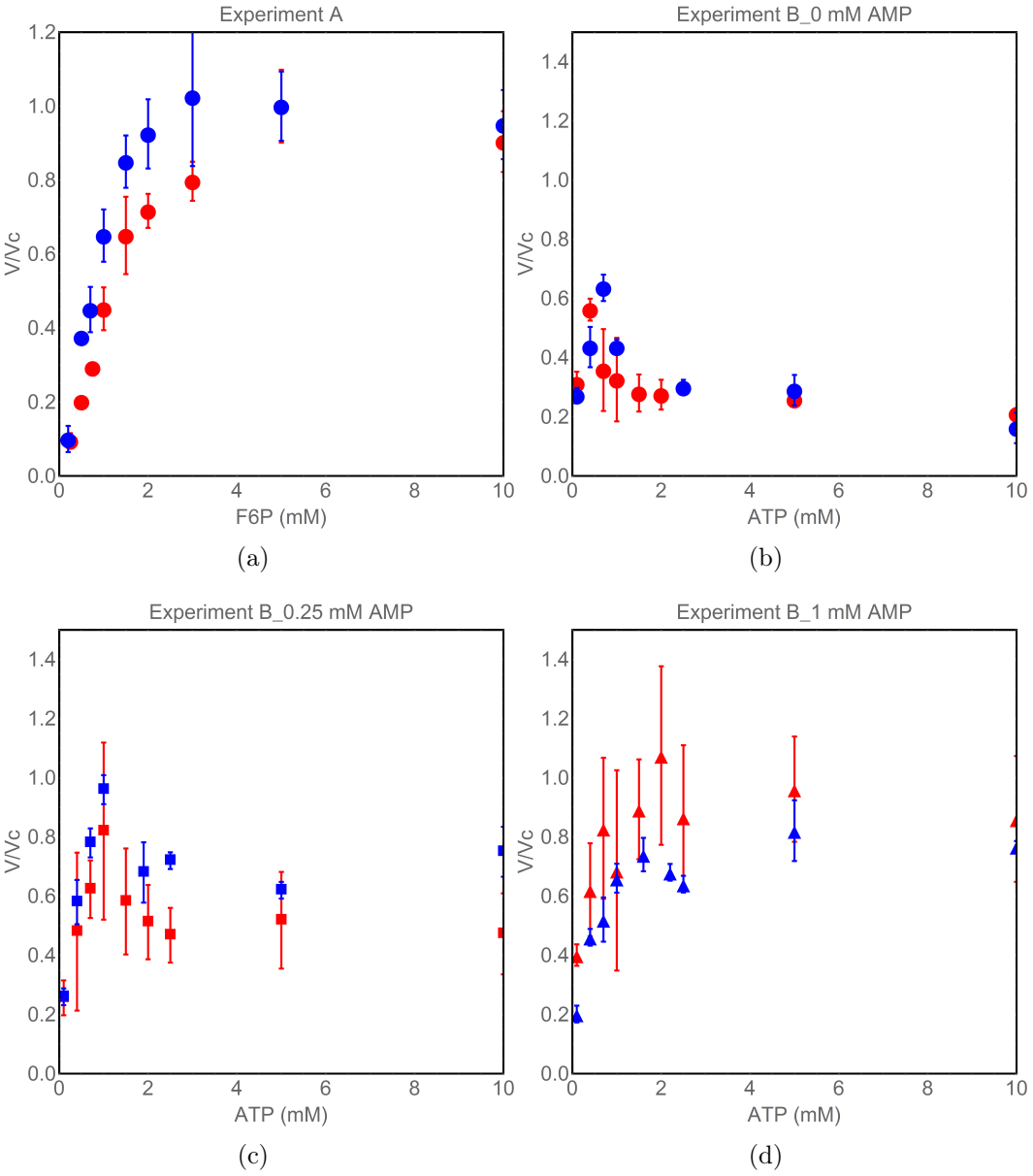

Figure 4.4: The biological duplicates for X2180 strain where blue and red symbols represent the different lysates from the two cultures in (a) experiment A, showing the F6P saturation plots at 1 mM ATP; (b) experiment B, scanning ATP at 1 mM F6P with 0 mM AMP (circular symbol); (c) experiment B, scanning ATP at 1 mM F6P with 0.25 mM AMP (square symbol) and (d) experiment B, scanning ATP at 1 mM F6P with 1 mM AMP (triangular symbol). For all the experiments, the normalised lysate activities appear to be comparable. The mean of the experimental data is presented symbolically with error bars indicating the standard deviation of the triplicate data (normalised to the control rates).

4.3.2 Rate equation fits

As described in Section 4.2.2, the rate equation fits were performed using the rate equation from the Teusink model [22] which was also used in the Du Preez model [10, 11] describing PFK. Initially we attempted to estimate all 15 parameters from the experimental data using the PFK model. However, with the limited experimental dataset the PFK model was unable to determine those parameter values unambiguously. Since the data available was for the investigation of the ATP,AMP and F6P dependence of PFK, only the parameters pertaining to those metabolites were fitted while the rest were used as reported for the non-oscillatory model in [10, 11]. The parameters that were fitted are shown in Table 4.2 and 4.3 for X2180 and VIN13, respectively. Good fits were obtained for the X2180 parameters with relatively smaller standard error values than the predicted parameters. However in the fits for VIN13 some of the determined parameters have larger standard error. A fit with one less parameter resulted in better standard errors but did not change the appearance of the fits noticeably.

Table 4.2: Parameter fit results for the X2180 strain

	Estimate	Standard error
CiPFKATP	3.76	0.741
CPFKATP	87.5	30.5
CPFKAMP	0.297	0.0350
KiPFKATP	3.73 mM	1.78
KmPFKATP	0.732 mM	0.154
KmPFKF6P	1.05 mM	0.251
KPFKAMP	0.127 mM	0.0263
$\frac{V_{max}}{V_c}$	1.17	0.0431

Table 4.3: Parameter fit results for the VIN13 strain

	Estimate	Standard error
CiPFKATP	19.7	72.2
CPFKATP	4.40	16.6
CPFKAMP	0.290	0.105
KiPFKATP	2.93 mM	1.94
KmPFKATP	0.181 mM	0.0433
KmPFKF6P	4.58 mM	0.716
KPFKAMP	0.135 mM	0.0687
$\frac{V_{max}}{V_c}$	1.16	0.0634

In Table 4.4 the first column provides the values used in the Du Preez model (dupreez1) and in the subsequent columns the parameters are presented as a percentage comparison, $\frac{\text{Parameter}_i}{\text{Parameter}_{\text{Du Preez}}} \times 100$, to the model where 100% indicates that the parameter as exactly the same as the one described in the model. As shown in Table 4.4 the specific activity of PFK in X2180 is higher than that of VIN13. The rates were calculated as a function of the normalised control rate (the reference rate deteremined at 5 mM F6P and 1 mM ATP in all repeats), thus the fitted V_{max} is $\frac{V_{max}}{V_c}$. By dividing the control rate with the $\frac{V_{max}}{V_c}$ fitted to the rate equation at the same conditions as the control rate (ATP 1 mM and F6P 5 mM) it is possible to determine the true V_{max} for the two strains. The average control rate for X2180 was 0.5 U/mg protein with a standard deviation of 0.0427 and for VIN13 the average was 0.13 U/mg protein with a standard deviation of 0.0196. Thus the calculated true V_{max} values were $V_{max} = 0.639$ U/mg protein and $V_{max} = 0.166$ U/mg protein for X2180 and VIN13, respectively. There is a notable difference in parameters between the X2180 strain, which has values closer to the model, and the VIN13 strain. The percentage comparison for KmPFKF6P is extremely high and can be attributed to the limited dataset where only one ATP concentration (1 mM) was used to investigate an F6P scan.

Table 4.4: Parameter comparison to the non-oscillatory model.

		% comparison	
	dupreez1 [10, 11]	X2180	VIN13
VmPFK	0.68 U/mg protein	93.9	24.4
KmPFKATP	0.71 mM	114	25.6
CiPFKATP	100	99.1	28.7
KPFKAMP	0.0995 mM	122	136
CPFKAMP	0.0845	345	341
CPFKATP	3	2914	146
KiPFKATP	0.65 mM	279	434
KmPFKF6P	0.1 mM	1069	4594
F26BP	0.02 mM	100	100
gR	5.12	100	100
L0	0.66	100	100
KPFKF26BP	0.000682 mM	100	100
CPFKF26BP	0.0174	100	100
KPFKF16BP	0.111 mM	100	100
CPFKF16BP	0.397	100	100

Figures 4.5 - 4.9 show the comparison between the experimental data, characterising PFK and the PFK model prediction for all the experimental conditions listed in Table 4.1. The mean of the experimental data is presented symbolically with error bars indicating the standard deviation of the triplicate data (normalised to the control rates) for both biological repeats pooled. The model prediction of the PFK rate equation with the fitted parameters is presented by the solid curve.

In Figure 4.5 is the data for condition assayed in experiment A investigating how PFK's substrate F6P behaves at the selected ATP concentration of 1 mM in both strains. For both strains the model prediction to the data is good and we see a clear substrate saturation curve. The curve for X2180 seems to attain saturation faster than VIN13 this is corroborated with the KmPFKF6P, where KmPFKF6P for X2180 shown in Table 4.2 is smaller then the KmPFKF6P for VIN13 in Table 4.3 .

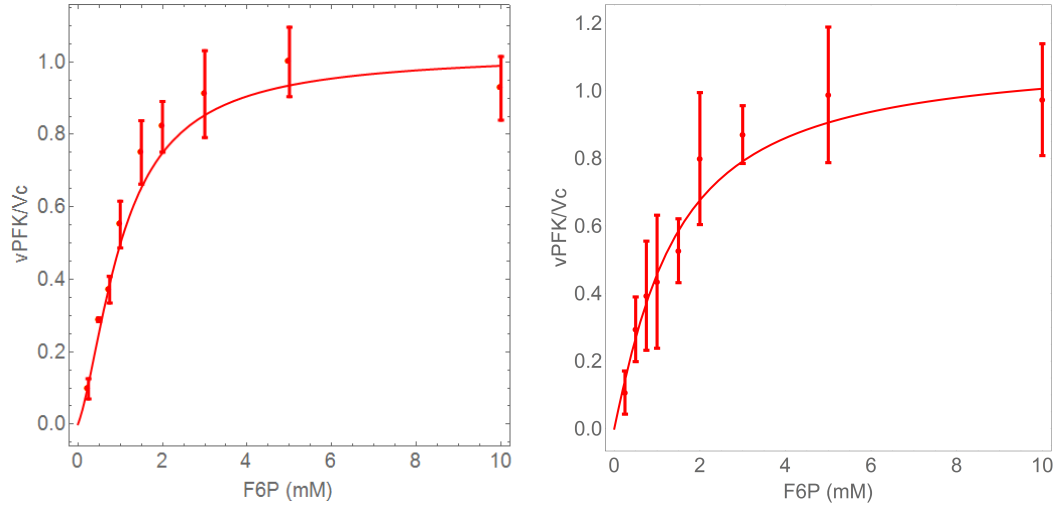

(a) (b)

Figure 4.5: A - PFK characterisation in terms of its substrate, F6P(0 mM - 10 mM) and ATP kept at 1 mM for (a) X2180 and (b) VIN13. The dots are the means of experimental data (with error bars indicating standard deviation) normalised to control rate conditions (1 mM ATP and 5 mM F6P) and the solid curve is the fitted rate equation. The model describes this behaviour well for the two strains. The mean of the experimental data is presented symbolically with error bars indicating the standard deviation of the triplicate data (normalised to the control rates)

Figures 4.6 to 4.9 all show the same type of experiment (Experiment B-E Table4.1) where the effect of a range of ATP concentrations (0 - 10 mM) and subsequent addition of AMP, where the red is with 0 mM AMP, the blue is with 0.25 mM AMP and the green is with 1 mM AMP, has on PFK enzyme

which is investigated at four F6P concentrations (0.25 - 1 mM). The experimental data for X2180 strains clearly depicts the ATP inhibition in the absence of allosteric activator (AMP) as described in literature. Also the allosteric activation of PFK in the presence of AMP can be seen by the alleviation of that inhibitory slope. Furthermore, the PFK model accurately describes the ATP inhibition and subsequent alleviation by the addition of AMP behaviour in both strains. The model shows how the increasing AMP concentration shifts the ATP inhibition curves upwards. However, this is not consistently reflected in the experimental data. The experiments do not show a dramatic difference between the low AMP of 0.25 mM and the high AMP value of 1 mM. Additionally, at lower F6P concentrations the ATP inhibition is more pronounced. The similarity between the two strains is that the experimental data seems to show ATP inhibition in X2180 and in VIN13. At higher concentrations of F6P however the ATP inhibition is not as clearly defined in VIN13 as it is for X2180. A difference between X2180 and VIN13 is that even though both strains show for higher AMP concentrations the alleviation of ATP inhibition, the effect i.e. shifting the graph upwards is not so obvious for the VIN13 data. All the individual data fits are shown in Appendix B.

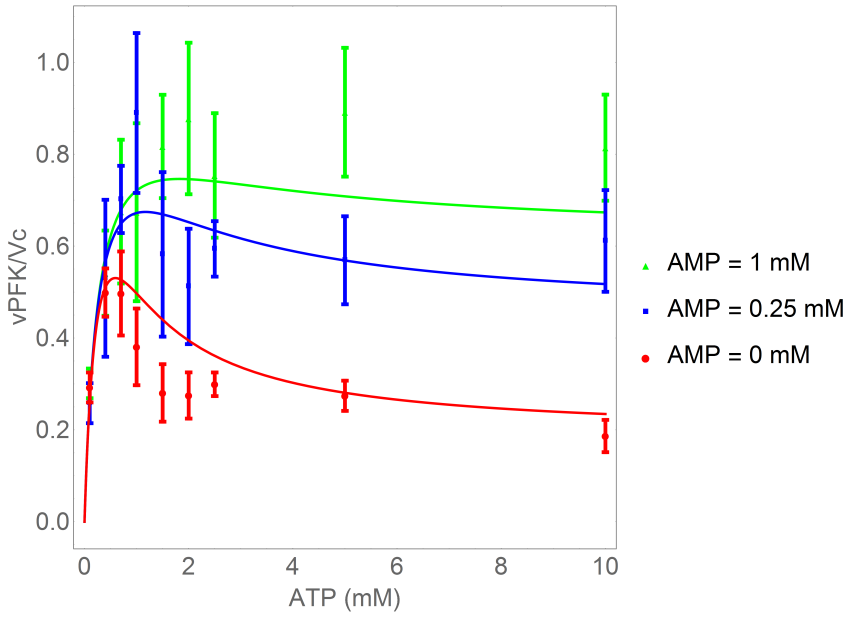

(a)

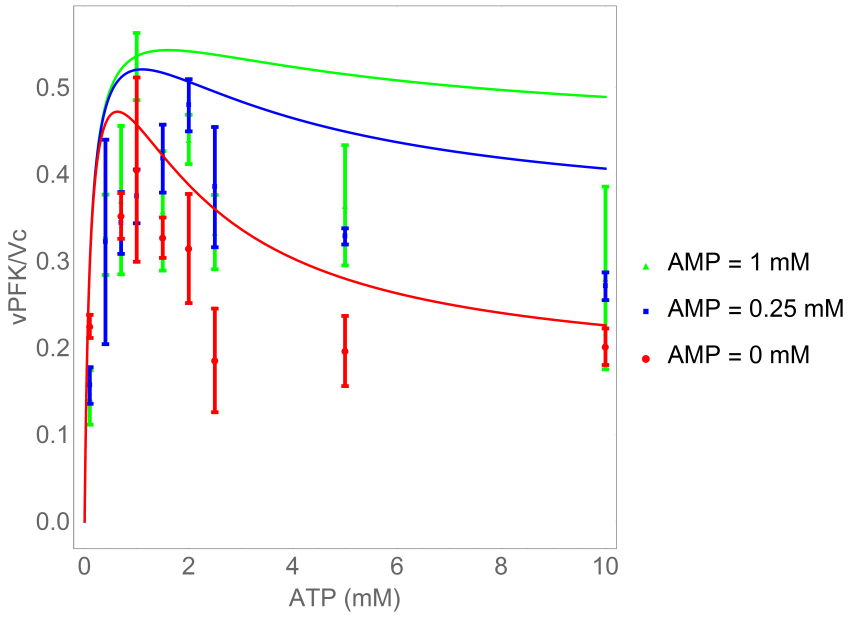

(b)

Figure 4.6: B - The effect of ATP on PFK at a F6P concentrations of 1 mM for (a) X2180 strain and (b) VIN13 strain and varying AMP concentrations of 0 mM AMP (red), 0.25 mM AMP (blue) and 1 mM AMP (green). The dots are the experimental data (with experimental error bars) and the solid curve is fitted rate equation. At this higher F6P concentration of 1 mM both the strains show ATP inhibition at higher ATP concentrations. The mean of the experimental data is presented symbolically with error bars indicating the standard deviation of the triplicate data (normalised to the control rates)

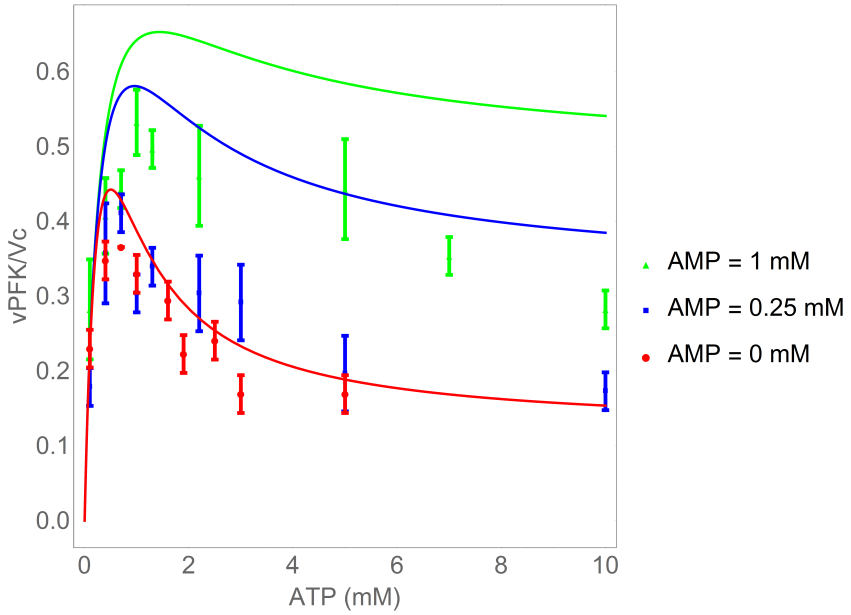

(a)

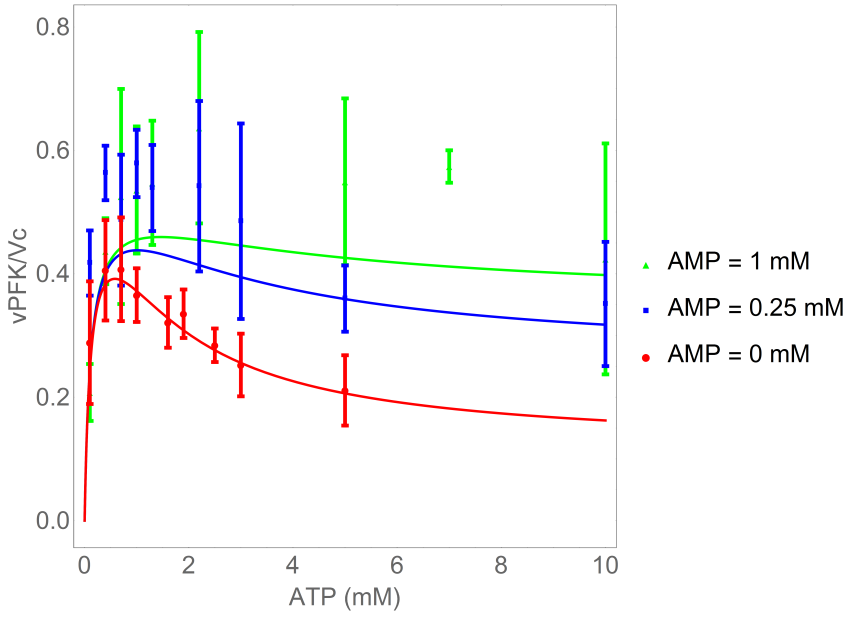

(b)

Figure 4.7: C - The effect of ATP on PFK at a F6P concentrations of 0.75 mM for (a) X2180 strain and (b) VIN13 strain and varying AMP concentrations of 0 mM AMP (red), 0.25 mM AMP (blue) and 1 mM AMP (green). The dots are the experimental data (with experimental error bars) and the solid curve is the fitted rate equation. The experimental data in both strains for this experiment does not fit the model prediction. The mean of the experimental data is presented symbolically with error bars indicating the standard deviation of the triplicate data (normalised to the control rates)

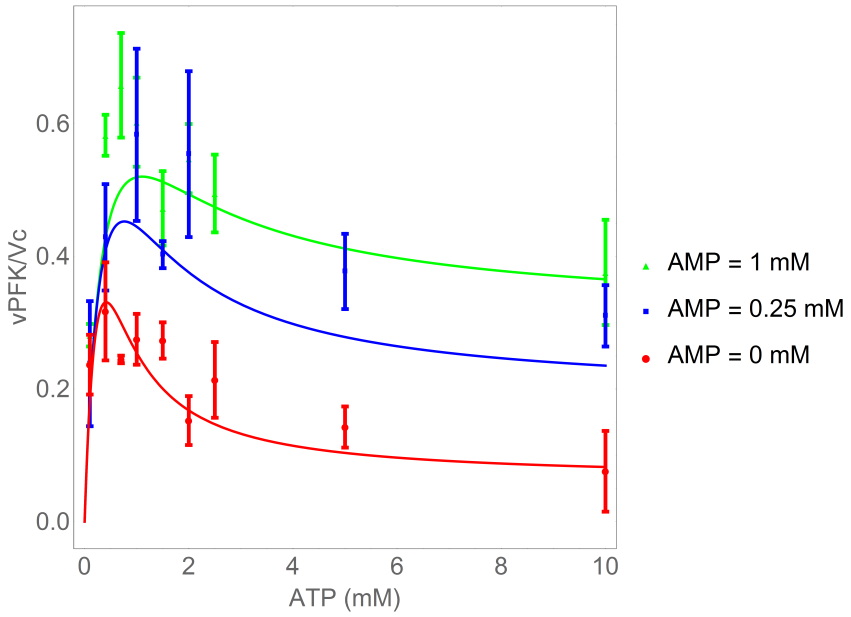

(a)

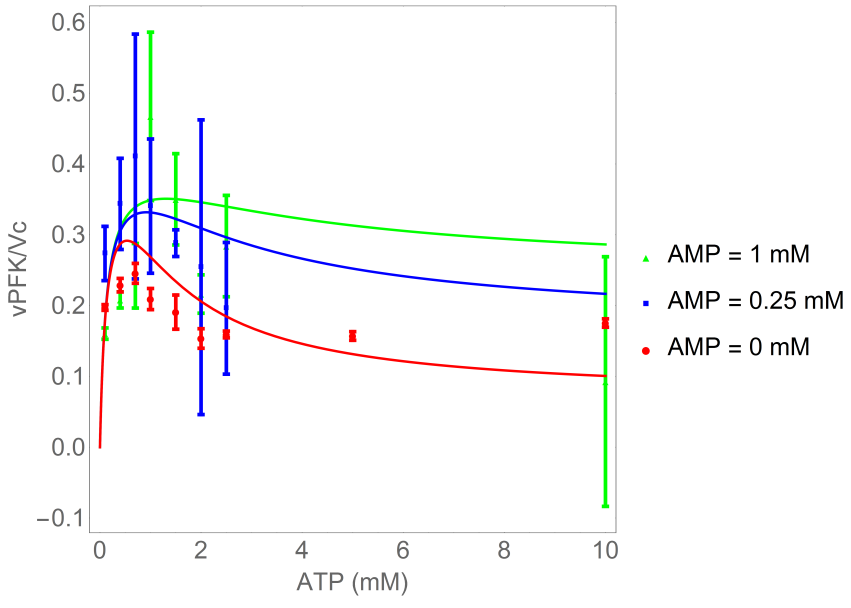

(b)

Figure 4.8: D - The effect of ATP on PFK at a F6P concentrations of 0.5 mM for (a) X2180 strain and (b) VIN13 strain and varying AMP concentrations of 0 mM AMP (red), 0.25 mM AMP (blue) and 1 mM AMP (green). The dots are the experimental data and the solid curve is the fitted rate equation. The mean of the experimental data is presented symbolically with error bars indicating the standard deviation of the triplicate data (normalised to the control rates).

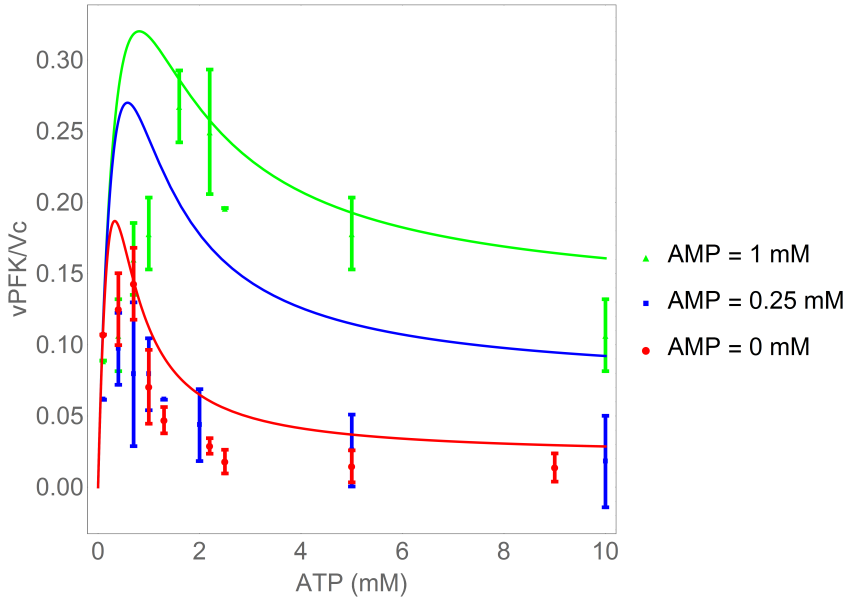

(a)

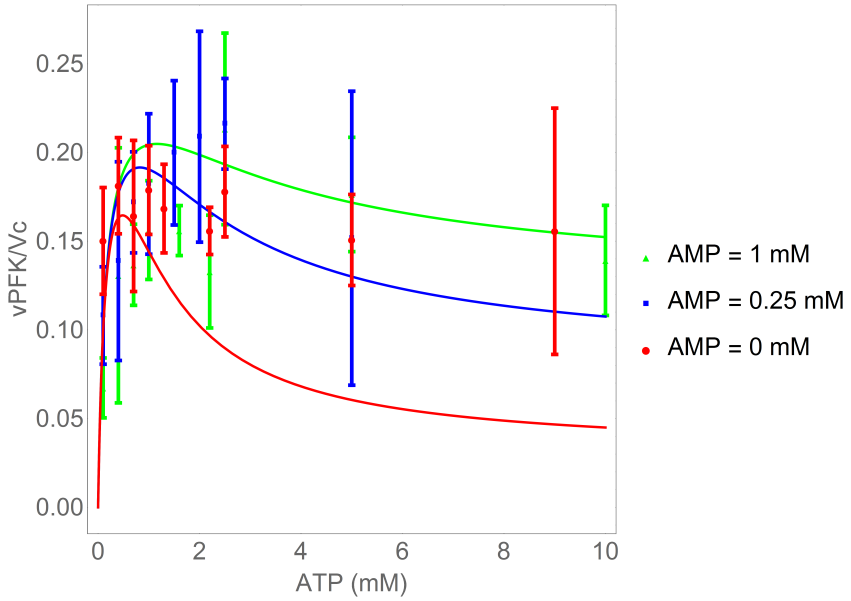

(b)

Figure 4.9: E - The effect of ATP on PFK at a F6P concentrations of 0.25 mM for (a) X2180 strain and (b) VIN13 strain and varying AMP concentrations of 0 mM AMP (red), 0.25 mM AMP (blue) and 1 mM AMP (green). The dots are the experimental data and the solid curve is the fitted rate equation. The mean of the experimental data is presented symbolically with error bars indicating the standard deviation of the triplicate data (normalised to the control rates).

4.3.3 Model analysis

Du Preez [10, 11] adapted the Teusink model [22] to show limit-cycle oscillations with minor changes to rate multipliers, as detailed in Section 2.5. The aim of this section is to follow these optimisation steps to obtain a model that oscillates and incorporates the PFK parameters determined experimentally in this study. For the X2180 strain the parameter values in Table 4.2 and the corresponding V_{max} from Section 4.3.2 were substituted into the dupreez1 model. The new model, however, failed to produce a steady state. Simulation results showed that the model ran out of ATP, probably due to the fact that the slowed-down lower part of glycolysis was unable to balance ATP production with the ATP demand of HK and PFK in upper glycolysis. Since we did not want to modify enzymatic parameters of any other reaction just yet, we decreased the external ethanol concentration to speed up the flux through lower glycolysis and a steady state reappeared (muiyserx2180 model). The PFK kinetics of the dupreez1 model as a function of substrate concentrations is shown in Figure 4.10(a). The black bar indicates the position of the steady state on the rate surface. For this simulation, AK was assumed to be in equilibrium and F16bP was fixed at its steady-state concentration. The kinetics of muiyserx2180 model is shown in Figure 4.10(b). Clearly the effect of ATP inhibition is more pronounced than in the wild type model (original dupreez1 model). This is similar to the results of the optimisation in [10], where the ATP inhibition effect appeared as a result of a directed search for parameters values leading to oscillations. Although the muiyserx2180 model does show ATP inhibition of PFK at its steady state (black bar in Fig. 4.10(b)), this does not seem to be sufficient for oscillations. The optimisation was then performed allowing all V_{max} values (except V_{max} for PFK) and the concentrations of external ethanol and glucose to vary. This was deemed reasonable as the activities of other enzymes were not experimentally determined. In this way oscillations were simulated in muiyserx2180opt. With A 5% step size in parameter adjustments an oscillatory model was obtained within 28 iterations. The results are shown in Table 4.5 where the first column shows the optimized parameters values for the muiyserx2180opt model and their % comparison to the dupreez1 model (note that the PFK parameters were unchanged from their values shown in Table 4.2). The PFK kinetics in the optimised model can be seen in Figure 4.10(c). Here the ATP inhibition effect is even more pronounced brought about by changes in the network as a result of the optimisation. The black oval indicates the limit cycle as determined from a time course simulation.

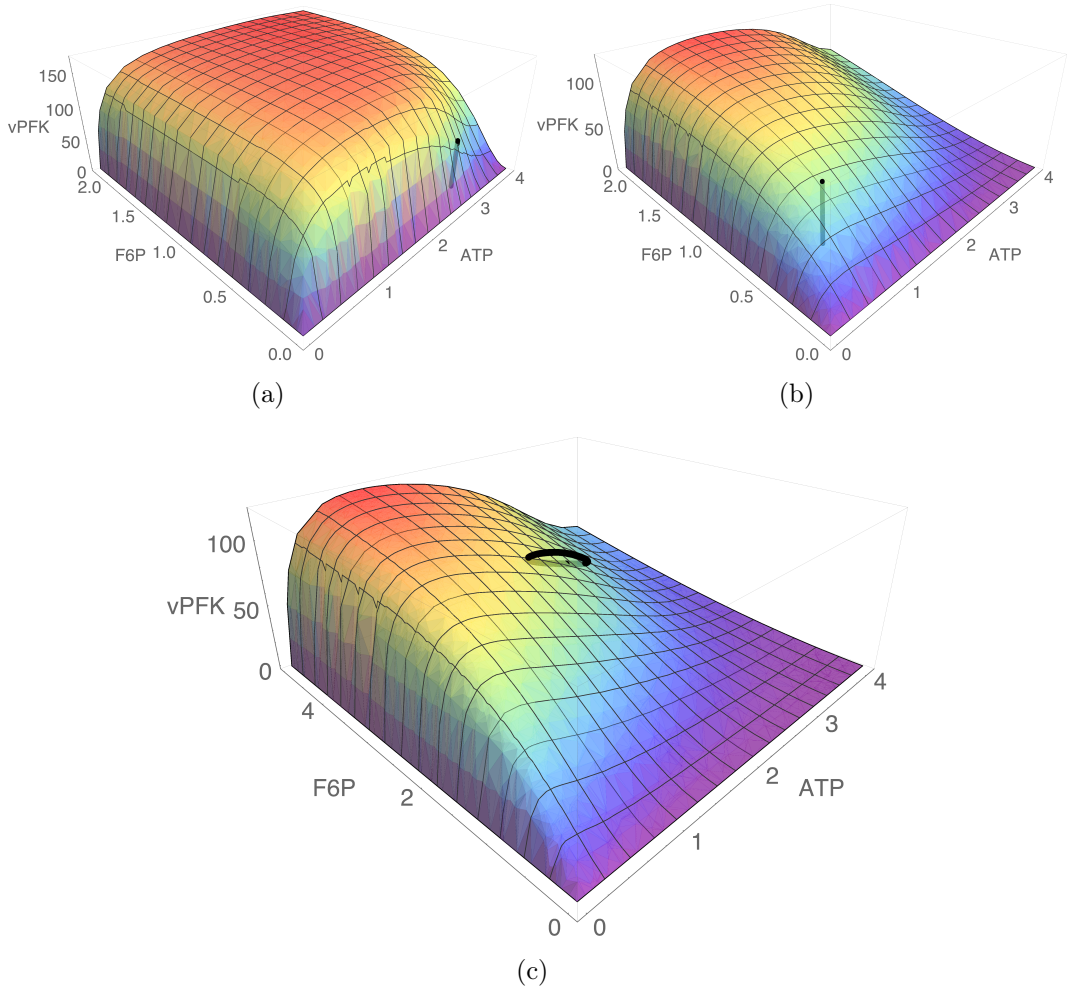

Figure 4.10: Comparison of PFK kinetics for (a) dupreez1, the non-oscillatory model showing the steady state concentrations on the graph with the bar, (b) muiyserx2180, the model created by including the fitted experimental parameters for PFK in the dupreez1 model showing the steady state concentrations on the graph with the bar and (c) muiyserx2180opt, the model optimized to simulate oscillation showing the limit cycle. The x-axis scans for ATP (mM), y-axis is the F6P (mM) and the z-axis shows the reaction rate (mM/min).

For the VIN13 strain the parameter values in Table 4.3 and the corresponding V_{max} from Section 4.3.2 were substituted into the dupreez1 model. The new model once again did not yield a steady state result and could not be rescued by decreasing the external ethanol (or changing the glucose concentration). A similar pattern of ATP depletion emerged, leading to a collapse of the pathway flux. The optimisation could therefore not be performed on this model and a thorough characterisation of other pathway enzymes (e.g. HK) might be required to rescue the model in a more directed fashion. If the V_{max} of PFK is left at its original dupreez1 value (muiyservin13 model), a steady

state is obtained but the optimisation does not yield an oscillating model. In fact, the optimisation fails due to one or more parameters once again crossing a boundary beyond which a valid numerical solution is no longer obtained and glycolysis halts. A PFK rate characteristic surface (Appendix B in Figure B.6) shows that the steady state in muiyservin13 model exhibits ATP activation and not inhibition which could contribute to the optimization failing.

Table 4.5: Optimized parameters for oscillations

	muiyserx2180opt	% comparison dupreez1 model
VmADH	895 mM/min	111
VmALD	236 mM/min	73.4
VmENO	361 mM/min	98.7
VmG3PA	457 mM/min	84.9
VmG3PDH	334 mM/min	69.9
VmGAPDH	372 mM/min	31.4
VmGLK	421 mM/min	186
VmGLT	121 mM/min	124
VmPCD	169 mM/min	97.0
VmPGI	920 mM/min	208
VmPGK	1351 mM/min	103
VmPGM	2567 mM/min	102
VmPYK	1237 mM/min	114
KSUCC	16.7 1/min	77.8
KTREHALOSE	0.410 1/mM/min	46.2
KATPASE	31.3 mM/min	33.6
KGLYCOGEN	0.708 1/mM/min	29.8
ETOH	8.49 mM	84.9
GLCo	50.4 mM	101

4.4 Conclusion

This chapter addressed the second and third objectives of the study: characterise and compare the ATP and AMP kinetic regulation of PFK in the two strains, and analyse the behaviour of the mathematical model of glycolytic oscillations using the experimentally determined PFK kinetic parameters.

We optimised the enzyme assay methodology for PFK in [22] to include an AK inhibitor based on work done by [77]. The AK inhibitor was used to prevent the added AMP from stimulating the AK to utilize AMP and ATP in the system. This ensures that the concentrations of ATP and AMP are well defined for the kinetic characterisation of PFK. This could also be important for

other assays where both ATP and AMP are added to extract containing AK. We experimentally characterised the ATP inhibitory effect on PFK and AMP alleviating that effect. Fitting the PFK rate equation of [22] to the data, with certain constraints regarding species characterised, resulted in a good qualitative description of F6P saturation, ATP inhibition and AMP activation and had varying levels of success in quantitative reproduction. Although the standard errors were smaller or of similar order as the fitted values, the unfitted parameters could certainly have an effect on the equation's behaviour and a more detailed dataset (encompassing characterisations for all metabolites affecting PFK in addition to more combinations of metabolites) could result in a better description when fitting all the parameters. Other mechanistic rate equations for PFK can also be investigated for compatibility with the data and improved predictive power. It was however shown that the parameters related to the effects of AMP and ATP on PFK, and experimentally determined in this study, resulted in a PFK rate characteristic surface plots similar to what was observed in the full optimisation study of Du Preez. In the case of the X2180 strain, the new parameters did result in a full model of glycolysis that exhibits oscillations after an additional optimisation of other enzyme concentrations. In the case of VIN13, no oscillating model could be obtained. However, an exhaustive search for parameters that could possibly still lead to oscillations in the VIN13 model was not performed and an extensive fine-tuning of the optimisation algorithm was not conducted. These could be avenues for investigation. Some additional characterisation of other pathway enzymes, such as hexokinase (HK) in the top part of glycolysis and phosphoglycerate kinase (PGK) or pyruvate kinase (PYK) for the bottom part of glycolysis,which are implicated in the energy regulation and sensitive to ATP levels, might also be required.

Chapter 5

Conclusions and Future work

5.1 Summary of findings

In this study the oscillatory yeast strain, X2180, showed sustained oscillations in the individual cells of the population. The visualisation was done using an optimized microscope detection method documented in Chapter 3. In comparison the VIN13 yeast strain exhibited no oscillation when harvested and treated following the exact protocol used for the X2180 strain. For the oscillatory signal observed the synchronization of the oscillations was tested. The population as a whole did not show synchronization, localised synchronization amongst neighbouring cells were reported. The study then investigated the PFK kinetic behaviour with respect to ATP and another effector of PFK, AMP. Overall the PFK experimental data obtained for X2180 showed better correlation to the model prediction than the VIN13. The ATP inhibition at higher concentrations is observed in both strains, and at first glance the PFK kinetics do not appear that different for the two strains. The kinetic parameters determined for X2180 were able to induce oscillations in a model for steady state glycolysis following the optimisation steps detailed in [11]. This was not the case for the experimentally determined VIN13 PFK parameters.

5.2 Recommendation for future work

In [55] they denote the inter-strain differences in the enzymatic make up can promote different behavioural characteristics. Such a difference in PFK enzyme kinetic properties is hypothesised as a possible reason for the observed difference between the X2180 and VIN13 strains with respect to oscillations. The PFK kinetics were therefore characterised for both strains. Even though the strains do show minor differences, it is unlikely that the observed difference in oscillatory behaviour can be attributed solely to PFK regulation by its allosteric effectors. Despite this, we were able to obtain oscillations in a non-oscillatory model of glycolysis using the X2180 PFK parameters and sub-

sequent optimisation whereas this was not possible for VIN13.Thus in the case of VIN13 more enzymes should be characterised to see if an oscillatory solution can be obtained from the existing models given that its PFK also shows ATP inhibition and AMP activation experimentally.

Another possible reason for not observing oscillations in the VIN13 yeast strain is the fact that VIN13 is a commercially used strain in wine production. As such, the alcoholic fermentation that takes place when the glucose is added results in higher concentrations of ethanol and acetaldehyde [78] than that found in budding yeast cells and it could be that these high concentrations are suppressing oscillations. The capturing of acetaldehyde (and other carbonyl-containing compounds in glycolysis) by cyanide is in fact one of the reasons that cyanide is deemed neccessary for oscillations [79]. It could be that these reactions regulate the flux through glycolysis and specifically ADH thererby maintaining NADH in a concentration range favourable for oscillations. To be consistent and to be able to compare the two different strains, the concentration of cyanide used as described in [7] was the same for both strains and optimizing the protocol for detection of any possible oscillations in the VIN13 strain was left for future work. Thus it is recommended that higher cyanide concentrations are investigated.

The phenomenon of synchronization of oscillations between yeast cells in a population has been of interest since the initial discovery of oscillating populations. Here we have presented some progress towards experimental detection and numerical analysis of synchronization between single cells in a batch environment (unlike the high-flow microfluidic environment of [7] where synchronization will not be possible). Future work can include optimizing the batch environment and investigating how the changes (e.g variation in cyanide/acetaldehyde concentrations) in the external environment alter the oscillatory signal and subsequent synchronization.

Appendix A

Microscope results

In Chapter 3 the results highlight the objective to visualise oscillation in the two yeast strains, however only selected results are presented in the chapter. The full set of oscillation data for both Vin 13 Figure A.1 - Figure A.4 and X2180 Figure A.5 - Figure A.8 are documented in Appendix A. Also some additional Hilbert transform analysis results are shown in Figure A.9 and the specification data sheet for the Olympus IX81 inverted fluorescent microscope is included in Figure A.10.

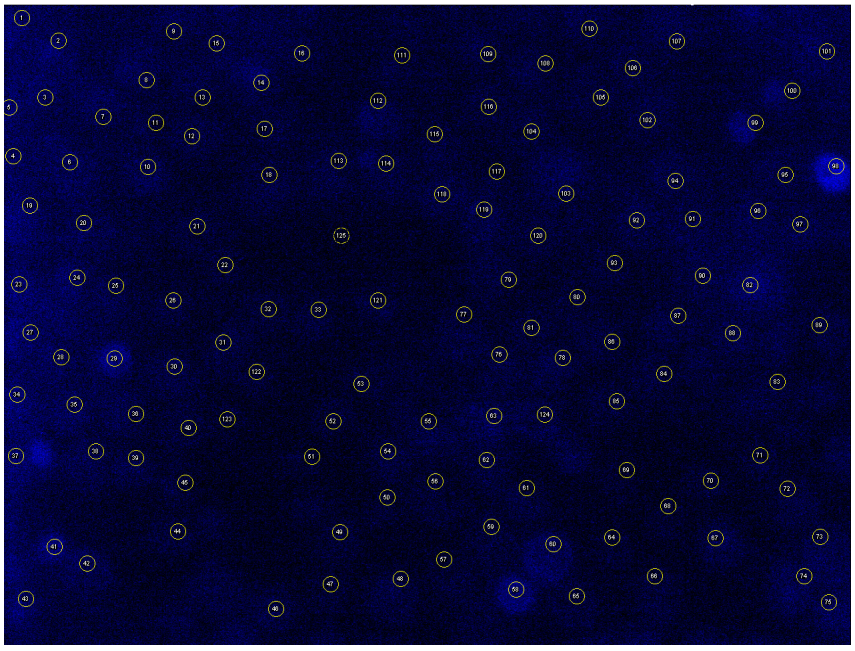

Figure A.1: The image captured during the experiment of Vin 13 and using Image J all the cells are encapsulated with ROI's measuring the NADH fluctuations in each image.

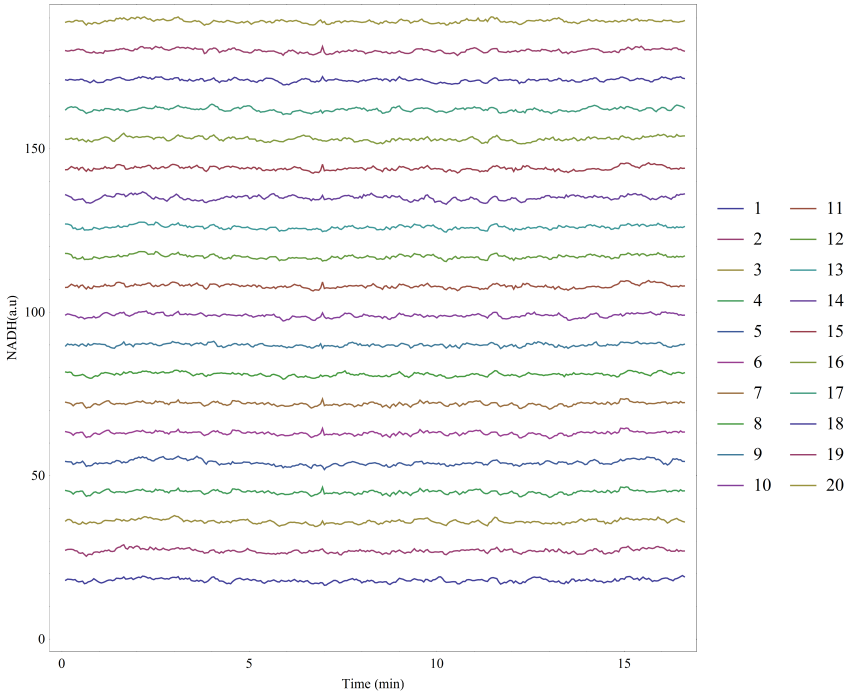

(a)

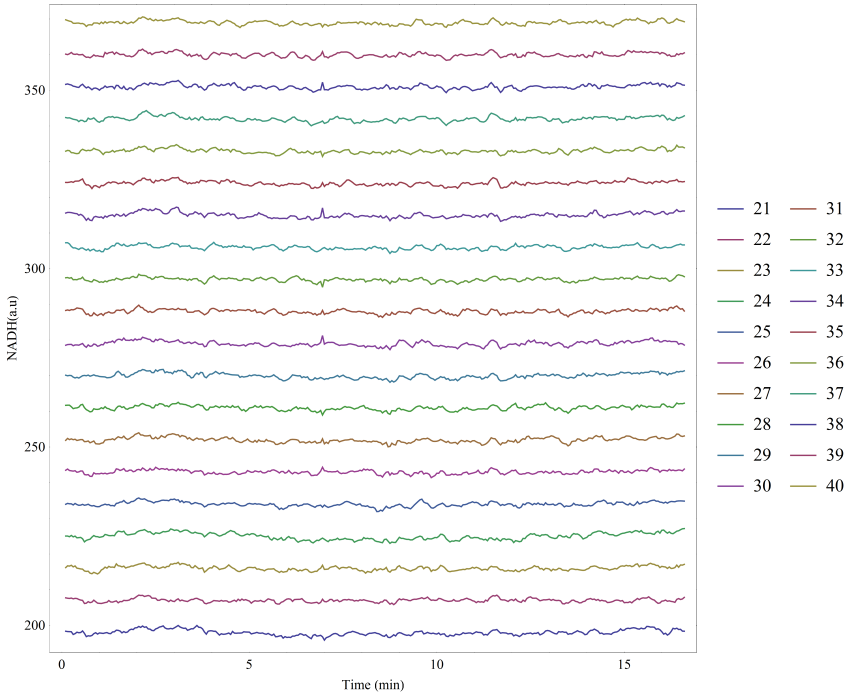

(b)

Figure A.2: The NADH signal of (a) ROI 1-20 and (b) ROI 21-40 of the Vin 13 strain. The curves are offset by 10 arbitrary units of intensity so that the can be easily visualised. The oscillations were induced at t = 0 by exposing the cells to a mixed solution containing 20 mM glucose + 5 mM cyanide.

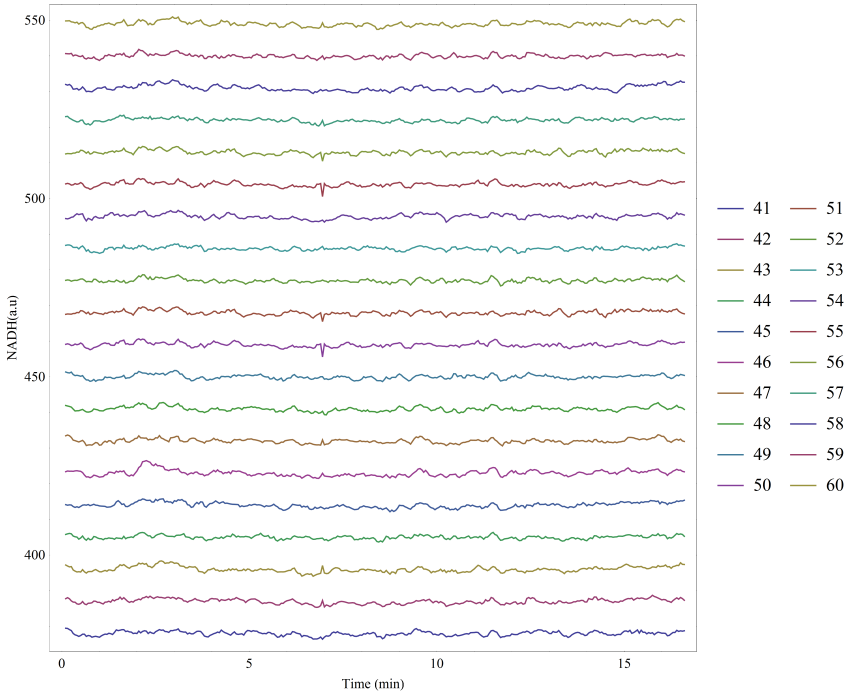

(a)

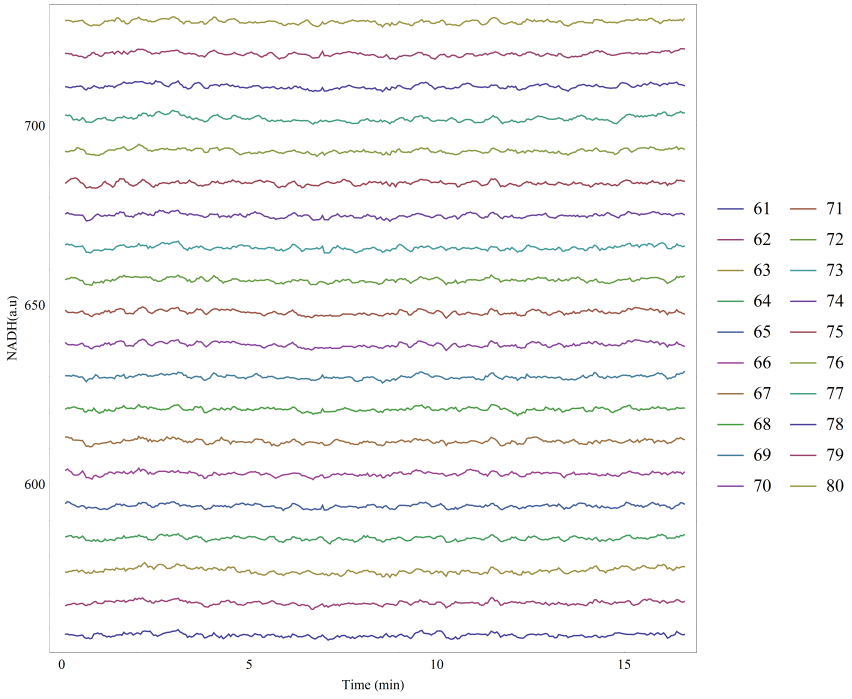

(b)

Figure A.3: The NADH signal of (a) ROI 41-60 and (b) ROI 61-80 of the Vin 13 strain. The curves are offset by 10 arbitrary units of intensity so that the can be easily visualised. The oscillations were induced at t = 0 by exposing the cells to a mixed solution containing 20 mM glucose + 5 mM cyanide.

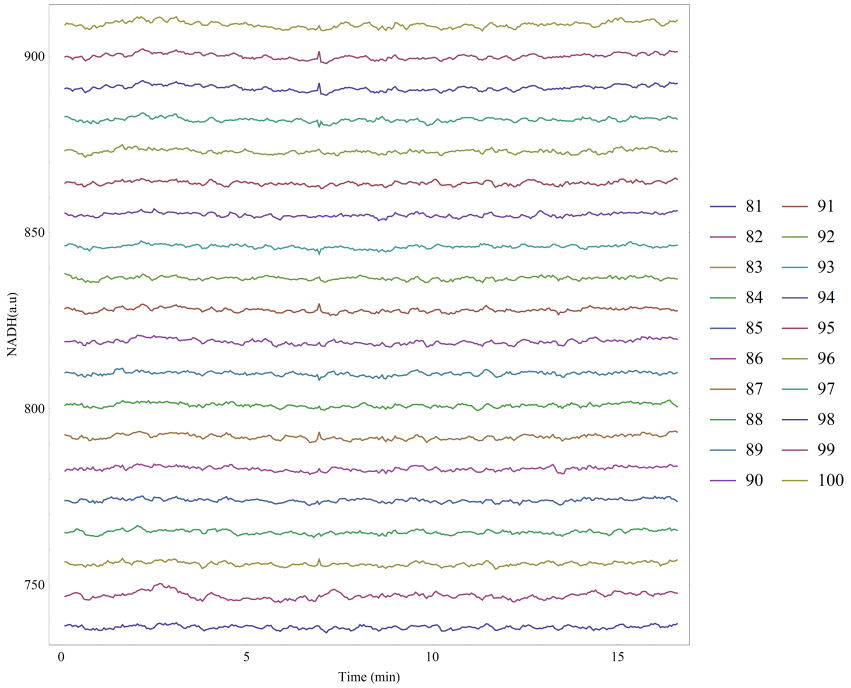

Figure A.4: The NADH signal of ROI 81-100 of the Vin 13 strain. The curves are offset by 10 arbitrary units of intensity so that the can be easily visualised. The oscillations were induced at t = 0 by exposing the cells to a mixed solution containing 20 mM glucose + 5 mM cyanide.

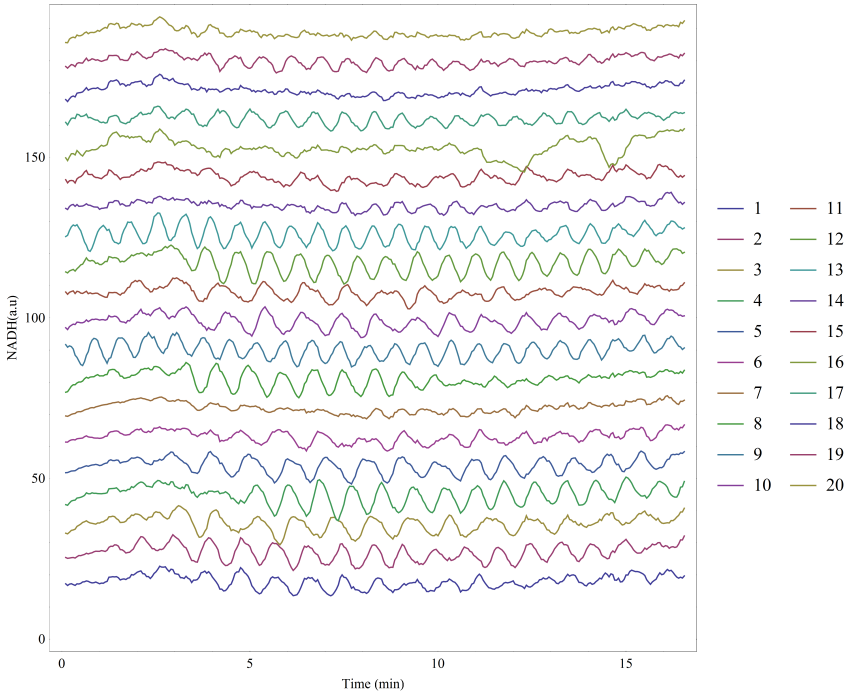

(a)

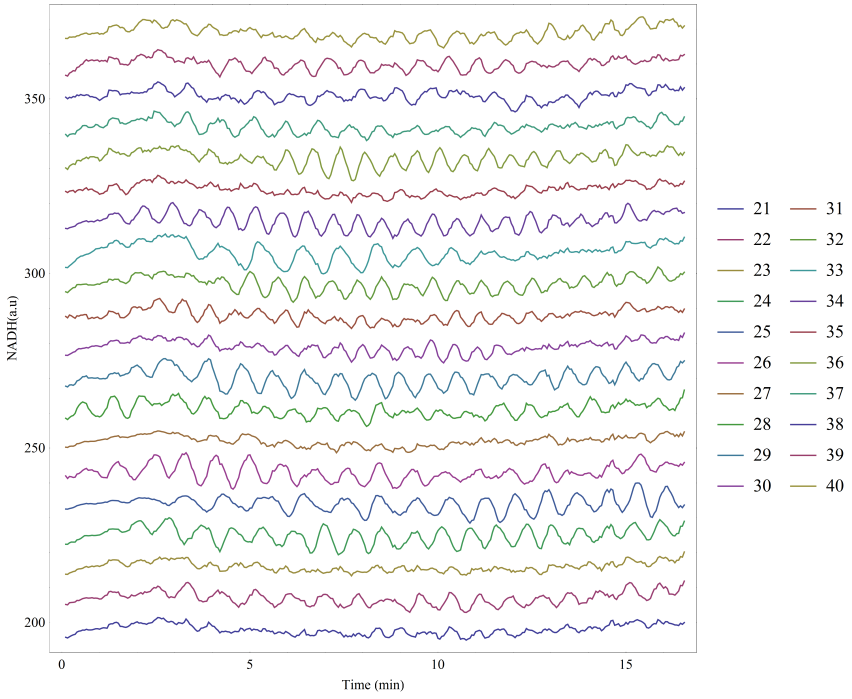

(b)

Figure A.5: The NADH signal of (a) ROI 1-20 and (b) ROI 21-40 of the X2180 strain. The curves are offset by 10 arbitrary units of intensity so that the can be easily visualised. The oscillations were induced at t = 0 by exposing the cells to a mixed solution containing 20 mM glucose + 5 mM cyanide.

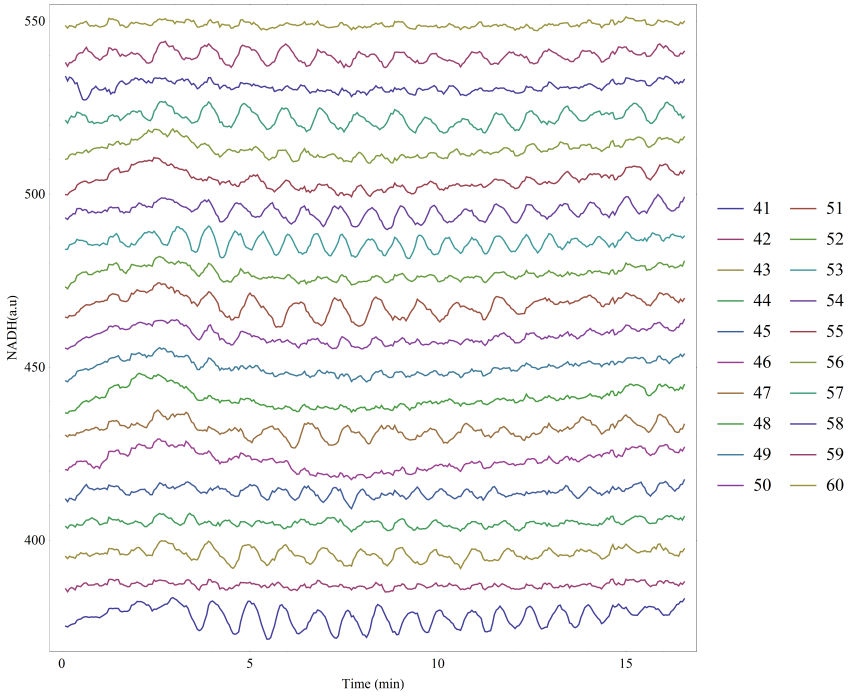

(a)

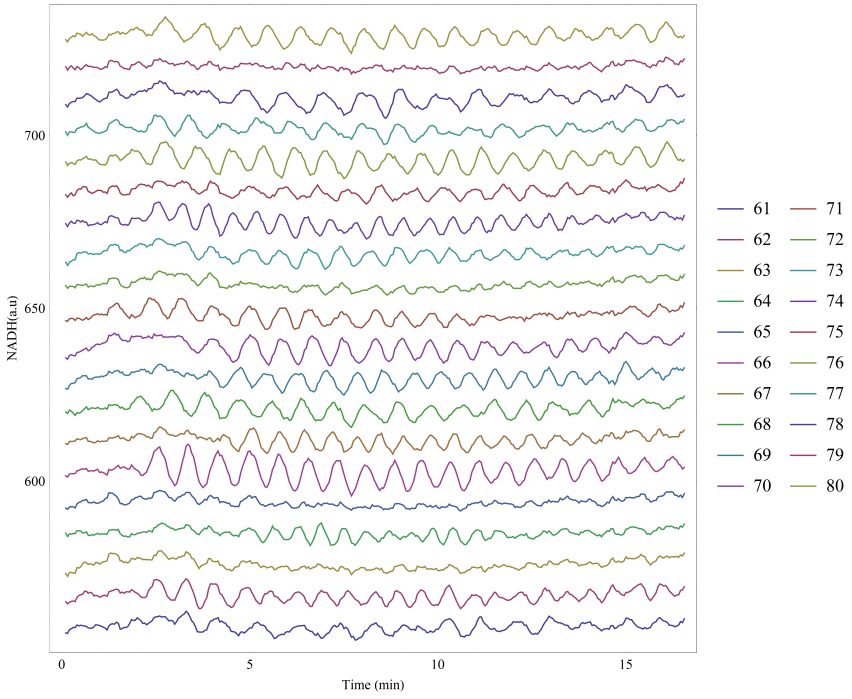

(b)

Figure A.6: The NADH signal of (a) ROI 41-60 and (b) ROI 61-80 of the X2180 strain. The curves are offset by 10 arbitrary units of intensity so that the can be easily visualised. The oscillations were induced at t = 0 by exposing the cells to a mixed solution containing 20 mM glucose + 5 mM cyanide.

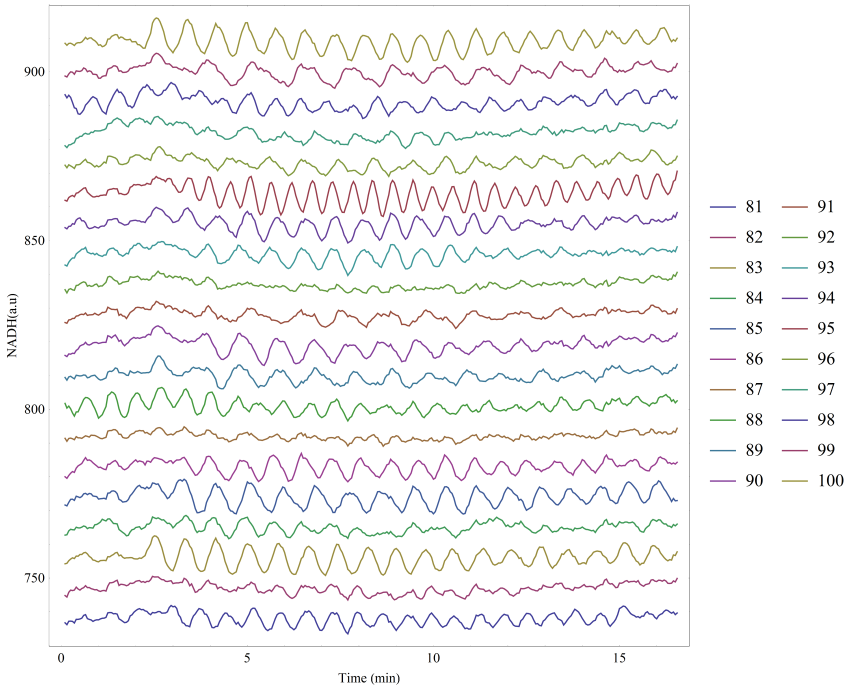

(a)

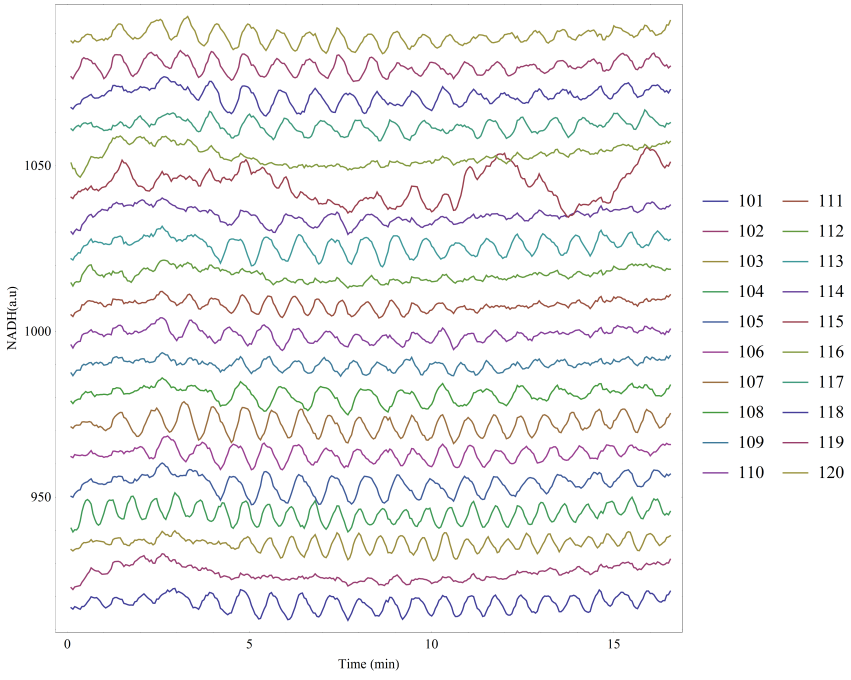

(b)

Figure A.7: The NADH signal of (a) ROI 81-100 and (b) ROI 101-120 of the X2180 strain. The curves are offset by 10 arbitrary units of intensity so that the can be easily visualised. The oscillations were induced at t = 0 by exposing the cells to a mixed solution containing 20 mM glucose + 5 mM cyanide.

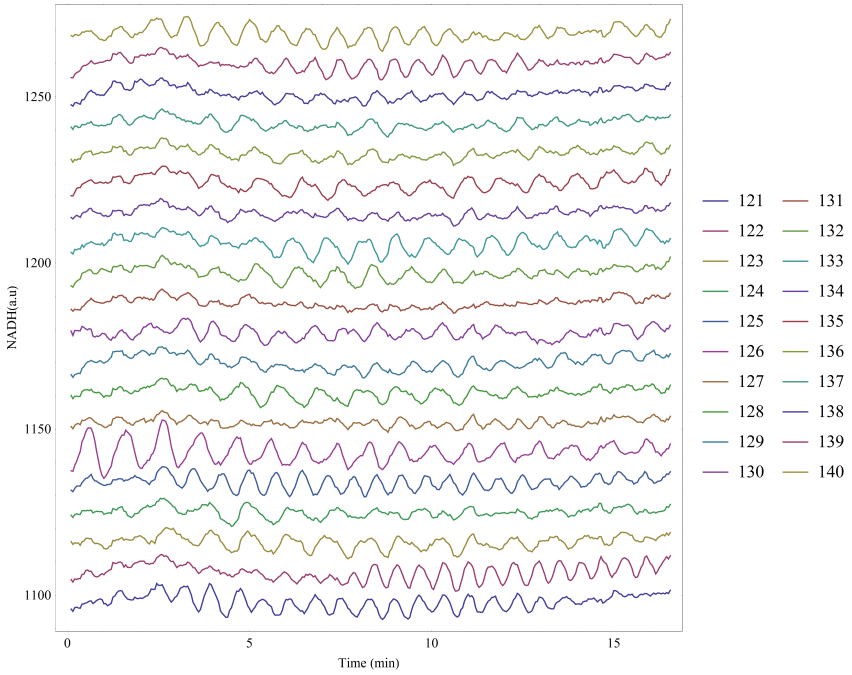

(a)

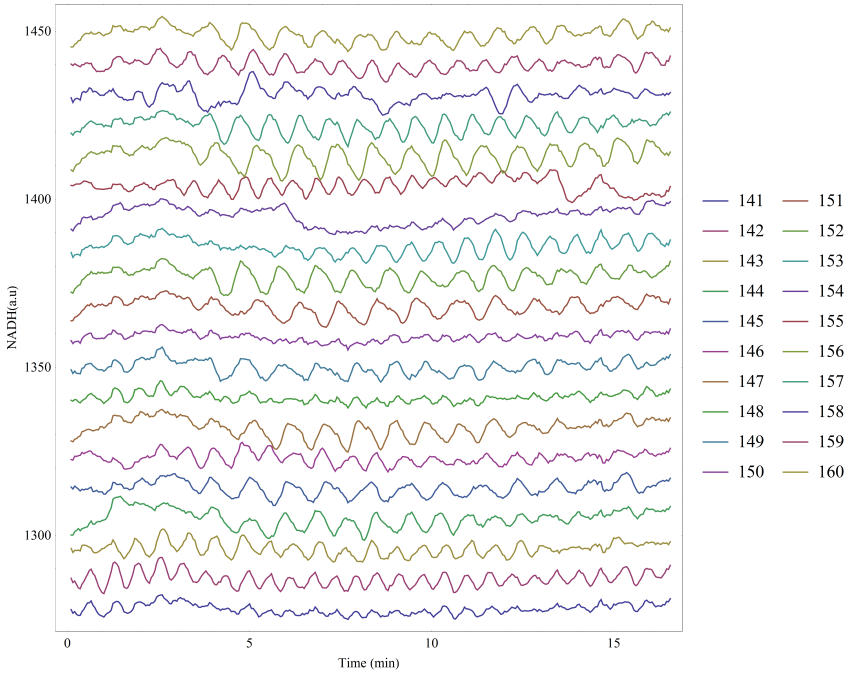

(b)

Figure A.8: The NADH signal of (a) ROI 121-140 and (b) ROI 141-160 of the X2180 strain. The curves are offset by 10 arbitrary units of intensity so that the can be easily visualised. The oscillations were induced at t = 0 by exposing the cells to a mixed solution containing 20 mM glucose + 5 mM cyanide.

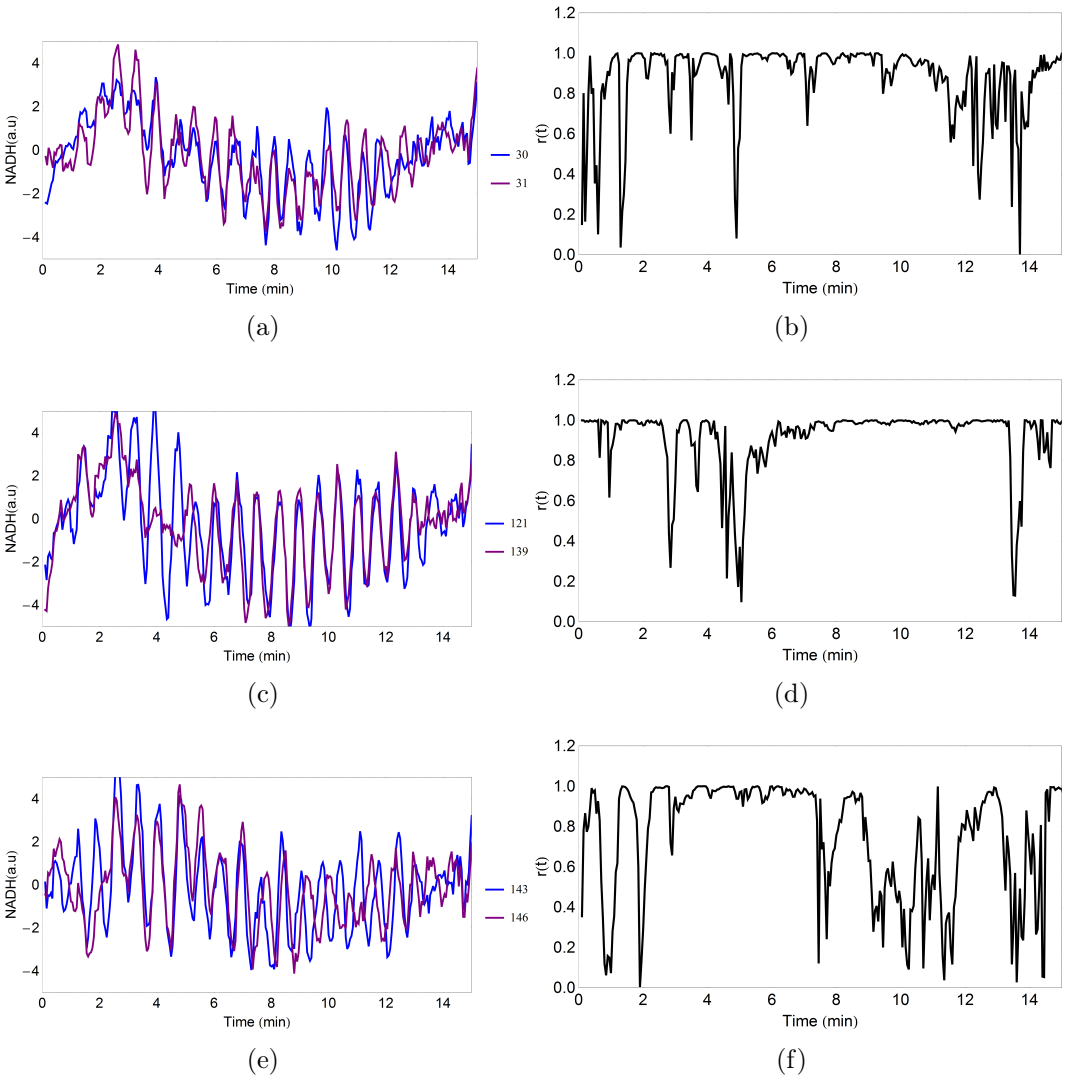

Figure A.9: Here the NADH signal of the neighbouring cells, as shown in (a),(c) and (e), is used to calculated the instantaneous phase ϕ_n of oscillation using the Hilbert transform. The graph in (b),(d) and (f) show the order parameter, $r(t)$, calculated from the determined ϕ_n. The values close to zero indicates the signal is out of phase with one another and at one the cells are synchronised.

Olympus IX81 inverted fluorescent microscope for Live cell imaging

Microscope system: Olympus Cell^R system (from Olympus Biosystems GMBH)

Camera: F-view-II cooled CCD camera (Soft Imaging systems)

Light source: Xenon-Arc burner (Olympus Biosystems GMBH) as light source

Excitation filters:
360 nm (for blue staining)
492 nm (for green staining)
572 nm (for red staining)
340 nm Fura
380 nm Fura
470 nm GFP
430 nm CFP
500 nm YFP

Emission filters:
UBG triple-bandpass emission filter cube (Chroma)
CFP/YFP filter set for FRET imaging

Objectives:
Olympus UPlanFI 4x/0.13 ∞/-
Olympus UPlanFLN 10x/0.30 ∞/-/FN26.5
Olympus LUCPlanFLN 20x/0.45 Ph1 ∞/0-2 FN22
Olympus LUCPlanFLN 40x/0.60 Ph2 ∞/0-2 FN22
Olympus Plan APO N 60x/1.42 Oil ∞/0.17/FN26.5
Olympus UPlanApo N 100x/1.40 Oil ∞/0.17/FN26.5

Software: Cell^R imaging software

Figure A.10: Specification sheet Olympus IX81- Showing the setup used to visualise glycolytic oscillations.

Appendix B

PFK results

In Chapter 4 the results show the PFK kinetic characterisation of the grouped experiments done for the different strains and fitting the data to the rate equation presented in the [22] model. This section will present the individual experiments shown by the dots with error bars (A - E: Figure B.1 - Figure B.5) and its fitted model prediction result shown by a solid curve for both X2180 and Vin 13 including the 95% confidence bands.

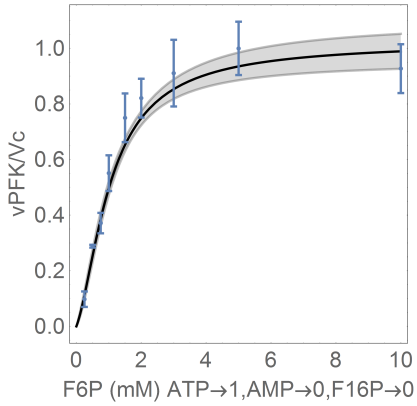

(a)

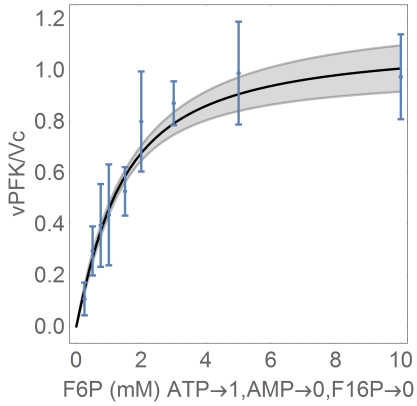

(b)

Figure B.1: A - PFK characterisation in terms of its substrate, F6P and ATP kept at 1 mM for (a) X2180 and (b) Vin 13. The dots are the experimental data and the solid curve is fitted rate equation

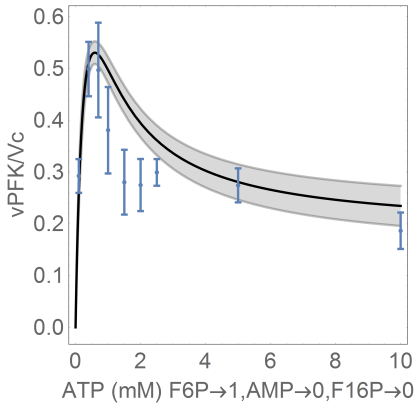

(a)

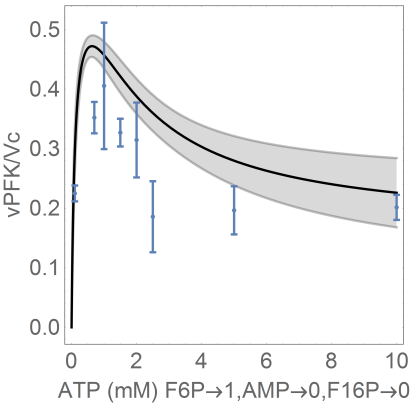

(b)

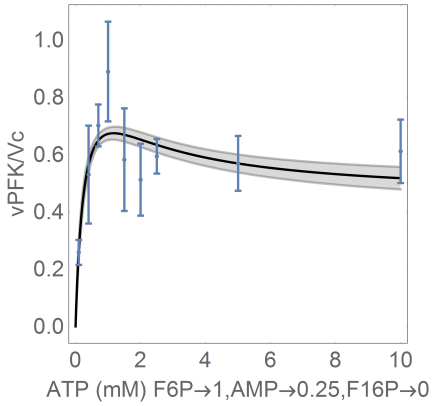

(c)

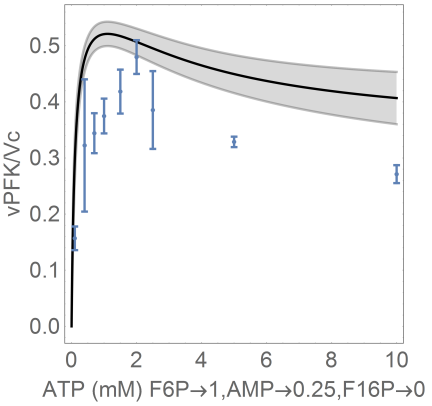

(d)

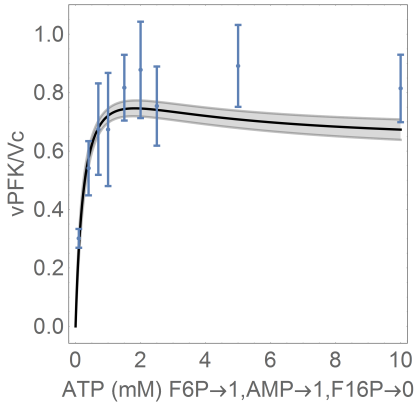

(e)

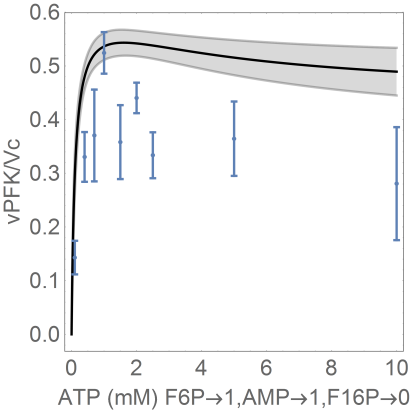

(f)

Figure B.2: B - The effect of ATP on PFK at a F6P concentrations of 1 mM for (a) 0 mM AMP in X2180 strain, (b) 0 mM AMP in Vin 13 strain, (c) 0.25 mM AMP in X2180 strain, (d) 0.25 mM AMP in Vin 13 strain, (e) 1 mM AMP in X2180 strain and (f) 1 mM AMP in X2180 strain. The dots are the experimental data and the solid curve is fitted rate equation

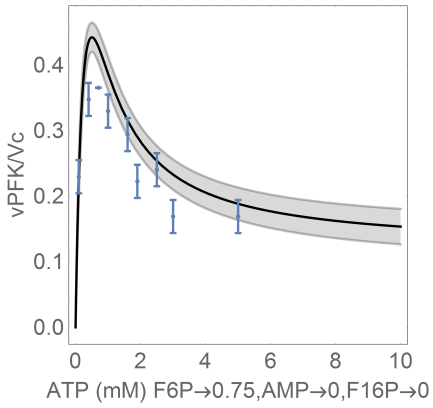

(a)

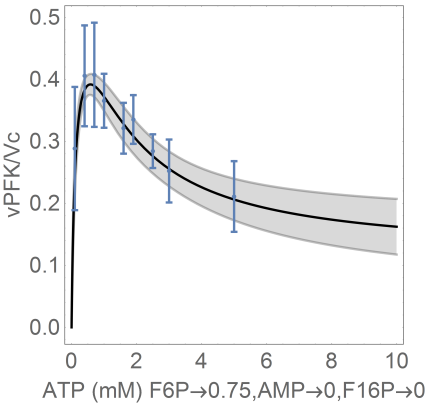

(b)

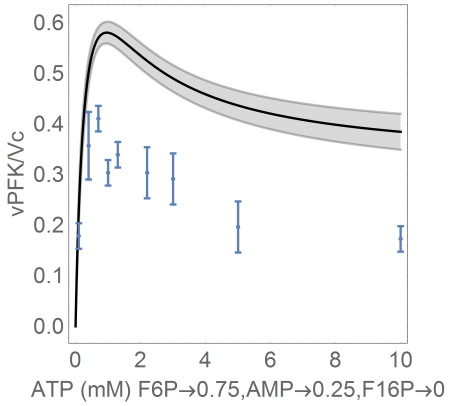

(c)

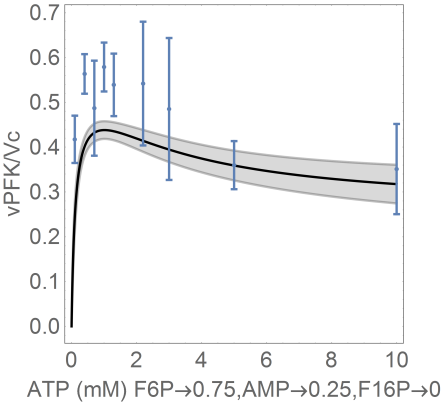

(d)

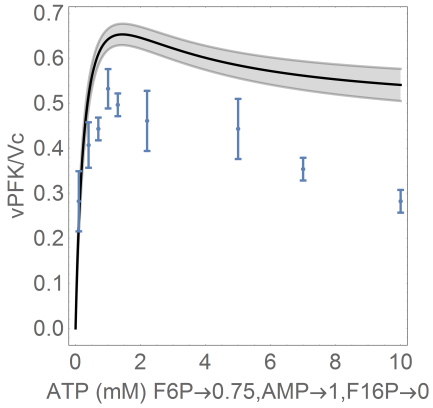

(e)

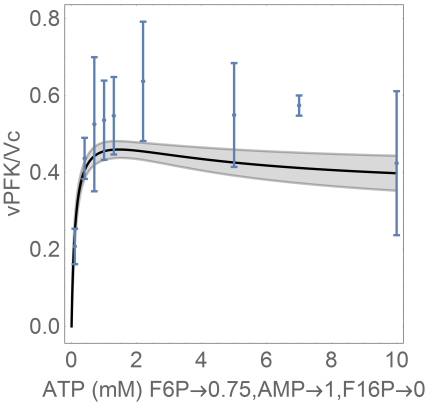

(f)

Figure B.3: C - The effect of ATP on PFK at a F6P concentrations of 0.75 mM for (a) 0 mM AMP in X2180 strain, (b) 0 mM AMP in Vin 13 strain, (c) 0.25 mM AMP in X2180 strain, (d) 0.25 mM AMP in Vin 13 strain, (e) 1 mM AMP in X2180 strain and (f) 1 mM AMP in X2180 strain. The dots are the experimental data and the solid curve is fitted rate equation

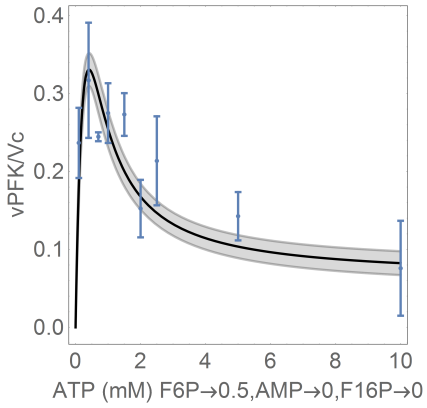

(a)

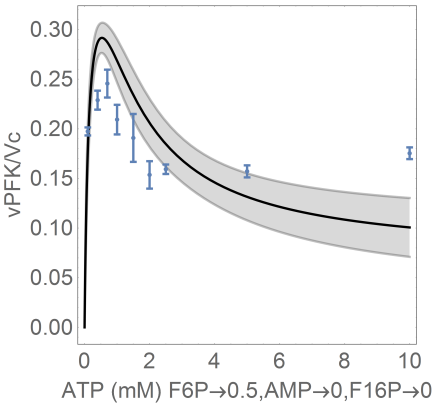

(b)

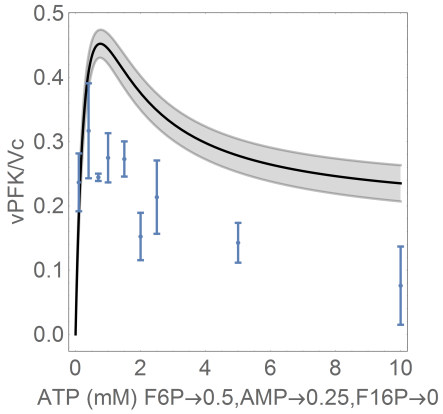

(c)

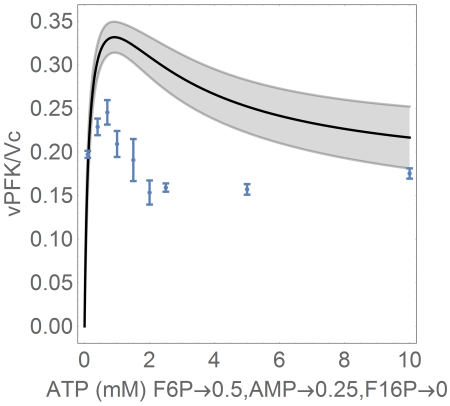

(d)

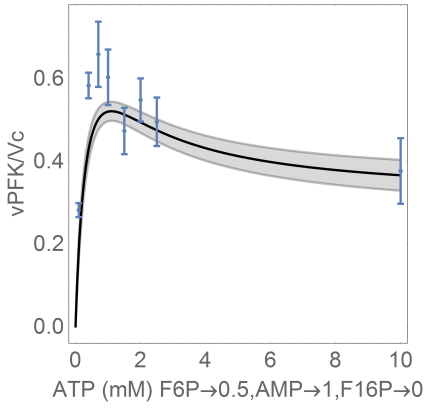

(e)

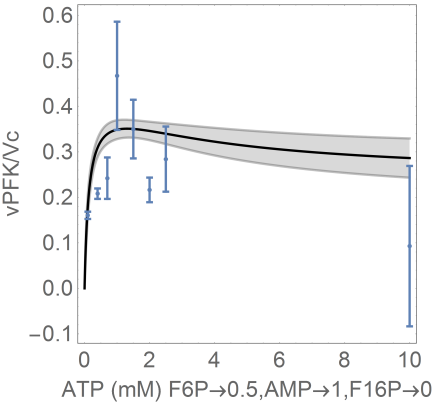

(f)

Figure B.4: D - The effect of ATP on PFK at a F6P concentrations of 0.5 mM for (a) 0 mM AMP in X2180 strain, (b) 0 mM AMP in Vin 13 strain, (c) 0.25 mM AMP in X2180 strain, (d) 0.25 mM AMP in Vin 13 strain, (e) 1 mM AMP in X2180 strain and (f) 1 mM AMP in X2180 strain. The dots are the experimental data and the solid curve is fitted rate equation

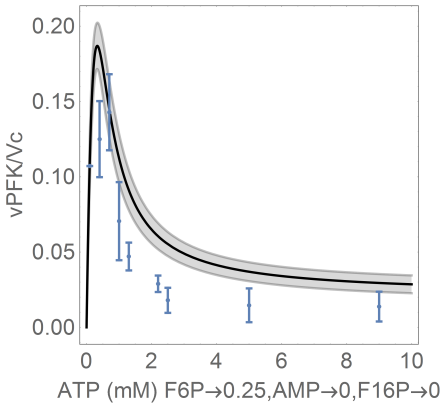

(a)

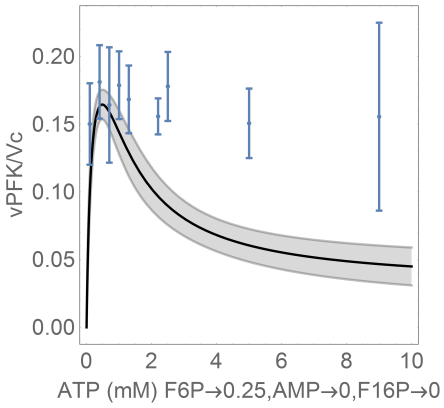

(b)

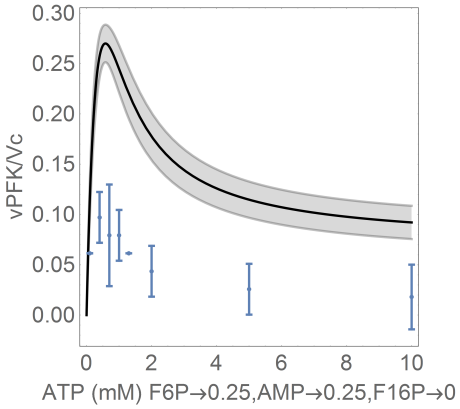

(c)

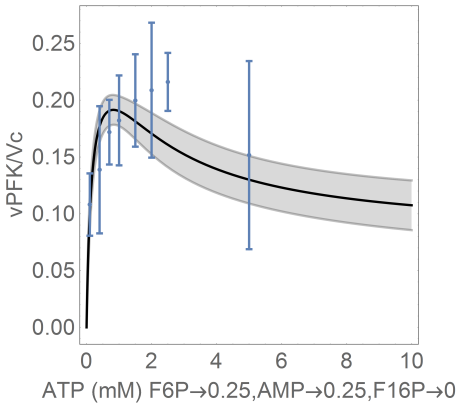

(d)

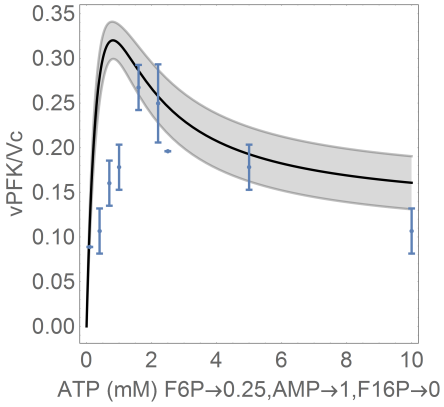

(e)

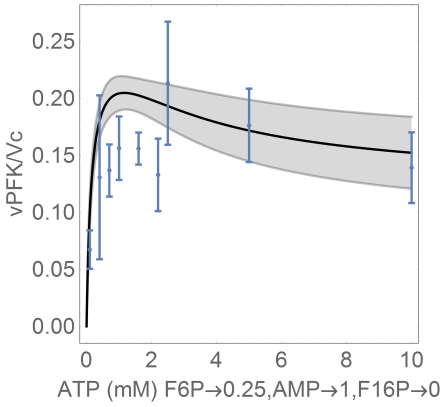

(f)

Figure B.5: E - The effect of ATP on PFK at a F6P concentrations of 0.25 mM for (a) 0 mM AMP in X2180 strain, (b) 0 mM AMP in Vin 13 strain, (c) 0.25 mM AMP in X2180 strain, (d) 0.25 mM AMP in Vin 13 strain, (e) 1 mM AMP in X2180 strain and (f) 1 mM AMP in X2180 strain. The dots are the experimental data and the solid curve is fitted rate equation

A PFK rate characteristic surface for the VIN13 strain is shown in Figure B.6. The steady state in muiyservin13 model exhibits ATP activation and not inhibition which could contribute to the optimization failing.

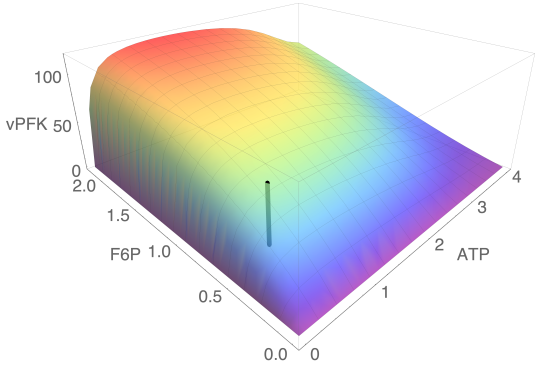

Figure B.6: PFK kinetics for muiyservin13, the model created by including the fitted experimental parameters for VIN13 PFK in the dupreez1 model showing the steady state concentrations on the graph with the bar. The x-axis scans for ATP (mM), y-axis is the F6P (mM) and the z-axis shows the reaction rate (mM/min).

List of References

[1] Nielsen, J. (2017) Systems biology of metabolism. *Annual review of biochemistry* **86**, 245–275

[2] Betz, A. and Chance, B. (1965) Influence of inhibitors and temperature on the oscillation of reduced pyridine nucleotides in yeast cells. *Archives of biochemistry and biophysics* **109**, 579–584

[3] Hess, B. and Boiteux, A. (1968) Control of glycolysis. *Regulatory functions of biological membranes* **2**, 149–167

[4] Richard, P., Diderich, J.A., Bakker, B.M., Teusink, B., van Dam, K. and Westerhoff, H.V. (1994) Yeast cells with a specific cellular make-up and an environment that removes acetaldehyde are prone to sustained glycolytic oscillations. *FEBS Letters* **341**, 223–226

[5] Danø, S., Sørensen, P.G. and Hynne, F. (1999) Sustained oscillations in living cells. *Nature* **402**, 320

[6] Danø, S., Hynne, F., De Monte, S., d'Ovidio, F., Sorensen, P.G. and Westerhoff, H. (2002) Synchronization of glycolytic oscillations in a yeast cell population. *Faraday Discuss.* **120**, 261–275

[7] Gustavsson, A.K., van Niekerk, D.D., Adiels, C.B., du Preez, F.B., Goksï¿½r, M. and Snoep, J.L. (2012) Sustained glycolytic oscillations in individual isolated yeast cells. *FEBS Journal* **279**, 2837–2847

[8] Goldbeter, A. and Lefever, R. (1972) Dissipative structures for an allosteric model: application to glycolytic oscillations. *Biophysical Journal* **12**, 1302–1315

[9] Selkov, E.E. (1975) Stabilization of energy charge, generation of oscillations and multiple steady states in energy metabolism as a result of purely stoichiometric regulation. *European Journal of Biochemistry* **59**, 151–157

[10] du Preez, F.B., van Niekerk, D.D., Kooi, B., Rohwer, J.M. and Snoep, J.L. (2012) From steady-state to synchronized yeast glycolytic oscillations i: model construction. *FEBS Journal* **279**, 2810–2822

[11] du Preez, F.B., van Niekerk, D.D. and Snoep, J.L. (2012) From steady-state to synchronized yeast glycolytic oscillations ii: model validation. *FEBS Journal* **279**, 2823–2836

[12] Goldbeter, A. and Nicolis, G. (1976) An allosteric enzyme model with positive feedback applied to glycolytic oscillations. *Prog. Theor. Biol* **4**, 157

[13] Goldbeter, A. (1974) Modulation of the adenylate energy charge by sustained metabolic oscillations. *Febs Letters* **43**, 327–330

[14] Teusink, B., Bakker, B.M. and Westerhoff, H.V. (1996) Control of frequency and amplitudes is shared by all enzymes in three models for yeast glycolytic oscillations. *Biochimica et Biophysica Acta (BBA) - Bioenergetics* **1275**, 204 – 212

[15] Reijenga, K.A., van Megen, Y.M., Kooi, B.W., Bakker, B.M., Snoep, J.L., van Verseveld, H.W. et al. (2005) Yeast glycolytic oscillations that are not controlled by a single oscillophore: a new definition of oscillophore strength. *Journal of Theoretical Biology* **232**, 385 – 398

[16] Wolf, J., Passarge, J., Somsen, O.J., Snoep, J.L., Heinrich, R. and Westerhoff, H.V. (2000) Transduction of intracellular and intercellular dynamics in yeast glycolytic oscillations. *Biophysical Journal* **78**, 1145–1153

[17] Gustavsson, A.K., Niekerk, D.D., Adiels, C.B., Kooi, B., Goksör, M. and Snoep, J.L. (2014) Allosteric regulation of phosphofructokinase controls the emergence of glycolytic oscillations in isolated yeast cells. *The FEBS journal* **281**, 2784–2793

[18] Snoep, J.L. (2005) The silicon cell initiative: working towards a detailed kinetic description at the cellular level. *Current Opinion in Biotechnology* **16**, 336–343

[19] Nielsen, K., Sørensen, P.G., Hynne, F. and Busse, H.G. (1998) Sustained oscillations in glycolysis: an experimental and theoretical study of chaotic and complex periodic behavior and of quenching of simple oscillations. *Biophysical chemistry* **72**, 49–62

[20] Bier, M., Bakker, B.M. and Westerhoff, H.V. (2000) How yeast cells synchronize their glycolytic oscillations: A perturbation analytic treatment. *Biophysical Journal* **78**, 1087 – 1093

[21] Hynne, F., Danø, S. and Sørensen, P.G. (2001) Full-scale model of glycolysis in saccharomyces cerevisiae. *Biophysical chemistry* **94**, 121–163

[22] Teusink, B., Passarge, J., Reijenga, C.A., Esgalhado, E., van der Weijden, C.C., Schepper, M. et al. (2000) Can yeast glycolysis be understood in terms of in vitro kinetics of the constituent enzymes? testing biochemistry. *European Journal of Biochemistry* **267**, 5313–5329

[23] Gustavsson, A.K., van Niekerk, D.D., Adiels, C.B., Goksör, M. and Snoep, J.L. (2014) Heterogeneity of glycolytic oscillatory behaviour in individual yeast cells. *FEBS letters* **588**, 3–7

[24] Gustavsson, A.K., Adiels, C.B., Mehlig, B. and Goksör, M. (2015) Entrainment of heterogeneous glycolytic oscillations in single cells. *Scientific reports* **5**, 9404

[25] Garrett, R, H. and Grisham, C, M. (1997) Biochemistry **18**, 535–546

[26] Botstein, D., Chervitz, S.A. and Cherry, M. (1997) Yeast as a model organism. *Science* **277**, 1259–1260

[27] Engel, S.R., Dietrich, F.S., Fisk, D.G., Binkley, G., Balakrishnan, R., Costanzo, M.C. et al. (2014) The reference genome sequence of Saccharomyces Cerevisiae: then and now. *G3: Genes, Genomes, Genetics* **4**, 389–398

[28] Aon, M., Cortassa, S., Westerhoff, H., Berden, J., Van Spronsen, E. and Van Dam, K. (1991) Dynamic regulation of yeast glycolytic oscillations by mitochondrial functions. *Journal of cell science* **99**, 325–334

[29] Richard, P., Teusink, B., Westerhoff, H.V. and van Dam, K. (1993) Around the growth phase transition S. cerevisiae's make-up favours sustained oscillations of intracellular metabolites. *FEBS Letters* **318**, 80 – 82

[30] Olivier, B.G. and Snoep, J.L. (2004) Web-based kinetic modelling using JWS Online. *Bioinformatics* **20**, 2143–2144

[31] Duysens, L. and Amesz, J. (1957) Fluorescence spectrophotometry of reduced phosphopyridine nucleotide in intact cells in the near-ultraviolet and visible region. *Biochimica et biophysica acta* **24**, 19–26

[32] Rapp, P. (1987) Why are so many biological systems periodic? *Progress in neurobiology* **29**, 261–273

[33] Ghosh, A., Chance, B. and Pye, E. (1971) Metabolic coupling and synchronization of NADH oscillations in yeast cell populations. *Archives of Biochemistry and Biophysics* **145**, 319 – 331

[34] Richard, P., Bakker, B.M., Teusink, B., Van Dam, K. and Westerhoff, H.V. (1996) Acetaldehyde mediates the synchronization of sustained glycolytic oscillations in populations of yeast cells. *European Journal of Biochemistry* **235**, 238–241

[35] Ghosh, A. and Chance, B. (1964) Oscillations of glycolytic intermediates in yeast cells. *Biochemical and Biophysical Research Communications* **16**, 174 – 181

[36] Higgins, J. (1964) A chemical mechanism for oscillation of glycolytic intermediates in yeast cells. *Proceedings of the National Academy of Sciences* **51**, 989–994

[37] Boiteux, A., Goldbeter, A. and Hess, B. (1975) Control of oscillating glycolysis of yeast by stochastic, periodic, and steady source of substrate: a model and experimental study. *Proceedings of the National Academy of Sciences* **72**, 3829–3833

[38] Boiteux, A. and Hess, B. (1978) Visualization of dynamic spatial structures in oscillating cell free extracts of yeast. In: Electrons to Tissues, Elsevier, 789–797

[39] Chance, B., Hess, B. and Betz, A. (1964) DPNH oscillations in a cell-free extract of s. carlsbergensis. *Biochemical and biophysical research communications* **16**, 182–187

[40] Das, J. and Busse, H. (1991) Analysis of the dynamics of relaxation type oscillation in glycolysis of yeast extracts. *Biophysical journal* **60**, 369–379

[41] Chance, B., Schoener, B. and Elsaesser, S. (1964) Control of the waveform of oscillations of the reduced pyridine nucleotide level in a cell-free extract. *Proceedings of the National Academy of Sciences* **52**, 337–341

[42] Hess, B. (1979) The glycolytic oscillator. *Journal of Experimental Biology* **81**, 7–14

[43] Chance, B., Estabrook, R.W. and Ghosh, A. (1964) Damped sinusoidal oscillations of cytoplasmic reduced pyridine nucleotide in yeast cells. *Proceedings of the National Academy of Sciences* **51**, 1244–1251

[44] Wahlefeld, A. and Bergmeyer, H. (1974) Methods of enzymatic analysis. *Academic Press, Inc, New York* **2**, 18–31. Triglycerides determination after enzymatic hydrolysis. 2nd English ed.,

[45] Madsen, M.F., Danø, S. and Sørensen, P.G. (2005) On the mechanisms of glycolytic oscillations in yeast. *The FEBS journal* **272**, 2648–2660

[46] Aon, M.A., Cortassa, S., Westerhoff, H.V. and Van Dam, K. (1992) Synchrony and mutual stimulation of yeast cells during fast glycolytic oscillations. *Journal of General Microbiology* **138**, 2219–2227

[47] Poulsen, A.K., Petersen, M.Ø. and Olsen, L.F. (2007) Single cell studies and simulation of cell-cell interactions using oscillating glycolysis in yeast cells. *Biophysical Chemistry* **125**, 275 – 280

[48] Goldbeter, A. (1997) Biochemical oscillations and cellular rhythms: the molecular bases of periodic and chaotic behaviour. *Cambridge University Press* **1**, 31–88

[49] Goodwin, B.C. (1965) Oscillatory behavior in enzymatic control processes. *Advances in enzyme regulation* **3**, 425–437

[50] Hess, B., Boiteux, A. and Krüger, J. (1969) Cooperation of glycolytic enzymes. *Advances in enzyme regulation* **7**, 149–167

[51] Betz, A. and Chance, B. (1965) Phase relationship of glycolytic intermediates in yeast cells with oscillatory metabolic control. *Archives of Biochemistry and Biophysics* **109**, 585 – 594

[52] Becker, J.U. and Betz, A. (1972) Membrane transport as controlling pacemaker of glycolysis in saccharomyces carlsbergensis. *Biochimica et Biophysica Acta (BBA)-Biomembranes* **274**, 584–597

[53] Reijenga, K.A., Snoep, J.L., Diderich, J.A., van Verseveld, H.W., Westerhoff, H.V. and Teusink, B. (2001) Control of glycolytic dynamics by hexose transport in Saccharomyces Cerevisiae. *Biophysical Journal* **80**, 626–634

[54] Heinrich, R. and Rapoport, T. (1975) Mathematical analysis of multienzyme systems. ii. steady state and transient control. *Biosystems* **7**, 130–136

[55] Williamson, T., Adiamah, D., Schwartz, J.M. and Stateva, L. (2012) Exploring the genetic control of glycolytic oscillations in saccharomyces cerevisiae. *BMC systems biology* **6**, 108

[56] Hess, B. and Plesser, T. (1979) Temporal and spatial order in biochemical systems. *Annals of the New York Academy of Sciences* **316**, 203–213

[57] Goldbeter, A. (1976) Kinetic cooperativity in the concerted model for allosteric enzymes. *Biophysical chemistry* **4**, 159–169

[58] Zhou, G., Ho, P. and van Holde, K. (1989) An analytic solution to the Monod-Wyman-Changeux model and all parameters in this model. *Biophysical journal* **55**, 275

[59] Kitano, H. (2002) Systems biology: a brief overview. *Science* **295**, 1662–1664

[60] Richter, O., Betz, A. and Giersch, C. (1975) The response of oscillating glycolysis to perturbations in the nadh/nad system: a comparison between experiments and a computer model. *Biosystems* **7**, 137–146

[61] Pritchard, L. and Kell, D.B. (2002) Schemes of flux control in a model of saccharomyces cerevisiae glycolysis. *European journal of biochemistry* **269**, 3894–3904

[62] Albers, E., Larsson, C., Andlid, T., Walsh, M.C. and Gustafsson, L. (2007) Effect of nutrient starvation on the cellular composition and metabolic capacity of saccharomyces cerevisiae. *Applied and environmental microbiology* **73**, 4839–4848

[63] Den Hollander, J., Ugurbil, K., Brown, T., Bednar, M., Redfield, C. and Shulman, R. (1986) Studies of anaerobic and aerobic glycolysis in saccharomyces cerevisiae. *Biochemistry* **25**, 203–211

[64] Louis, E.J. (2016) Historical evolution of laboratory strains of saccharomyces cerevisiae. *Cold Spring Harbor Protocols* **2016**, 77–75

[65] Patnaik, P. (2003) Effect of fluid dispersion on cybernetic control of microbial growth on substitutable substrates. *Bioprocess and biosystems engineering* **25**, 315–321

[66] Keulers, M. and Kuriyama, H. (1998) Extracellular signaling in an oscillatory yeast culture. In: Information processing in cells and tissues. Springer, 85–94

[67] Swedlow, J.R. and Platani, M. (2002) Live cell imaging using wide-field microscopy and deconvolution. *Cell Structure and Function* **27**, 335–341

[68] Dodd, B.J. and Kralj, J.M. (2017) Live cell imaging reveals ph oscillations in saccharomyces cerevisiae during metabolic transitions. *Scientific Reports* **7**, 13922

[69] Onlinemedia (1993). AAVOS International kernel description. URL `https://aavos.eu/glossary/fourier-transform/`

[70] Cooley, J.W. and Tukey, J.W. (1965) An algorithm for the machine calculation of complex fourier series. *Mathematics of computation* **19**, 297–301

[71] Gabor, D. (1946) Theory of communication. part 1: The analysis of information. *Journal of the Institution of Electrical Engineers* **93**, 429–441. Part III: Radio and Communication Engineering

[72] Pikovsky, A., Rosenblum, M., Kurths, J. and Kurths, J. (2003) Synchronization: a universal concept in nonlinear sciences. *Cambridge university press* **12**, 362

[73] Shinomoto, S. and Kuramoto, Y. (1986) Phase transitions in active rotator systems. *Progress of Theoretical Physics* **75**, 1105–1110

[74] Alsuhaim, H., Vojisavljevic, V. and Pirogova, E. (2013) Effects of non-thermal microwave exposures on the proliferation rate of saccharomyces cerevisiae yeast. *World Congress on Medical Physics and Biomedical Engineering* 48–51

[75] Snoep, J., Mrwebi, M., Schuurmans, J., Rohwer, J. and De Mattos, M.T. (2009) Control of specific growth rate in saccharomyces cerevisiae. *Microbiology* **155**, 1699–1707

[76] De Monte, S., d'Ovidio, F., Danø, S. and Sørensen, P.G. (2007) Dynamical quorum sensing: Population density encoded in cellular dynamics. *Proceedings of the National Academy of Sciences* **104**, 18377–18381

[77] Kouril, T. (2012) Challenging metabolic networks at high temperature. The central carbohydrate metabolism of Sulfolobus solfataricus. Ph.D. thesis, Vrije Universiteit Amsterdam. Naam instelling promotie: VU Vrije Universiteit Naam instelling onderzoek: VU Vrije Universiteit

[78] Lilly, M., Lambrechts, M. and Pretorius, I. (2000) Effect of increased yeast alcohol acetyltransferase activity on flavor profiles of wine and distillates. *Applied and environmental microbiology* **66**, 744–753

[79] Hald, B.O., Smrcinova, M. and Sørensen, P.G. (2012) Influence of cyanide on diauxic oscillations in yeast. *The FEBS journal* **279**, 4410–4420